

**Studies on the Reaction Mechanism of Cyclodextrin  
Glycosyltransferase and Malto-hexaose Forming Amylase on the  
Basis of X-ray Crystallographic and Protein Engineering Analyses**

**February 2004**

**Ryuta KANAI**

**Studies on the Reaction Mechanism of Cyclodextrin  
Glycosyltransferase and Malto-hexaose Forming Amylase on the  
Basis of X-ray Crystallographic and Protein Engineering Analyses**

**A Dissertation Submitted to the Graduate School of Life and  
Environmental Sciences, the University of Tsukuba in Partial  
Fulfillment of the Requirements for the Degree of Doctor of  
Philosophy in Science.  
(Doctoral Program in Functional Biosciences)**

**Ryuta KANAI**



## Table of Contents

Abbreviations · · · · ·	1
Abstracts · · · · ·	2
General Introduction · · · · ·	4
Table and Figures · · · · ·	7
Chapter I · · · · ·	16
The Reaction Mechanism of Cyclodextrin Glycosyltransferase on the Basis of X-ray Crystallographic and Protein Engineering Analyses	
Section I · · · · ·	17
Crystal Structures of Cyclodextrin Glycosyltransferase Complexed with 1-Deoxy- nojirimycin and Acarbose: the Inhibition Mechanism and Substrate Binding	
Abstract · · · · ·	18
Introduction · · · · ·	19
Materials and Methods · · · · ·	20
Results · · · · ·	23
Discussion · · · · ·	25
Tables and Figures · · · · ·	28
Section II · · · · ·	39
Crystal Structures of the Native and Acarbose-Complexed forms of Cyclodextrin Glycosyltransferase in which Phe283 is replaced with leucine: Role of Phe283 in Enzymatic Reaction.	

Abstract · · · · ·	40
Introduction · · · · ·	41
Materials and Methods · · · · ·	43
Results · · · · ·	46
Discussion · · · · ·	50
Tables and Figures · · · · ·	53
 Chapter II · · · · ·	 68
The Reaction Mechanism of Malto-hexaose Forming Amylase on the Basis of X-ray Crystallographic Analysis: Crystal Structures of the Native and Pseudo-maltononaose- complexed Forms.	
Abstract · · · · ·	69
Introduction · · · · ·	70
Materials and Methods · · · · ·	72
Results · · · · ·	77
Discussion · · · · ·	82
Tables and Figures · · · · ·	85
 General Discussion · · · · ·	 105
Figure · · · · ·	107
 References · · · · ·	 109
 Acknowledgements · · · · ·	 117

## Abbreviations

BAA; Barley  $\alpha$ -amylase

BLA; *Bacillus licheniformis*  $\alpha$ -amylase

BSTA; *Bacillus stearothermophilus*  $\alpha$ -amylase

CD; cyclodextrin

CGTase; cyclodextrin glycosyltransferase

F283L; mutant CGTase replaced Phe283 with leucine

F283L\_ACA; F283L complex with acarbose

F283Y; mutant CGTase replaced Phe283 with leucine

F283Y\_ACA; F283Y complex with acarbose

G1; glucose

G2; maltose

G3; maltotriose

G4; maltotetraose

G5; maltopentaose

G6; maltohexaose

G6-amylase; maltohexaose forming amylase

G6AMY; maltohexaose forming amylase

G7; maltoheptaose

HPLC; high performance liquid chromatography

IC<sub>50</sub>; 50% inhibition concentration of maximal enzymatic activity

3KB-G5CNP; 3-ketobutylidene- $\beta$ -2-chloro-4-nitrophenylmalto-pentaoside

LB; Luria-Bertani

MBS; maltose binding site

PEG; polyethylene glycol

SDS-PAGE; sodium dodecyl sulfate-polyacrylamide gel electrophoresis

TLC; thin layer chromatography

## Abstract

Cyclodextrin glycosyltransferase (CGTase) converts starch and  $\alpha$ -1,4-glucans to circular  $\alpha$ -1,4-linked maltodextrins,  $\alpha$ ,  $\beta$ , and  $\gamma$ -cyclodextrins consisting of six, seven, and eight glucose units, respectively, by transglycosylation. Maltohexaose forming amylase (G6-amylase) hydrolyzes starch to linear maltohexaose. Both enzymes belonging to  $\alpha$ -amylase family are distinct from typical  $\alpha$ -amylase, which hydrolyzes starch to glucose and/or maltose. Biochemical experiments previously reported for CGTase and G6-amylase indicated their specific subsite structures to produce cyclodextrins or maltohexaose. Furthermore, the mutational analyses of CGTase showed some amino acid residues involving to the cyclization reaction. However, in CGTase and G6-amylase, the structural properties of the subsites specific for their products have been unknown and we have little information about the detailed structures of the amino acid residues involving in cyclization reaction of CGTase. In this study, as a final goal to reveal their reaction mechanisms to produce cyclodextrin or maltohexaose in each enzyme, I performed the experiments mainly using X-ray crystallographic techniques as follows.

In section I of chapter I, to elucidate each inhibition mechanism of 1-deoxynojirimycin and acarbose for the enzymatic reaction of CGTase and show the subsite structure of CGTase, the crystal structures of CGTase complexed with 1-deoxynojirimycin or acarbose were determined, respectively. The structure of acarbose-complexed CGTase showed that the pseudo-maltotetraose derived from acarbose is bound from subsites  $-2$  to  $+2$  and its N-glycoside bond locates between subsites  $-1$  and  $+1$ . Furthermore, Phe183/259 specifically conserved in CGTase make stack interaction with the glucosyl residue at subsite  $+2$  and seem to involve in guiding the glucosyl residue at non-reducing end to the acceptor-binding site (subsites  $+1$  and  $+2$ ). The structure of 1-deoxynojirimycin-complexed CGTase showed that 1-deoxynojirimycin neighboring to subsite  $-1$  contacts to a catalytic residue Asp229 with hydrogen bonds but doesn't form the stack interaction with Tyr100 frequently observed in sugar-enzyme complex.

In section II of chapter I, to elucidate the role of Phe283 conserved specifically in CGTase on enzymatic reactions more detailed, the native and acarbose-complexed crystal structures of the

mutant CGTase in which Phe283 is replaced with leucine have determined and showed that Phe283 plays an important role in enzymatic reactions resulting cyclization by fixing the motion of Phe259.

In chapter II, the native and pseudo-maltononaose-complexed crystal structures of G6-amylase were determined to elucidate the subsite structure of G6-amylase and revealed the presence of six subsites of non-reducing end and an importance of the hydrophobic interaction of aromatic residue Trp140 with a glucosyl residue at subsite –6.

Finally, the difference between the production mechanisms of CGTase and G6-amylase are discussed on the basis of these structures and I suggest that the change in their backbone structure mainly observed in domain B is responsible for each specific subsite structure and the amino acid residues specifically conserved in their subsites enable their effective production of cyclodextrins or maltohexaose.

## General Introduction

$\alpha$ -Amylase and related enzymes are one of the most fundamental components in sugar and energy metabolisms of all lives. Especially,  $\alpha$ -amylase family (glycoside hydrolase family 13 (B. Henrissat *et al.* 1997)) is not only essential for vital activity but also contains enzymes useful in our life (Table 1).

Cyclodextrin glycosyltransferase (CGTase; EC 2.4.1.19) belonging to  $\alpha$ -amylase family converts starch and related  $\alpha$ -1,4-glucans to circular  $\alpha$ -1,4-linked maltodextrin, cyclodextrin (CD), by intra-molecular transglycosylation differed from  $\alpha$ -amylase (Figure 1). In general, CDs consist of six, seven, or eight  $\alpha$ -1,4-linked glucosyl units and are each referred to  $\alpha$ -,  $\beta$ -,  $\gamma$ -CDs. Since CDs form inclusion complexes with a variety of guest molecules and change their physicochemical properties, they have been applied in pharmaceutical, chemical and food industries.

Maltohexaose-forming amylase (G6-amylase; EC 3.2.1.98) also belonging to  $\alpha$ -amylase family mainly produces maltohexaose by hydrolyzing starch (Figure 1). Since oligo-saccharides (maltotetraose, maltopentaose, and maltohexaose), which are not produced by usual  $\alpha$ -amylase, are useful for low sweetness, low viscosity, high moisturizing effect, and high efficiency for digestion and absorption, G6-amylase is an important enzyme in food and pharmaceutical industries. Both CGTase and G6-amylase are similar to  $\alpha$ -amylase in their substrates, starch and related  $\alpha$ -1,4-glucans, but their products are distinct from that of  $\alpha$ -amylase that finally hydrolyze to glucose and/or maltose (Figure 1).

In the previously reported biochemical and crystallographic analyses, the catalytic mechanisms are fundamentally common between  $\alpha$ -amylase family containing CGTase and G6-amylase (Figure 2) (A. Tsukamoto *et al.* 1988; M. Kubota *et al.* 1991; A. Nakamura *et al.* 1992; J.C.M. Uitdehaag *et al.* 1999). The catalytic residues are one aspartic acid as a nucleophile and one glutamic acid as a proton donor/acceptor. For the first step, the glutamic acid residue provides a proton to the oxygen atom of the glucosidic bond as a cleavage site and the aspartic acid residue nucleophilically attacks to the C1 atom of the cleaved bond (Figure 2). After formation of a covalently bonded sugar-enzyme intermediate, the glutamic acid residue accepts a proton from

the oxygen atom of acceptor molecules (sugar or water) in the second step and the nucleophilic oxygen atom attacks to the C1 atom covalently bonded to the aspartic acid residue (Figure 2) and the catalytic reaction finishes. When the acceptor molecule is a sugar, the reaction is transglycosylation and, when it is water, the reaction is hydrolysis (Figure 2).

The previous biochemical studies on the specific production mechanisms of CGTase and G6-amylase indicated the importance of their specific subsite structure (Figure 3) (T. Nakakuki *et al.* 1984; S. Abe *et al.* 1991; C. Klein *et al.* 1992). The subsite is in a particular region to bind one glucose unit and the subsites located at the reducing terminal side are defined with plus-signed number. CGTase and G6-amylase have six to eight and six subsites in the non-reducing terminal side, respectively. In contrast,  $\alpha$ -amylases except those from plant have only two to four subsites with non-reducing terminal side. Therefore, whether their products are oligo-saccharide or glucose/maltose would result from the differences of their subsite structures and substrate binding modes. Furthermore, CGTase would require the specific binding mode to cyclize linear oligo-saccharides. The biochemical analyses of CGTase previously reported that the some amino acid residues are critical for the cyclodextrin formation (A. Nakamura *et al.* 1994) and the X-ray structure analyses showed that the CGTase consists of five domains (A, B, C, D, and E) (Figure 4) (M. Kubota *et al.* 1991; C. Klein *et al.* 1992; C.L. Lawson *et al.* 1994; K. Harata *et al.* 1996; R.M.A. Knegtel *et al.* 1996). Domain A is constituted by a typical  $(\beta/\alpha)_8$  barrel structure with an additional  $\alpha$ -helix and a long loop region containing a  $\beta$ -sheet. The domain B, consisting of a short  $\alpha$ -helix, short strands and loops, is located on the wider side of the barrel, where the active site is situated. Only  $\beta$ -sheet structures are observed in domains C, D, and E (Figure 4). However, the relationship between the subsite structure and the process of the cyclization reaction is unclear and the structural information of the amino acid residues important in it is little. Moreover, the three-dimensional structure of G6-amylase has not been determined and its reaction mechanism of maltohexaose production is not clear.

In this study, as a final goal to elucidate the specific production mechanism of CGTase and G6-amylase, I performed the structure analyses mainly using X-ray crystallographic techniques

as follows. In section I of chapter I, I determined the two crystal structures of CGTase complexed with inhibitors, 1-deosynojirimycin or acarbose, to elucidate their inhibition mechanisms for the enzymatic reaction of CGTase. In section II of chapter I, to elucidate the role of Phe283 conserved specifically in all CGTases on enzymatic reaction, I determined the native and acarbose-complexed crystal structures of the mutant CGTase in which Phe283 is replaced with leucine. In chapter II, I determined the native and pseudo-maltononaose- complexed crystal structures of G6-amylase to elucidate the mechanism of maltohexaose formation. Then I discuss the mechanism of CGTase and G6-amylase to produce specific maltooligosaccharides, cyclodextrin and maltohexaose, respectively.



Enzyme names	E..C. num.	Major reaction	Substrate	Major products	3D strcuture
$\alpha$ -Amylase	3.2.1.1	$\alpha$ -1,4-Hydrolysis	Amylose, amylopectin	Malto-oligosaccharide, maltose, glucose	Determined
$\alpha$ -Glucosidase	3.2.1.20	$\alpha$ -1,4-Hydrolysis	Amylose	Glucose	Determined
Maltogenic amylase	3.2.1.133	$\alpha$ -1,4-Hydrolysis	Amylose, amylopectin	Maltose	Determined
Maltotetraose-forming amylase	3.2.1.60	$\alpha$ -1,4-Hydrolysis	Amylose, amylopectin	Maltotetraose	Determined
Maltopentaose-forming amylase	3.2.1.-	$\alpha$ -1,4-Hydrolysis	Amylose	Maltopentaose	Not determined
<b>Maltohexaose-forming amylase</b>	3.2.1.98	$\alpha$ -1,4-Hydrolysis	Amylose, amylopectin	Maltohexaose	Not determined
Cyclomaltodextrinase	3.2.1.54	$\alpha$ -1,4-Hydrolysis	Cyclodextrin	Malto-oligosaccharide	Determined
4- $\alpha$ -Glucanotransferase	2.4.1.25	$\alpha$ -1,4-Transglycosylation	Amylose	Amylose	Determined
<b>Cyclodextrin glycosyltransferase</b>	2.4.1.19	$\alpha$ -1,4-Transglycosylation	Amylose	Cyclodextrin	Determined
Pullulanase	3.2.1.41	$\alpha$ -1,6-Hydrolysis	Amylopectin, pullulan	Branched oligosaccharide, maltotriose	Not determined
Neopullulanase	3.2.1.135	$\alpha$ -1,4-Hydrolysis, $\alpha$ -1,6-Hydrolysis	Pullulan	Panose	Determined
Oligo- $\alpha$ -glucosidase	3.2.1.10	$\alpha$ -1,6-Hydrolysis	Isomalto-oligosaccharide	Glucose	Determined
Isoamylase	3.2.1.68	$\alpha$ -1,6-Hydrolysis	Amylopectin	Amylose	Determined
Glucodextranase	3.2.1.70	$\alpha$ -1,6-Hydrolysis	Amylopectin	Amylose	Not determined
Branching enzyme	2.4.18	$\alpha$ -1,6-Transglycosylation	Amylose	Amylopectin	Determined
Trehalose synthase	5.4.99.16	$\alpha$ , $\alpha$ -1,1-Transglycosylation	Maltose	$\alpha$ , $\alpha$ -1,1-Trehalose	Not determined
Trehalose-6-phosphate hydrolase	3.2.1.93	$\alpha$ , $\alpha$ -1,1-Hydrolysis	$\alpha$ , $\alpha$ -1,1-Trehalose-6-phosphate	Glucose, glucose-6-phosphate	Not determined
Amylosucrase	2.4.1.4	$\alpha$ -1,4-Transglycosylation	Sucrose, amylose	Fructose, amylose	Determined
Sucrose phosphorylase	2.4.1.7	Phosphorylation	Sucrose, phosphate	Fructose, glucose-1-phosphate	Not determined
Isomaltulose synthase	5.4.99.11	Transglycosylation	Sucrose	6-O- $\alpha$ -glucopyranosyl-D-fructofuranose	Determined

**Table 1. Enzymatic properties of glycoside hydrolase family 13.**

**Figure 1. Specific productions from starch by CGTase, G6-amylase and  $\alpha$ -amylase.** CGTase, G6-amylase and  $\alpha$ -amylase produce cyclodextrin, maltohexaose and glucose and/or maltose, respectively, from starch and related  $\alpha$ -1,4-glucans.

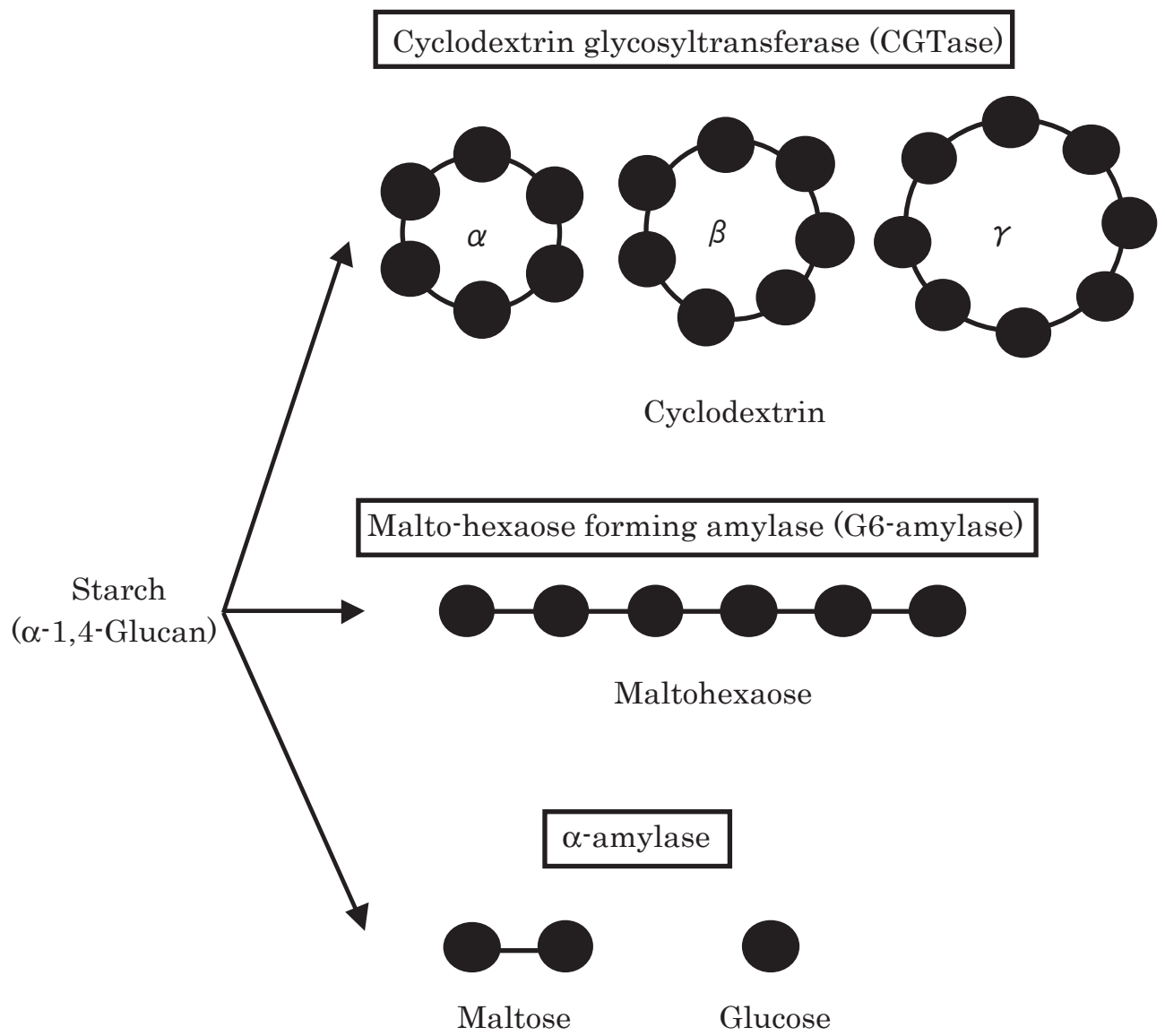


**Figure 2. Catalytic mechanism of  $\alpha$ -amylase family enzymes.** The active center consist of one aspartic acid as nucleophilic catalyst and one glutamic acid as proton donor/acceptor.

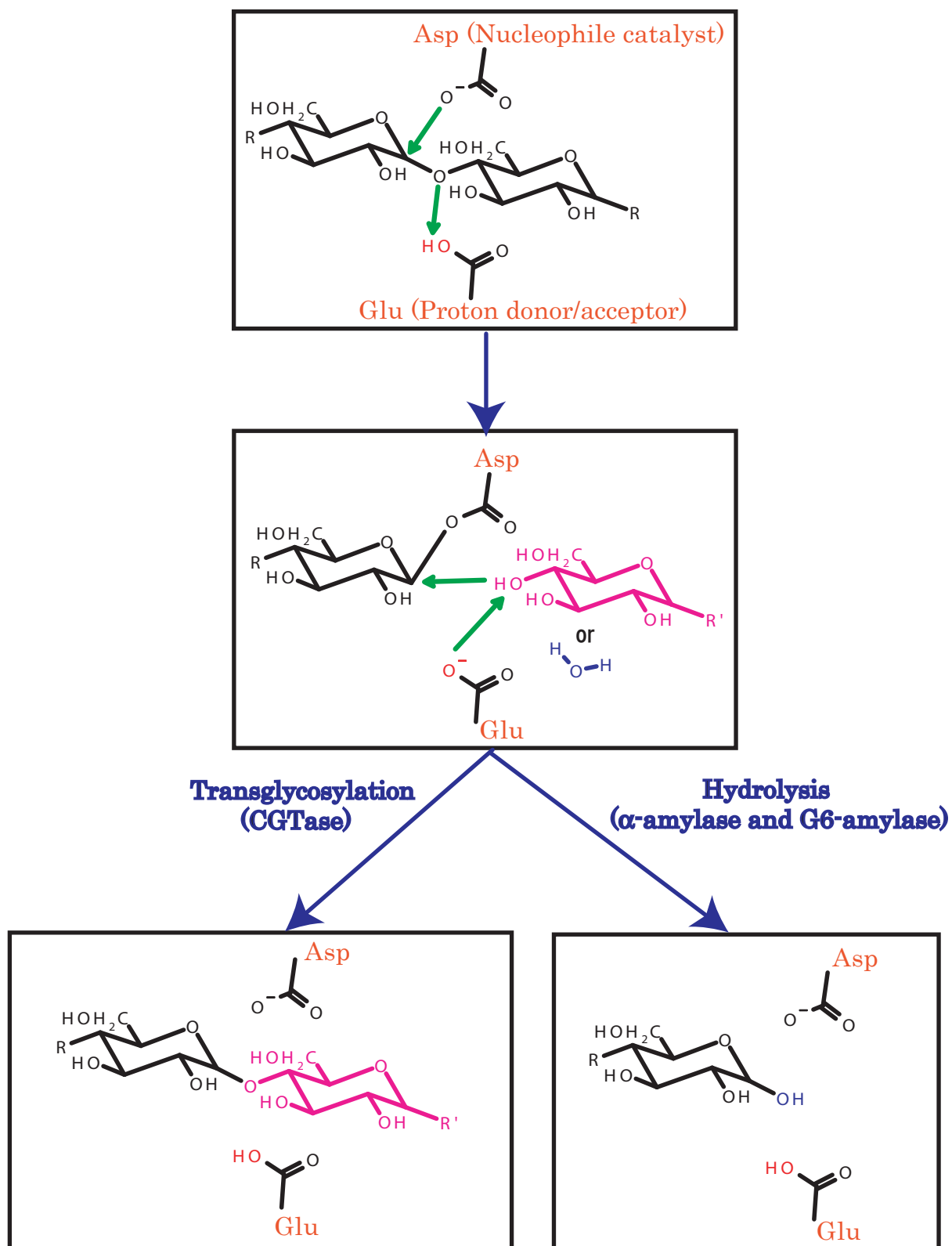


**Figure 3. Production mechanism of cyclodextrin and maltohexaose by CGTase and G6-amylase.**

Both enzymes have more subsites at the non-reducing side than that  $\alpha$ -amylase. In CGTase, cyclization additionally occurs after sugar-enzyme intermediate formation.

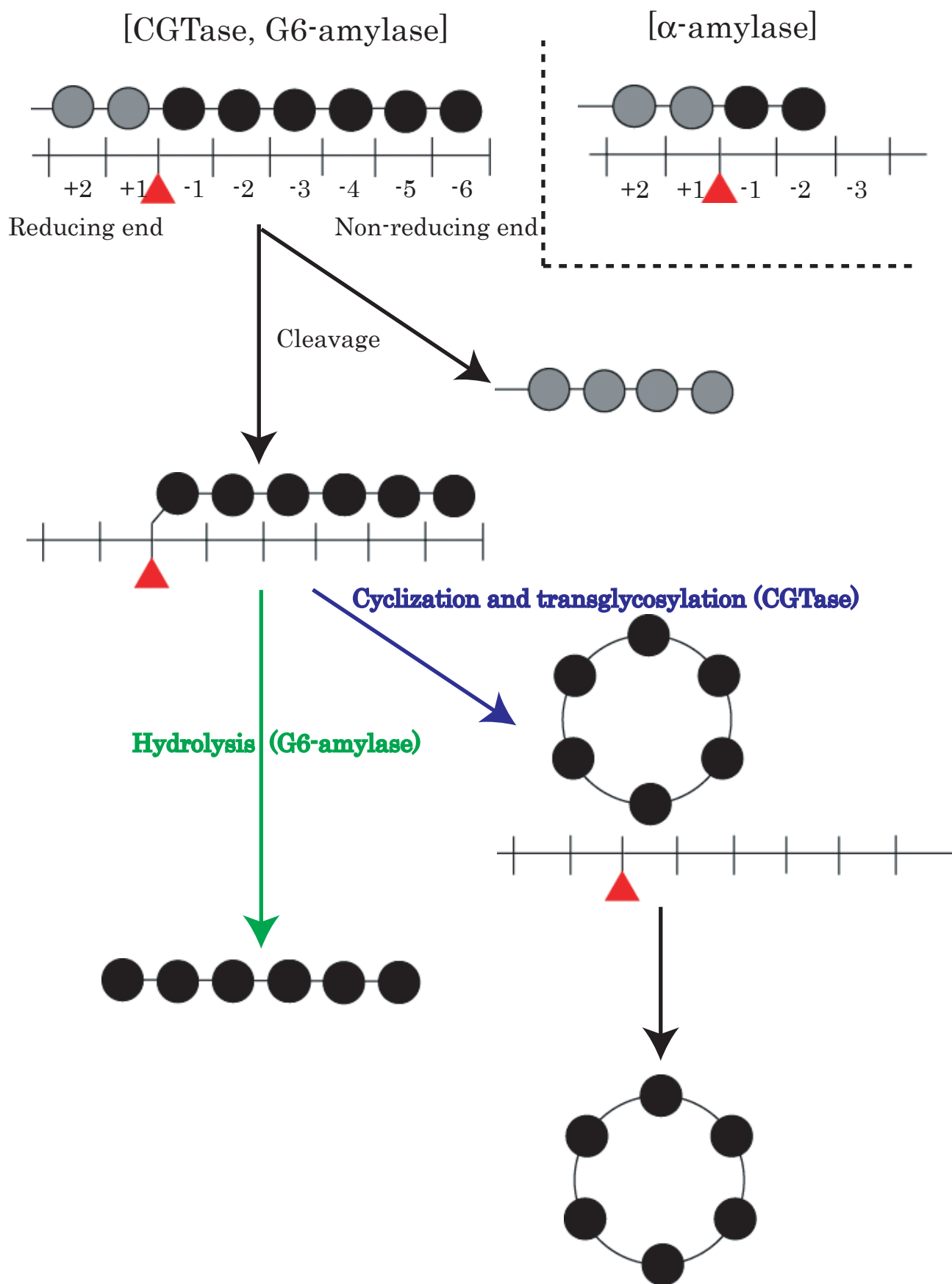
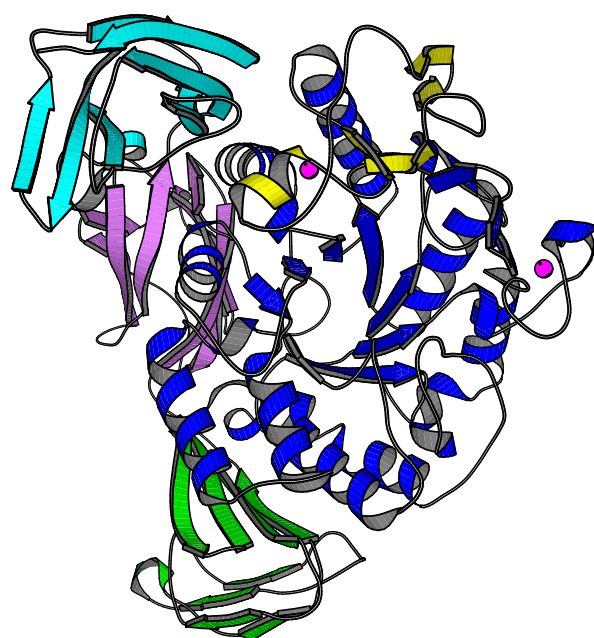
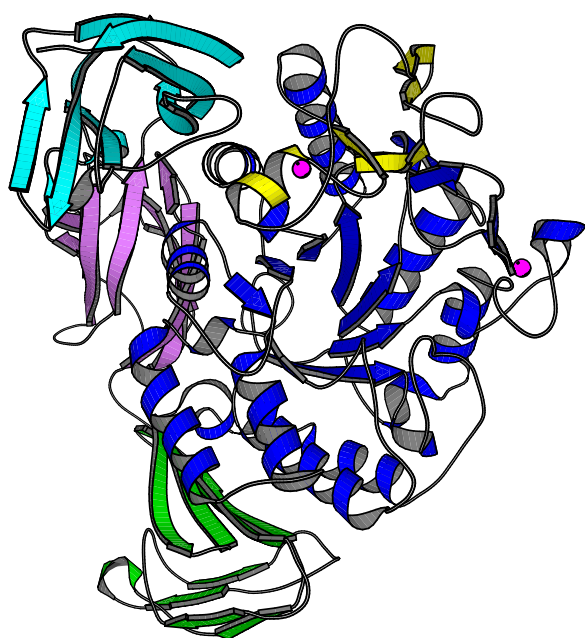


**Figure 4. Stereo view of the structure of cyclodextrin glycosyltransferase from *Bacillus* sp.1011 (K. Harata *et al.* 1996).** CGTase consists of five domains: A (1-406, blue), B (139-203, yellow), C (407-496, green), D (497-584, purple) and E (585-686, cyan). Calcium ions are shown by magenta circles.





## **Chapter I**

### **The Reaction Mechanism of Cyclodextrin Glycosyltransferase on the Basis of X-ray Crystallographic and Protein Engineering Analyses**

## Section I

**Crystal Structures of Cyclodextrin Glycosyltransferase Complexed with 1-Deoxy-  
nojirimycin and Acarbose: the Inhibition Mechanism and Substrate Binding**

## Abstract

1-Deoxynojirimycin, a pseudo-glucose, and acarbose, a pseudo-maltotetraose, are inhibitors for glucosyl hydrolases. Acarbose shows powerful inhibition in the enzymatic reaction of cyclodextrin glycosyltransferase (CGTase) and glucoamylase, and 1-deoxynojirimycin is a strong inhibitor for glucoamylase, although it weakly affects for CGTase. To elucidate the difference in the inhibition abilities and the subsite structure of CGTase, the crystal structures of the CGTase from alkalophilic *Bacillus* sp.1011 complexed with 1-deoxynojirimycin or acarbose were determined at 2.0 Å resolution.

The acarbose-complexed structure showed the four subsites in the active cleft of CGTase. One pseudo-maltotetraose molecule occupies subsites from -2 to +2 with many hydrogen bonds and hydrophobic interaction and its N-glycosidic bond is located between subsites -1 and +1. These would result in the strong inhibition of acarbose in the enzymatic reaction of CGTase. Moreover, Phe183 and Phe259 conserved specifically in CGTase are in the hydrophobic stacking interaction with the glucosyl residue at subsite +2. This indicates that these amino acid residues are involved in guiding the glucosyl residue at the non-reducing terminal of sugar chain to the acceptor-binding site (subsites +1 and +2) in cyclization.

In 1-deoxynojirimycin-complexed structure, one 1-deoxynojirimycin molecule is bound to the active center near the subsite -1 by hydrogen bonds with catalytic residues and water molecules, but doesn't make stacking interaction with Tyr100 as observed in acarbose-complexed structure. The lack of stacking interaction with the aromatic side chain of Tyr100 would be responsible for the weak inhibition of 1-deoxynojirimycin in the enzymatic action of CGTase.

## Introduction

Cyclodextrin glucanotransferase (EC 2.4.1.19, CGTase) belonging to  $\alpha$ -amylase family (glycoside hydrolases family 13 (B. Henrissat *et al.* 1997)) mainly produces cyclic  $\alpha$ -1,4-linked maltohexaose, maltoheptaose and malto-octaose called  $\alpha$ ,  $\beta$  and  $\gamma$ -cyclodextrins, respectively. The cyclization reaction that is not observed in  $\alpha$ -amylase is the most attractive property of CGTase. The key to the cyclization reaction is how the non-reducing end of the donor molecule instead of the other sugar and water molecules is transferred at subsites +1 and +2 of the acceptor-binding site in CGTase. The biochemical analyses reported previously indicated the specific subsite structures (subsites -4 to +2, etc) to cyclize linear oligosaccharide (S. Abe *et al.* 1991) and the X-ray structure of CGTase from *Bacillus stearothermophilus* has first been determined at 1991 (M. Kubota *et al.*) and the structures of CGTase from alkalophilic *Bacillus* sp.1011 have been reported (K. Harata *et al.* 1996), but the structural information about the subsites is not obscure.

Since the structure of inhibitors normally is similar to the native substrates, the structure of inhibitor-enzyme complex provides much important clues to the elucidation of substrate recognition and binding. Acarbose and 1-deoxynojirimycin have been used as inhibitors for sugar-catalyzing enzymes (Figure 5). 1-Deoxynojirimycin is a strong inhibitor for exo-type glycosyl hydrolase like glucoamylase ( $IC_{50}$  for starch degrading activity = 0.096  $\mu$ M (E. Truscheit *et al.* 1981)) that hydrolyzes  $\alpha$ -1,4-linked glucan and produces only  $\beta$ -glucose, but its inhibition power is weak for endo-type glycosyl hydrolase like CGTase ( $IC_{50}$  for starch degrading activity = 480  $\mu$ M). In contrast, acarbose is a strong inhibitor for most glycosyl hydrolases (glucoamylase;  $IC_{50}$  = 0.0065  $\mu$ M (E. Truscheit *et al.* 1981), CGTase;  $IC_{50}$  = 0.6  $\mu$ M). To elucidate the inhibition mechanisms of 1-deoxynojirimycin and acarbose for CGTase and the substrate recognition and interaction of CGTase, we determined the crystal structures of CGTase from alkalophilic *Bacillus* sp.1011 complexed with 1-deoxynojirimycin and acarbose, respectively.

## Materials and methods

### *Chemicals and enzymes*

All restriction and modification enzymes used for recombinant DNA manipulations were purchased from Takara Shuzo Co., Ltd., or Toyobo Co., Ltd. Tetracycline and ampicillin were from Wako Pure Chemical Industry Ltd. Soluble starch was from E. Merck. Acarbose was a gift from Drs. A. Mullen and K. Hornberg (Bayer AG). 1-Deoxynojirimycin was a gift from Prof. H. Seto (University of Tokyo). All other chemicals were of reagent grade.

### *Bacterial strains and plasmids*

CGTase was produced in the protease-deficient mutant *E. coli* ME8417 [*lon*::Tn10(*tet*<sup>r</sup>) *thr leu lacy* ], provided by Dr. H. Takahashi (University of Tokyo). Plasmid pTUE254 contains the CGTase gene region of alkalophilic *Bacillus* sp.1011 (K. Kimura *et al.* 1987).

### *Expression and purification of wild type CGTase*

The wild type CGTase was expressed and purified as described (A. Nakamura *et al.* 1992; K. Haga *et al.* 1994). ME8417 containing the plasmid pTUE254 encoding the CGTase was incubated in Luria-Bertani medium containing ampicillin (50 µg/ml) and tetracycline (20 µg/ml) for 14 hr at 37 °C. Target proteins were abstracted by osmotic shock (S.J. Chan *et al.* 1981). The supernatant obtained after ammonium sulfate (28%) precipitation was loaded onto TOYOPEARL HW55-F equilibrated with 28% ammonium sulfate-10 mM sodium phosphate buffer (pH 6.0). The resin was washed and then the target proteins were eluted with 10 mM sodium phosphate buffer (pH 6.0). The proteins were desalted over a Bio-Gel column (BioRad) equilibrated by Milli-Q and concentrated to 25 mg/ml using an Amicon concentration kit. The proteins were over 99% pure according to SDS-PAGE. Protein concentrations were determined using the BCA protein assay reagent (Pierce) with standard bovine serum albumin.

### *Crystallization of CGTase complexed with acarbose and 1-deoxynojirimycin*

All crystals were obtained by the co-crystallization with acarbose or 1-deoxynojirimycin by hanging drop vapor diffusion (K. Haga *et al.* 1994). The CGTase complexes were crystallized in 20% (w/v) PEG3000, 20% (v/v) 2-propanol, 100 mM sodium citrate, 1 mM calcium chloride, and additive 1 mM acarbose or 1-deoxynojirimycin. Rod-like crystals of about  $1.0 \times 0.3 \times 0.2$  mm appeared within two weeks at room temperature.

### *Data collection*

X-ray diffraction data of the acarbose-complexed CGTase were collected to 2.0 Å resolution by using a Bruker SMART 6000 diffractometer (50 kV, 90mA) at 290K. The number of the unique reflections was 91,157 with  $R_{\text{merge}}(I)$  value of 13.2% and completeness of 96.0%. X-ray diffraction data of the CGTase complex with 1-deoxynojirimycin were collected to 1.8 Å resolution on an Enraf-Nonius FAST diffractometer equipped with a FR571 generator (40 kV, 50 mA) at 286 K. Eight data sets of independent reflections obtained from two crystals were merged to the set of 100,410 unique reflections with the  $R_{\text{merge}}(I)$  value of 7.6% and completeness of 81.5%. Results are summarized in Table 2.

### *Structure determination and refinement*

All structures were resolved by molecular replacement using the coordinates of native wild type alkalophilic *Bacillus* sp.1011 CGTase (K. Harata *et al.* 1996) and refined by the program *X-PLOR* (A.T. Brünger *et al.* 1987) using the diffraction data between 10.0 - 2.0 Å resolution and above the 2 and 1  $\sigma$  level in the acarbose-complexed and 1-deoxynojirimycin-complexed structures, respectively. The 1-deoxynojirimycin and the pseudo-maltotetraose molecules derived from acarbooses were respectively introduced in the model structures by reference to their  $|3F_o - 2F_c|$  and  $|F_o - F_c|$  electron density maps ( $> 1.5 \sigma$ ). Difference electron density peaks above  $3\sigma$  in the  $|F_o - F_c|$  map and in intermolecular contacts in the range of 2.5 - 3.3 Å with protein were considered as water. However, those with an isotropic temperature factor above 60 Å<sup>2</sup> were omitted during refinement. The refinements converged at the  $R$  values of 18.4% ( $R_{\text{free}} = 24.6\%$ ) for

the 1-deoxynojirimycin-complexed structure and 15.4% ( $R_{\text{free}} = 21.4\%$ ) for the acarbose-complexed structure. The stereo-chemical qualities of these structures were confirmed by the program PROCHECK (A.R. Laskowski *et al.* 1993). The program TURBO-FRODO examined the graphics and drew the structures. Atomic coordinates have been deposited with Protein Data Bank (acarbose complex: 1UKQ, 1-deoxynojirimycin complex: 1I75). The refinement statistics are summarized in Table 2.



## Results

### *Crystal Structure*

The crystals of CGTase complexed with acarbose and 1-deoxynojirimycin are isomorphous with that of native CGTase belonging to the triclinic space group *P*1 and the asymmetric unit contains two independent CGTase molecules (molecules 1 and 2). In the acarbose-complexed structure, the electron density map showed that a pseudo-maltotetraose molecule derived from acarbose locates at subsites from -2 to +2 of the catalytic active site (Figure 6) in the two independent molecules. An acarbose is composed of an unsaturated cyclitol (A) at the non-reducing end, a 4,6-dideoxy-4-amino-D-glucose (B), and two D-glucose residues (C, D) in that order. The pseudo-maltotetraose molecules described here consist of A - B - C and one glucose residue (G) at the non-reducing end (G - A - B - C). As a result, its N-glycosidic bond locates at between subsites -1 and +1. The processing mechanism is unclear but this conversion has been confirmed elsewhere (M. Qian *et al.* 1994; R. Mosi *et al.* 1998; K. Haga *et al.* 2004). In 1-deoxynojirimycin-complexed structure, two 1-deoxynojirimycin molecules are located at the active center of domain A and the maltose binding site 1 (MBS1) of domain E (Figure 7). In both complexed CGTase, the backbone structures are almost identical to that of native one (K. Harata *et al.* 1996).

### *Interaction of the pseudo-maltotetraose derived from acarbose with CGTase*

The pseudo-maltotetraose is bound to subsites from -2 to +2 by many hydrogen bonds with the amino acid residues (Trp101, His140, Tyr195, Glu257, Phe259, Asp328, Asp371, and Arg375) and water molecules in the two independent molecules and the pyranose ring of the glycosyl residue at subsite +2 in molecule 1 is parallel within about 4 Å distance to the aromatic ring of Phe259 and that in molecule 2 is sandwiched by the aromatic rings of Phe183 and Phe259 (Figure 6). These indicate that Phe259 and/or Phe183 make stack interaction with the glucosyl residues at subsite +2. Moreover, the pyranose ring of the cyclitol residue at subsite -1 is parallel within about 4 Å distance to the aromatic ring of Tyr100.

### *Interaction of CGTase with 1-deoxynojirimycin*

1-Deoxynojirimycin is located near the subsite –1 in the active site cleft and bound by hydrogen bonds with the catalytic residues Asp229, Glu257 or Asp328 in the two independent molecules (Figure 7). In sugar complexes of CGTase, the pyranose ring of a cyclitol residue located at subsite –1 is in stacking interaction with the aromatic ring of Tyr100, as observed in the crystal structure of CGTase complexed with acarbose (Figures 6 and 8). In contrast, since the pyranose ring of 1-deoxynojirimycin in both molecules 1 and 2 is not parallel but is rather perpendicular to the aromatic side chain of Tyr100, such stack interaction is not formed between the 1-deoxynojirimycin and Tyr100 (Figures 7 and 8).

The 1-deoxynojirimycin molecules located at MBS1 form hydrogen bonds with the side chain of Asn667. In molecule 1, the pyranose ring of 1-deoxynojirimycin is nearly parallel to the indole moiety of Trp662 while 1-deoxynojirimycin in molecule 2 is faced to the indole moiety of Trp616.

## Discussion

### *Inhibition of acarbose for CGTase*

As the result of the crystallographic analysis, in crystal, the acarbose (A-B-C-D) was processed to the pseudo-maltotetraose (G-A-B-C). The processing mechanism is unclear but this conversion has been confirmed by crystallographic and biochemical analyses (R. Mosi *et al.* 1998; I. Przytylski *et al.* 2000; K. Haga *et al.* 2004). Its N-glycosidic bond locates between subsites -1 and +1 and blocks the catalytic reaction (Figure 6). Moreover, since the pseudo-maltotetraose is bound to the subsites -2 to +2 by hydrogen bonds and stack interaction (Figure 6), the inhibition for CGTase reaction by acarbose would result from not only the block of cleavage reaction for the glycoside bond by the replacement of oxygen atom in it with nitrogen atom but also strong interaction of the pseudo-maltotetraose with the subsites.

### *Importance of interaction of Phe183/259 in substrate binding*

In the acarbose-complexed structure, Phe183 and/or Phe259 conserved specifically in CGTase make stack interaction with the glucosyl residue at subsite +2 (Figure 6). In molecule 2, Phe259 partly makes stack interaction with that at subsite +1 (Figure 6). These indicate that these amino acid residues are involved in guiding the glucosyl residue at the non-reducing terminal of sugar chain to the acceptor-binding site (subsites +1 and +2) in cyclization (Figure 9). This suggestion is supported by the biochemical analyses of the mutant CGTases in which phenylalanines are replaced with leucines (F183L and F259L) (A. Nakamura *et al.* 1994). Nakamura *et al.* reported that the replacement of Phe183 or Phe259 with leucine induced low activities of starch degradation and  $\beta$ -cyclodextrin formation and increased  $K_m$  values for linear substrates as acceptors (A. Nakamura *et al.* 1994). Furthermore, biochemical analysis of the mutant CGTase replaced Phe183/259 with leucines (F183L/F259L) indicated that Phe183 and Phe259 are cooperatively involved in acceptor binding and play a critical role in cyclization.

### *Inhibition of 1-deoxynojirimycin for CGTase*

In the enzyme reaction, Glu257 plays to donate/accept a proton, Asp229 is a nucleophilic catalyst and Asp328 stabilizes the intermediate state (A. Nakamura *et al.* 1992; J.C.M. Uitdehaag *et al.* 1999b). Direct or indirect binding of 1-deoxynojirimycin to Asp229, Glu257 and Asp328 would achieve the inhibition of 1-deoxynojirimycin for CGTase reaction. However, the number of hydrogen bonds of 1-deoxynojirimycin in the CGTase complex is fewer one third or half than that in glucoamylase complex (E.M.S. Harris *et al.* 1993) and, in spite of the presence of multiple subsites as shown in the acarbose-complexed structure, only one molecule of 1-deoxynojirimycin bound to the active center near subsite -1. These suggest the weak inhibition of 1-deoxynojirimycin for CGTase.

#### *Binding property of subsite -1 to glucosyl residue*

The active site cleft of CGTase has multiple subsite structure for sugar binding, however, 1-deoxynojirimycin is only bound near subsite -1. As observed in the acarbose-complexed structure, the cyclitol residue strongly binds subsite -1 by many hydrogen bonds with Trp101, Asp227, Asp229, His327, Asp328 and stack interaction with Tyr100. Since the stable binding of the glucosyl residue to the subsite -1 is essential for the reaction process, the subsite -1 is expected to have higher affinity to a glucosyl residue than the other subsites. This may be the reason for it why 1-deoxynojirimycin, pseudo-glucose, binds to only the subsite -1.

As shown in the acarbose-complexed structure and elsewhere (R. Mosi *et al.* 1998; J.C.M. Uitdehaag *et al.* 1999a; J.C.M. Uitdehaag *et al.* 1999b), the cyclitol residue located at the subsite -1 is in the stacking interaction with the aromatic ring of the Tyr100. This is a common structure in the recognition and binding of substrate, but in the present structure, 1-deoxynojirimycin at subsite -1 has no such stacking interaction (Figures 7 and 8). The present structure suggests two reasons for it. The first is that the active site cleft stably binds the substrate only if the substrate is an oligo-saccharide. In other words, each binding between subsite and glucosyl residue is weak and the stacking interaction of the glucosyl residue is supported by hydrogen bonds and stacking interaction of the neighboring glucosyl residues. The

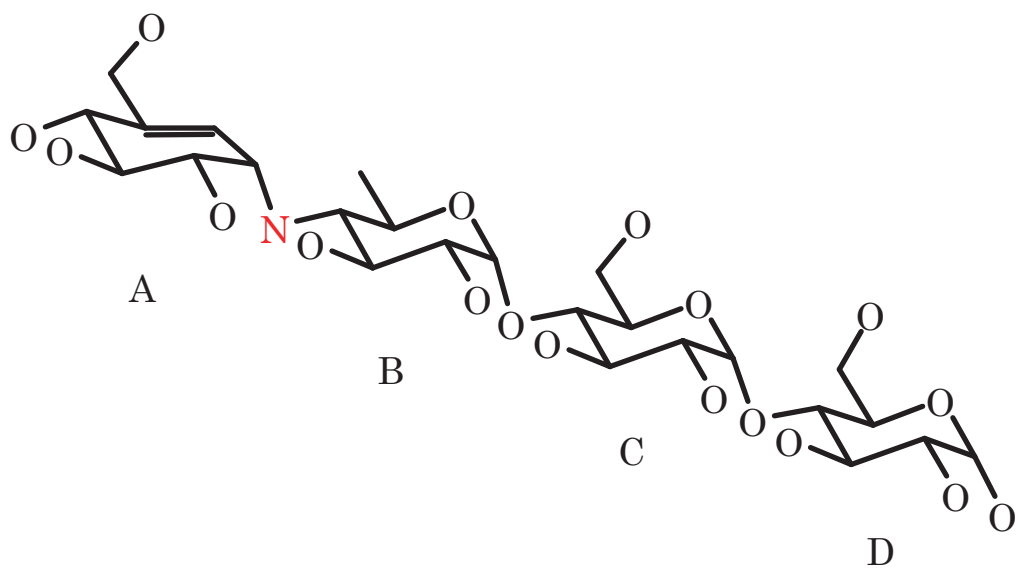
second reason is that the interaction of 1-deoxynojirimycin differs from the glucosyl residue since the charge distribution in the pyranose ring is different from that of native substrate because of the replacement of O5 with N5 (Figure 5). Therefore, this may prevent 1-deoxynojirimycin from the formation of stacking contact with Tyr100.

**Table 2. Summaries of data collection and refinement statistics of alkalophilic *Bacillus* sp.1011 CGTase complexed with 1-deoxynojirimycin or acarbose.**

<i>Data collection</i>	(1-Deoxynojirimycin complex)	(Acarbose complex)
Space group	P1	P1
Cell dimensions (a,b,c, $\alpha,\beta,\gamma$ )	64.78, 74.24, 79.03 Å, 85.03, 104.88, 101.02°	64.94, 74.49, 79.10 Å 85.13, 105.02, 101.02°
Resolution range	27.89-1.84 Å	48.56-2.00 Å
No. of unique reflections	106,410	91,157
Completeness	81.5%	96.0%
$R_{\text{merge}}$	7.6%	13.2%
<i>Structure refinement</i>		
Resolution range	10.0-2.0 Å	10.0-2.0 Å
No. of unique reflections used	86,468 ( $F > 2\sigma$ )	82,018 ( $F > 1\sigma$ )
Completeness	96.3%	87.0%
Final $R$ value	0.154	0.184
Final $R_{\text{free}}$ value for 6% data	0.214	0.246
Root mean square deviation from ideality		
bond length	0.013 Å	0.015 Å
bond angle	2.70°	2.91°

**Figure 5. Structures of acarbose (A) and 1-deoxynojirimycin (B).** The glycosyl residues of acarbose are referred to A, B, C, and D in order from the non-reducing end. N-glycosidic bond not cleavaged by sugar catalyzing enzymes locates between A and B.

(A)



(B)

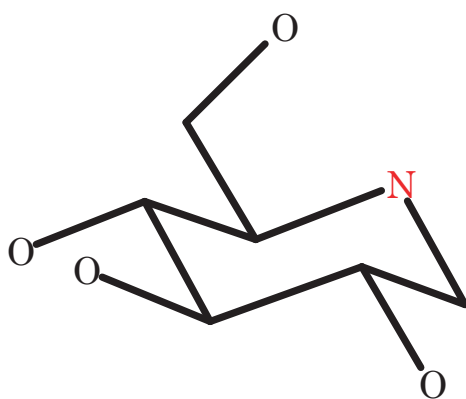
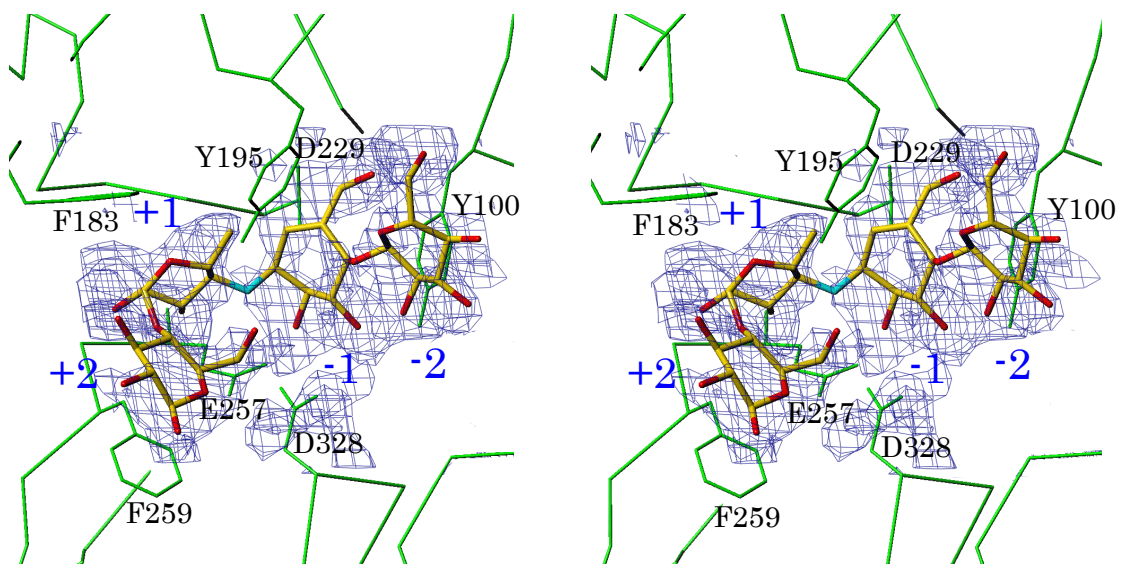
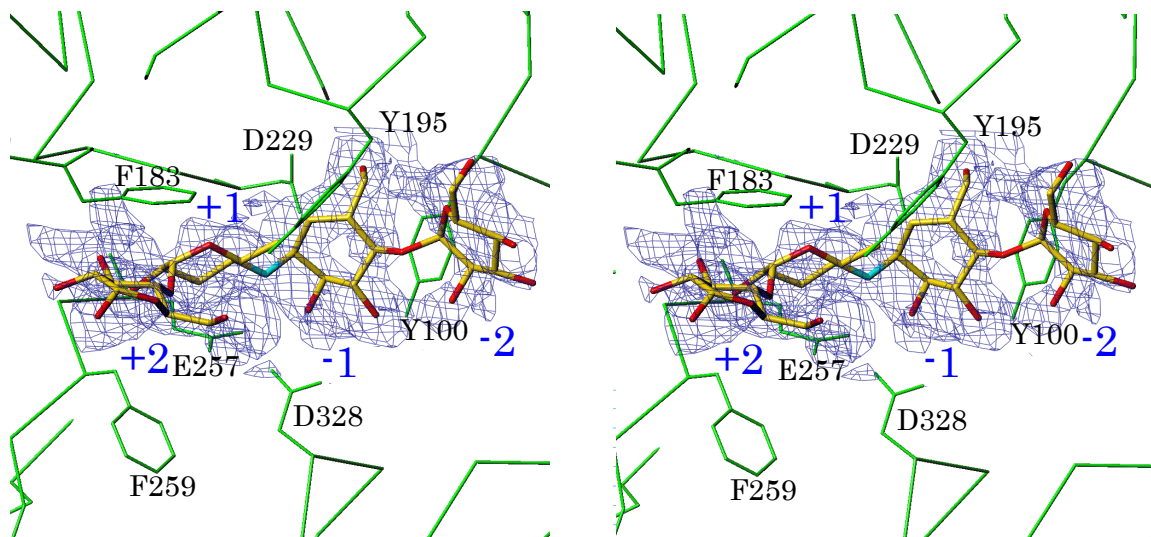




**Figure 6. Steroview of the pseudo-maltotetraose and the catalytic active site in two independent molecules 1 (A) and 2 (B) of CGTase complexed with acarbose.** CGTases and the pseudo-maltotetraose molecules are represented by thin and thick lines, respectively. Omit  $|3F_o - 2F_c|$  electron density maps are contoured at  $1\sigma$  level.



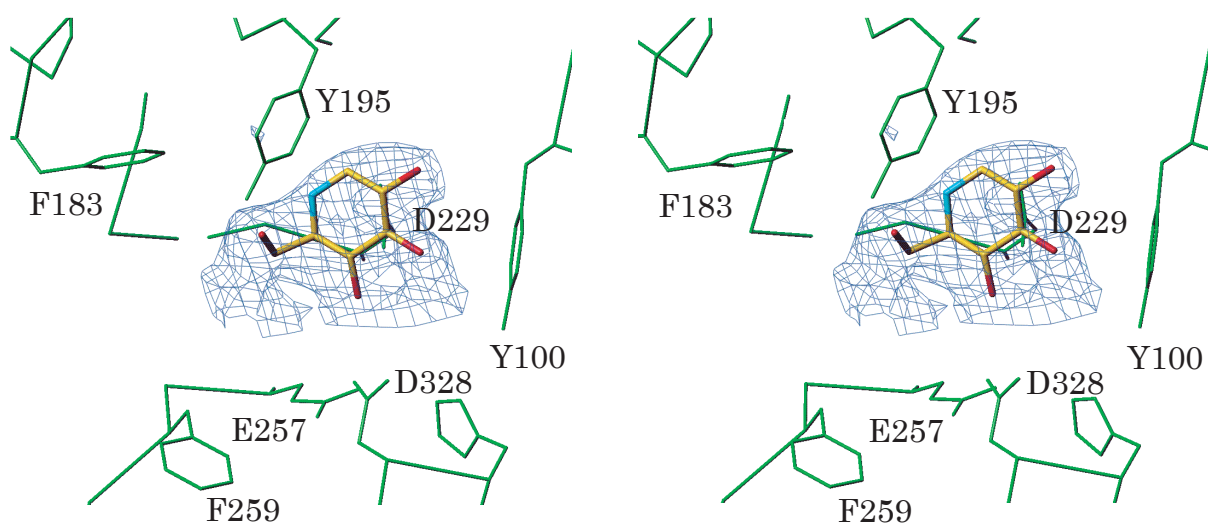
(A)



(B)

**Figure 7. Steroview of the 1-deoxynojirimycin and the catalytic active site in two independent molecules 1 (A) and 2 (B) of CGTase complexed with 1-deoxynojirimycin.** CGTase and the 1-deoxynojirimycin molecules are represented by thin and thick lines, respectively. Omit  $|3F_o - 2F_c|$  electron density maps are contoured at  $1\sigma$  level.

(A)



(B)

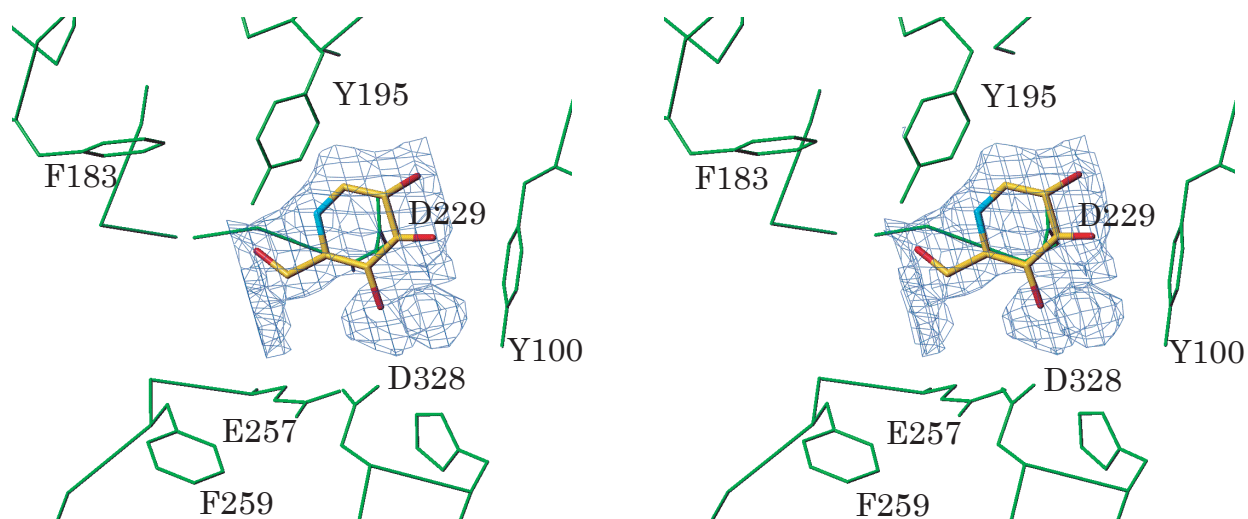


**Figure 8. Positional relationship of the cyclitol residue and Tyr100 at subsite -1.** The pyranose ring of the cyclitol residue (thin green line) at subsite -1 is parallel to the aromatic ring of Tyr100 (thick line). In contrast, the pyranose ring of 1-deoxynojirimycin (thick magenta line) is not parallel and is rather perpendicular to it.

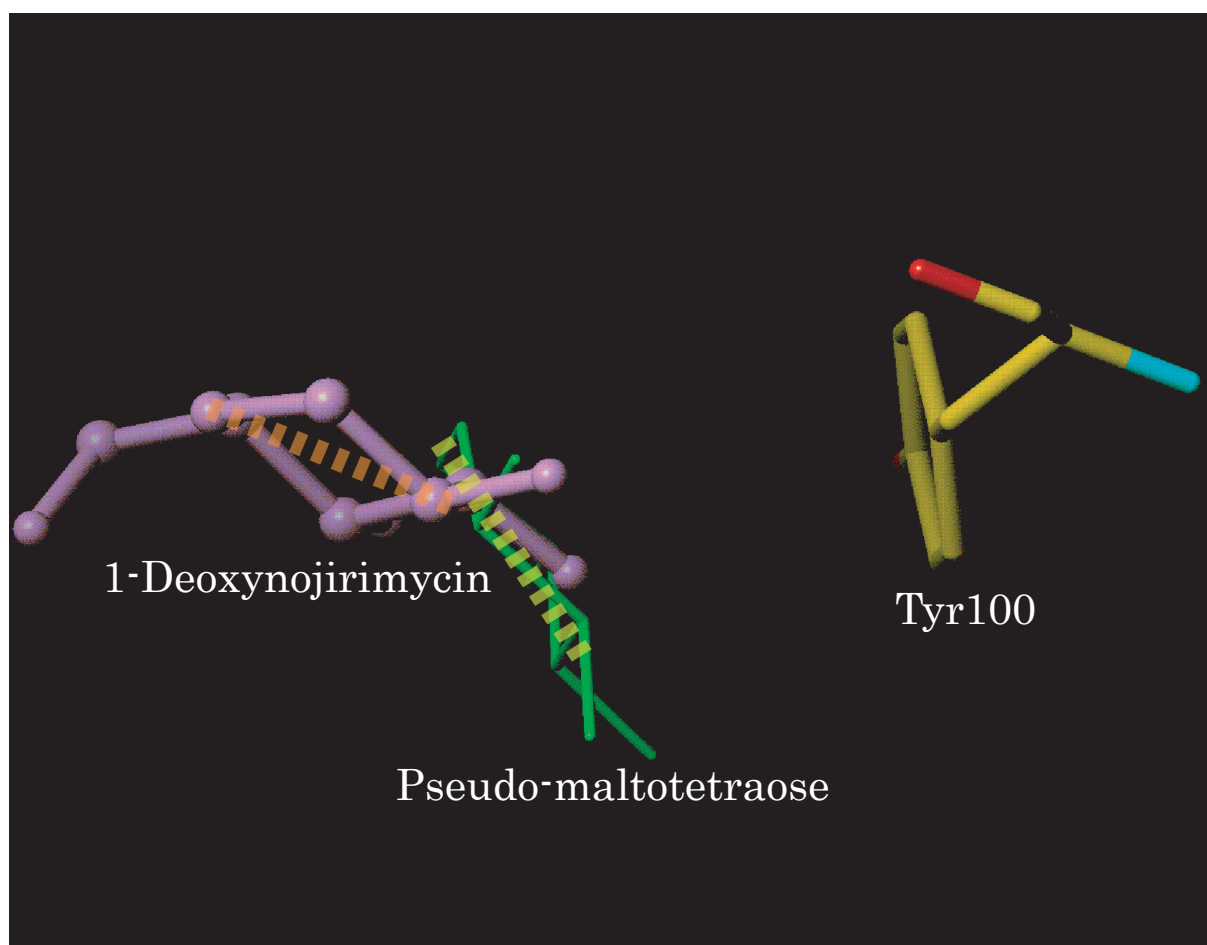
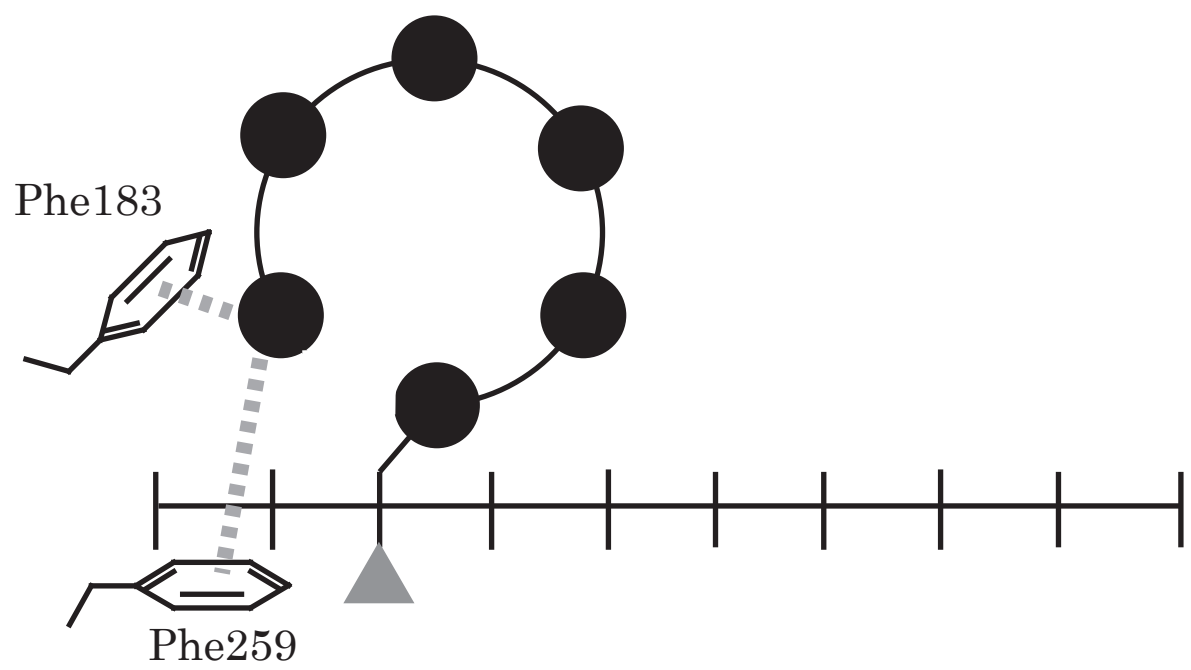


**Figure 9. Diagram of interaction of Phe183/259 with glucosyl residue at the non-reducing terminal side for cyclization.** Phe183/259 would guide the glucosyl residue at the non-reducing side to acceptor-binding site (subsites +1 and +2).





## Section II

Crystal Structures of the Native and Acarbose-Complexed forms of Cyclodextrin Glycosyl-transferase in which Phe283 is replaced with leucine: Role of Phe283 in Enzymatic Reaction.

## Abstract

Cyclodextrin glycosyltransferase (CGTase) belonging to the  $\alpha$ -amylase family mainly catalyzes transglycosylation and produces cyclodextrins from starch and related  $\alpha$ -1,4-glucans. The catalytic site of CGTase specifically conserves four aromatic residues, Phe183, Tyr195, Phe259, and Phe283, which are not found in  $\alpha$ -amylase. To elucidate the structural role of Phe283, we determined the crystal structures of native and acarbose-complexed mutant CGTases in which Phe283 was replaced with leucine (F283L) or tyrosine (F283Y). The temperature factors of the region 259 - 269 in native F283L increased more than 10 Å<sup>2</sup> compared with that in the wild type. The complex formation with acarbose not only increased the temperature factors (> 10 Å<sup>2</sup>) but also changed the structure of the region 257 - 267. This region is stabilized by interactions of Phe283 with Phe259 and Leu260 and plays an important role in the cyclodextrin binding. The conformation of the side chains of Glu257, Phe259, His327 and Asp328 in the catalytic site was altered by the mutation of Phe283 with leucine and this suggests that Phe283 partly arranges the structure of the catalytic site through contacts with Glu257 and Phe259. The replacement of Phe283 with tyrosine decreased the enzymatic activity in the basic pH range. The hydroxyl group of Tyr283 forms hydrogen bonds with the carboxyl group of Glu257 and the p*K*<sub>a</sub> of Glu257 in F283Y may be lower than that in the wild type.

## Introduction

Cyclodextrin glycosyltransferase (CGTase, EC 2.4.1.19), which belongs to the  $\alpha$ -amylase family [glycosyl hydrolase family 13 (B. Henrissat *et al.* 1997)], catalyzes the conversion of starch and related  $\alpha$ -1,4-glucans to cyclodextrins. The enzyme also catalyzes a coupling reaction and a disproportionation reaction through intermolecular transglycosylation, but its hydrolyzing activity is weak. Most CGTases from bacteria (*Bacillus macerans*, *B. stearothermophilus*, *B. circulans*, etc) show a bell-shaped pH profile (pH 5.5 - 7.5) (S. Kobayashi *et al.* 1978; M. Tanaka *et al.* 1991; L. Nitschke *et al.* 1990) and some CGTases from alkalophilic bacteria (*Bacillus* sp.1011, *B. ohbensis*, *Bacillus* sp.37-2) can function over a wide pH range (pH 4.5 - 10) (A. Nakamura *et al.* 1993; K.A. Sin *et al.* 1991; T. Kaneko *et al.* 1990). The mechanism of the alkalophilic catalysis is not clearly understood, but the  $pK_a$  value of the proton donor/acceptor residue in alkalophilic CGTase must be higher than that in other CGTases.

The cyclization reaction that is not observed in  $\alpha$ -amylase is the most attractive property of CGTase. The key to the cyclization reaction is how the non-reducing end of the donor molecule instead of the other sugar and water molecules is transferred at subsites +1 and +2 of the acceptor-binding site in CGTase. Nakamura *et al.* (1994) have reported the biochemical analysis of the four mutant CGTases in which the specifically conserved aromatic amino acid residues (Phe183, Tyr195, Phe259, and Phe283) of the catalytic active site (Figure 10) are replaced with leucine. Stochastic reaction path calculations of the process to form  $\gamma$ -CD from malto-octaose showed that Phe183 transports the non-reducing end of a donor molecule to subsite +1 at the acceptor binding site through the stacking interaction between the aromatic ring of phenylalanine and the pyranose ring of the sugar molecule and Tyr195 cooperatively acts with Phe183 as a hydrophobic center to guide linear substrates to the acceptor-binding site where they are cyclized compactly (J.C.M. Uitdehaag *et al.* 2001). Phe259 plays an important role in binding the substrate, especially an acceptor residue, to cooperatively cyclize it on Phe183 (A. Nakamura *et al.* 1994; A.K. Schmidt *et al.* 1998; J.C.M. Uitdehaag *et al.* 2001). Furthermore, Nakamura *et al.* (1994) have shown that the  $K_m$  values of F283L CGTase for some linear substrates are similar

to those of the wild type enzyme whereas those for CDs are higher. However, the relationship between the enzymatic property and the structural change caused by the mutation of Phe283 has remained unknown in spite of the significance of this residue that is specifically conserved in CGTase.

Here, we discuss the structural role of Phe283 on substrate binding and the catalytic reaction based on four crystal structures of mutant CGTases replaced with leucine (F283L) or tyrosine (F283Y) and their complexes with acarbose (F283L\_ACA and F283Y\_ACA), which is a powerful inhibitor for most glucoside hydrolases.

## Materials and methods.

### *Chemicals and enzymes*

All restriction and modification enzymes used for recombinant DNA manipulations were purchased from Takara Shuzo Co., Ltd., or Toyobo Co., Ltd. Tetracycline and ampicillin were from Wako Pure Chemical Industry Ltd. Soluble starch was from E. Merck. Acarbose was a gift from Drs. A. Mullen and K. Hornberg (Bayer AG). All other chemicals were of reagent grade.

### *Bacterial strains and plasmids*

Recombinant DNA was manipulated in *Escherichia coli* JM109 [*recA1 endA1 gyrA96 thi hsdR17 supE44 relA1 Δ(lac proAB)* / F<sup>+</sup>: *traD36 proAB lacF* ZAM15]. Mutant CGTases were produced in the protease-deficient mutant *E. coli* ME8417 [*lon*::Tn10(*tet*<sup>r</sup>) *thr leu lacY*], provided by Dr. H. Takahashi (University of Tokyo). Plasmid pTUE254 contains the CGTase gene region of an alkalophilic *Bacillus* sp.1011 (K. Kimura *et al.* 1987).

### *Construction of mutant CGTase genes*

The F283L mutant CGTase gene was constructed as described (A. Nakamura *et al.* 1994). The F283Y mutant CGTase gene was prepared in the same manner as that of F283L (A. Nakamura *et al.* 1994). The oligonucleotide, 5'-GCTCGATTACCGCTTTG-3', was used in site-directed mutation of the F283Y mutant CGTase gene.

### *Expression and purification of mutant CGTases*

Mutant CGTases were expressed and purified as described (A. Nakamura *et al.* 1992; K. Haga *et al.* 1994). ME8417 containing the plasmid pTUE254 encoding mutant CGTase was incubated in Luria-Bertani medium containing ampicillin (50 µg/ml) and tetracycline (20 µg/ml) for 14 hours at 37 °C. Target proteins were abstracted by osmotic shock (S.J. Chan *et al.* 1981). The supernatant obtained after ammonium sulfate (28%) precipitation was loaded onto TOYOPEARL HW55-F and then the target proteins were eluted with 10 mM sodium phosphate

buffer (pH 6.0). The proteins were desalted over a Bio-Gel column (BioRad) and concentrated to 25 mg/ml using an Amicon concentration kit. The proteins were over 99% pure according to SDS-PAGE.

#### *Enzyme assay*

All reactions proceeded at 37 °C in Britton-Robinson buffer (50 mM phosphoric, acetic and boric acids and adjusted to suitable pH by NaOH) with various pH values. Starch degrading activity was measured by the blue value method with slight modification (A. Nakamura *et al.* 1993). The enzyme digest was composed of 600 µl of 0.5%(w/w) soluble starch and 300 µl of enzyme (finally about 3-5 U/ml). The reaction mixture was incubated for 5, 10, and 15 minutes. The reaction was halted and starch was colored by adding stop solution (0.17 mM I<sub>2</sub>, 1.7 mM KI, 1.7 mM HCl). One unit of starch degrading activity was defined as the amount that generated a 1 % decrease per minute of absorbance at 660 nm.

Disproportionation activity between 3KB-G5CNP as a donor and glucose as an acceptor in various pH conditions (5.0 – 9.0) were determined as described (A. Nakamura *et al.* 1994) and the kinetic parameters  $k_{cat}$  and  $K_m$  were determined by the nonlinear least squares methods with Taylor expansion (M. Sakoda *et al.* 1976).

#### *Crystallization of F283L and F283Y and their acarbose complexes*

All crystals were prepared according to Haga *et al.* (1994) and the acarbose complexes were obtained by co-crystallization with acarbose. Crystallization was performed by hanging drop vapor diffusion using 2.5% protein solution and a reservoir solution containing 20% (w/v) PEG3000, 20% (v/v) 2-propanol, 100 mM sodium citrate, 1 mM calcium chloride, and additive 1 mM acarbose for the co-crystallization. Rod-like crystals of  $1.0 \times 0.3 \times 0.2$  mm were grown within two weeks at room temperature.

#### *Data collection*

X-ray diffraction data of F283L crystals were collected to 1.8 Å resolution at 286K using an Enraf-Nonius FAST diffractometer (40 kV, 50 mA) at three goniometer settings as described (K. Harata *et al.* 1996). X-ray diffraction data of the crystals of F283Y, F283L\_ACA, and F283Y\_ACA were collected at 290K using a Bruker SMART 6000 diffractometer (50 kV, 90 mA). The  $R_{\text{merge}}(I)$  values for these data were below 11%. Table 3 summarizes the statistics of data collection.

### *Structure determination and refinement*

All the four structures were determined by molecular replacement using the coordinates of the wild type structure (K. Harata *et al.* 1996) and refined by using the program *X-PLOR* (A.T. Brünger *et al.* 1987). In the starting model, the residue 283 was glycine, which was replaced with leucine or tyrosine after  $|3F_o - 2F_c|$  electron density maps ( $> 1 \sigma$ ) confirmed their shape. The pseudo-tetraose molecules derived from acarbose were introduced in the structures of F283L\_ACA and F283Y\_ACA by reference to their  $|3F_o - 2F_c|$  and  $|F_o - F_c|$  electron density maps ( $> 1.5 \sigma$ ). Water molecules were introduced in the structures as the same manner as previously described (K. Harata *et al.* 1996). The stereo-chemical qualities of these structures were confirmed by the program PROCHECK (A.R. Laskowski *et al.* 1993). The program TURBO-FRODO examined the graphics and drew the structures. The results are summarized in Table 3. Atomic coordinates have been deposited with Protein Data Bank (F283L: 1V3J, F283Y: 1V3K, F283L\_ACA: 1V3L, F283Y\_ACA: 1V3M).

## Results

### *Enzyme assays of F283L and F283Y mutants*

Nakamura *et al.* (1994) have reported that F283L CGTase has about half of the starch degrading activity of the wild type within a neutral pH range (Figure 11A). The activity was considerably decreased at both acidic and basic pH ranges (Figure 11B). In contrast, the starch degrading activity of F283Y CGTase was similar to that of the wild type between the acidic and neutral pH ranges but decreased to 10% at pH 10.0. The pH value of half activity at basic pH side was shifted to 8.6 from 10.0 of the wild type (Figure 11B).

Replacement of Phe283 with leucine resulted in 23-67% decreases in the  $K_m$  values for 3-ketobutylidene- $\beta$ -2-chloro-4-nitrophenylmalto-pentaoside (3KB-G5CNP), which is a maltopentaose with its non-reducing end blocked and with aglycon at its reducing end, in the disproportionation reaction, and no significant correlation to pH was detected. On the other hand, the  $k_{cat}$  values for the disproportionation reaction at various pH conditions decreased to 1.6-4.4% compared with those of the wild type.

### *Crystal structures of two mutants, F283L and F283Y, and their acarbose complexes (F283L\_ACA and F283Y\_ACA)*

The crystallographic properties of these mutant enzymes (Table 3) are almost identical to those of the wild type CGTase (K. Harata *et al.* 1996; K. Haga *et al.* 2004) and the asymmetric unit contains two independent molecules (MOL1, MOL2). F283L\_ACA and F283Y\_ACA bind a pseudo-tetraose derived from acarbose at subsites from -2 to +2 in the active site pocket (Figures 12 and 13). Acarbose is composed of an unsaturated cyclitol (A) at the non-reducing end, a 4,6-dideoxy-4-amino-D-glucose (B), and two D-glucose residues (C, D) in that order. However, it was converted to a pseudo-tetraose consisting of A-B-C and one glucose residue (G) at the non-reducing end (G-A-B-C). This conversion has been also confirmed in other CGTase complexes (R. Mosi *et al.* 1998; K. Haga *et al.* 2004).



### *Structural change in the catalytic active site of F283L*

The backbone structure of F283L is almost identical to the wild type CGTase. However, the isotropic temperature factors of C $\alpha$  atoms of the residues 259-269 of F283L, that construct subsites +1 to +3 (B.A. van der Veen *et al.* 2001; K. Haga *et al.* 2004), increased by more than 10 Å<sup>2</sup> (Figure 14A). Therefore, the structure of this region is more flexible in F283L than in the wild type.

In F283L, the phenyl group of Phe259 is moved towards the carboxyl group of Glu257, the proton donor/acceptor group, for about 1 Å with a +30° change in the  $\chi^1$  angle of Phe259 (Figure 15A). The side chain of Glu257 is also shifted by about 0.5 Å towards Leu283. This indicates that Phe283 sterically regulates the conformation of Glu257 because the C $\zeta$  atom of Phe283 is within 4.0 Å to the carboxyl group of Glu257 and the replacement of Phe283 with leucine creates a space into which the side chain of Glu257 can move. The side chains of Asp328 and His327 are moved by about 0.4 Å, but they still form hydrogen bonds with the carboxyl group of Glu257 as observed in the wild type (Figure 15A).

### *Structural change in the catalytic active site of F283L\_ACA*

When wild type CGTase forms the complex with acarbose (R. Mosi *et al.* 1998; K. Haga *et al.* 2004), the structural change was minimal compared with the native enzyme. In contrast, several significant changes were found between native F283L and its complex. The isotropic temperature factors of the regions 257-278 and 310-317 of F283L are increased more than 10 Å<sup>2</sup> by the complex formation with acarbose (Figure 14B). In addition, region 257-267 undergoes the remarkable structural changes as shown by the positional difference ( $> 0.5$  Å) of the equivalent C $\alpha$  atoms between F283L and F283L\_ACA (Figure 14C). Therefore, these regions in F283L are more flexible in the complexed state than those in the native state. Furthermore, since the regions 269-280 and 314-320 are connected to each other by four and five hydrogen bonds in MOL1 and MOL2, respectively, and these hydrogen bonds are conserved in the native and acarbose-complexed structures of F283L and wild type, the structure of these regions may alter

cooperatively through hydrogen bonding interactions in between the native and complexed states. The electron density of the aromatic ring of Phe259 in F283L\_ACA is much weaker than that observed in F283L. This indicates the high flexibility of the side chain of Phe259. Contacts between the glucose residue and Phe259 may be flexible but not weak because the  $K_m$  for 3KB-G5CNP in the disproportionation is rather decreased in F283L compared with the wild type enzyme.

The C $\alpha$  atoms of Phe259 are shifted by 1.3 Å (MOL 1) and 1.7 Å (MOL 2) towards substrates (Figure 15B) compared with the wild type complexed with acarbose (K. Haga *et al.* 2004). Glu257 is shifted 1.5 Å towards Leu283 in MOL1 and 0.89 Å in MOL2, but the carboxyl group of Glu257 forms a hydrogen bond with the carboxyl group of Asp328 as observed in the wild type (Figure 15B). The carboxyl group of Asp229 is shifted toward the bottom of the active cleft by 0.9 Å in MOL1 and 0.6 Å in MOL2 (Figure 12).

#### *Binding of pseudo-tetraose derived from acarbose in F283L\_ACA*

The torsion angles of the cleavage sites [ $\phi$ : C7(A)-C1(A)-N4(B)-C4(B) and  $\psi$ : C1(A)-N4(B)-C4(B)-C5(B)] of the pseudo-tetraose molecule of F283L\_ACA differ from those of acarbose complexed with the wild type [ $\Delta\phi$  = -37° (MOL1), -23° (MOL2) and  $\Delta\psi$  = 26° (MOL1), -48° (MOL2)] (Figure 12). The torsion angles of the glycosidic linkage that connects sugar residues at subsites +1 and +2 in MOL2 were also changed by -17°( $\Delta\phi$ ) and 58°( $\Delta\psi$ ). In MOL2 of F283L\_ACA, Phe259 was shifted 1.6 Å toward the 4-amino-4,6-dideoxyglucose (GLD) residue at subsite +1 from its position in the wild type complex. This movement of Phe259 disrupted the hydrogen bonds between GLD and Glu257, and Phe259 was in close contacts within 4 Å distance with the GLD residue at subsite +1 (Figure 15B).

The distance between the N4 atom of the pseudo-glycosidic bond and the carboxyl group of Glu257 was not significantly changed by the mutation of F283L while the distance between the C1 atom of the cyclitol residue at subsite -1 and the carboxyl group of Asp229 was changed more than 0.3 Å (MOL1) and 0.1 Å (MOL2) (Figure 12). This indicates that the efficiency of

nucleophilic attack by Asp229 is decreased in F283L.

As observed in the wild type complex (R. Mosi *et al.* 1998; K. Haga *et al.* 2004), the unsaturated cyclitol ring of the sugar residue in F283L\_ACA is parallel to the aromatic ring of Tyr100, and the pyranose ring located at the subsite +2 is also parallel to the aromatic ring of Phe259 or Phe183 (Figure 12). As a result, their intermolecular contacts are mostly conserved. This may be the reason for the relatively low  $K_m$  values of F283L for linear substrates (A. Nakamura *et al.* 1994).

#### *Structural change in the catalytic active site of F283Y and F283Y\_ACA*

The hydroxyl group of Tyr283 in F283Y forms de novo hydrogen bonds with the carboxyl groups of Glu257 (2.6 Å in MOL1 and MOL2) and the side chain of Asn326 (2.9 Å in MOL1 and 3.1 Å in MOL2) (Figure 15C). Compared with the wild type (K. Harata *et al.* 1996), the  $\chi^2$  angle of Glu257 in F283Y was changed by 7.9° in MOL1 and 4.5° in MOL2 and the carboxyl oxygen atoms of Glu257 are shifted 0.3-0.4 Å although they still retained the hydrogen bonds with Asp328 and His327 (Figure 15C).

Compared with the wild type CGTase-acarbose complex (R. Mosi *et al.* 1998; K. Haga *et al.* 2004), the carboxyl oxygen atoms of Glu257 in F283Y\_ACA were shifted 0.3 - 0.8 Å by the rotation of  $\chi^2$  or  $\chi^3$  and formed hydrogen bonds with the hydroxyl group of Tyr283. The imidazolyl group of His327 forms a *de novo* hydrogen bond with the O2H hydroxyl group of the cyclitol residue with the distance of 2.7 Å in MOL1 and 2.6 Å in MOL2 (Figure 13). The other contacts between the protein and sugar molecules in F283Y\_ACA are mostly conserved in the wild type complexed with acarbose. These findings indicate that the change in pseudo-tetraose binding was caused by structural changes of Glu257, Phe259, His327, and Asp328 induced by the mutation.

## Discussion

### *Phe283 represses the flexibility of region 259-269 neighboring the catalytic site*

The crystal structure of F283L revealed the increased flexibility of the region 259-269, which constructs subsite +2 and +3 (Figure 14). In the wild type, the aromatic ring of Phe283 is situated about 3.3 Å far from the H $\alpha$ -C $\alpha$  of Phe259 and perpendicular to the aromatic ring of Phe323 with the H $\zeta$  atom of Phe323 2.8 Å away (Figure 16A) (K. Harata *et al.* 1996). This geometry indicates that the aromatic ring of Phe283 is in the CH- $\pi$  interaction with Phe259 and Phe323. In F283L, the replacement of Phe283 with leucine breaks the CH- $\pi$  interaction and the side chain of Leu283 causes steric hindrance with the phenyl groups of Phe259 and Phe323 (Figure 16A). This is supported by the fact that such changes are not evident in the structure of F283Y (Figure 15C). In addition, the C $\beta$ , C $\gamma$  and C $\delta$ 1 atoms of Phe283 are 4.0 Å far from Leu260 (Figures 15B and 16A), indicating that Phe283 suppresses the structural flexibility of Leu260 through close contact. Except for such interactions, the region 259-269 that is exposed to solvent has few interactions. Therefore, the increased flexibility of this region may result from the disruption of the CH- $\pi$  interaction of Phe283 with Phe259 and close contacts with Leu260.

### *Phe283 maintains the structure of the catalytic site*

We compared the conformational changes of residues Phe259, Glu257, His327, and Asp328 of the native and acarbose-complex of F283L with the wild type (K. Harata *et al.* 1996; K. Haga *et al.* 2004) (Figure 15A and B). The replacement of Phe283 by leucine induces movement of the side chain of Glu257 by disrupting the close contact of the carboxyl group with the phenyl group. This conformational change of Glu257 is associated with movement of the side chains of Asp328 and His327 to retain hydrogen bonds with the carboxyl group of Glu257. Moreover, the conformation of the side chain of Phe259 alters to move toward the side chain of Glu257. These findings suggest that the phenyl group of residue 283 plays an important role in maintaining the structure of the “active” catalytic site by regulating the conformation of the side chains of Phe259 and Glu257 via CH- $\pi$  interaction and close contact, and indirectly arranges the structure of the

side chains of His327 and Asp328 (Figure 16B). Since the  $k_{\text{cat}}$  value of F283L CGTase for  $\beta$ -CD formation was about 40% of the wild type (A. Nakamura *et al.* 1994), these structural changes may slightly affect the catalytic reaction. In fact, the distance between the carboxyl group of Asp229 and the C1 atom of the cyclitol residue at subsite -1 in F283L\_ACA was increased by 0.3 and 0.1 Å in MOL1 and MOL2, respectively (Figure 12), and the efficiency of Asp229 as a nucleophile would be lower than that of the wild type enzyme.

*Phe283 may play important role in substrate binding by repressing the flexibility of region 259-269*

The  $K_m$  values of F283L for various linear substrates in coupling, disproportionation, and hydrolysis were similar to or less than those of the wild type, whereas the  $K_m$  values for  $\alpha$ -,  $\beta$ -, and  $\gamma$ -CD were increased 1.3 to 3.0-fold in cyclization, coupling, and hydrolysis (A. Nakamura *et al.* 1994). These results indicate that the region 259-269 involved in the binding of linear sugars has such flexibility that slightly affects the catalytic reaction but does not reduce binding affinity. However, the increased structural flexibility of Phe259 in F283L causes the increase of  $K_m$  values for  $\alpha$ ,  $\beta$ ,  $\gamma$ -CD. In fact, while the glucose residue at subsite +2 of maltononaose is sandwiched between Phe183 and Phe259 (J.C.M. Uitdehaag *et al.* 1999b), the glucose residue of  $\gamma$ -CD at subsite +2 is in the stack interaction with only Phe259 (J.C.M. Uitdehaag *et al.* 1999a). This indicates that Phe259 is more important for cyclodextrin binding than Phe183. Therefore, we suggest that Phe283 plays an important role in the binding of substrates, especially CD, by repressing the flexibility of the region 259-269 (Figure 16B).

*New hydrogen bond with the carboxyl group of Glu257 in F283Y may reduce enzymatic activity in the basic pH region*

F283Y CGTase is less active at the basic pH region than wild type CGTase in the starch degradation (Figure 11). The crystal structure of F283Y shows that a new hydrogen bond is formed between the hydroxyl group of Tyr283 and the carboxyl group of Glu257 (Figure 15C).

Therefore, pH profile of F283Y CGTase may be changed because the proton of the carboxyl group of Glu257 will be easily released by the hydrogen bond formation with the hydroxyl group of Tyr283, which decreased the  $pK_a$  value. Although the experimental  $pK_a$  value of Glu257 was not measurable, the present results indicate that the  $pK_a$  value of wild type Glu257 is relatively high to maintain its protonation state in the basic pH range.

**Table 3. Data processing and structure refinement of the residue 283 mutant CGTases**

<i>Data processing</i>		(F283L)	(F283Y)	(F283L_ACA)	(F283Y_ACA)
Cell axis	a (Å)	63.9	64.9	65.0	64.1
	b	73.7	74.4	73.7	73.6
	c	78.2	79.0	80.1	78.3
	$\alpha(^{\circ})$	85.1	85.2	85.5	84.9
	$\beta$	105.0	105.1	105.5	105.1
	$\gamma$	101.0	101.0	101.5	101.0
Resolution range(Å)		29.1-1.83	29.1-1.83	48.4-1.80	18.9-1.82
No. of unique reflections		102,927	92,133	83,161	103,110
$R_{\text{merge}}$		7.3%	10.1%	8.6%	9.5%
<i>Structure refinement</i>					
Resolution range(Å)		10.0-2.0	10.0-2.0	10.0-2.1	10.0-2.0
No. of unique Reflections ( $F > 2\sigma$ )		78,142	84,562	67,131	83,723
Completeness		86.2%	90.1%	82.8%	92.2%
Final $R$ factor		17.0%	15.5%	16.9%	16.3%
Final $R_{\text{free}}$ factor		24.2%	20.0%	23.2%	21.7%
RMSD					
Bond length(Å)		0.015	0.013	0.013	0.013
Bond angle( $^{\circ}$ )		2.94	2.64	2.90	2.76

**Figure 10. Four aromatic residues (Phe183, Tyr195, Phe259, and Phe283) conserved specifically in the catalytic active site of CGTase.** Phe183, Tyr195 and Phe259 are colored by cyan and Phe283 are represented by red line.  $\gamma$ -Cyclodextrin shown with green line is bound to the active site of *B. circulans* 251 CGTase (J.C.M. Uitdehaag *et al.* 1999a).



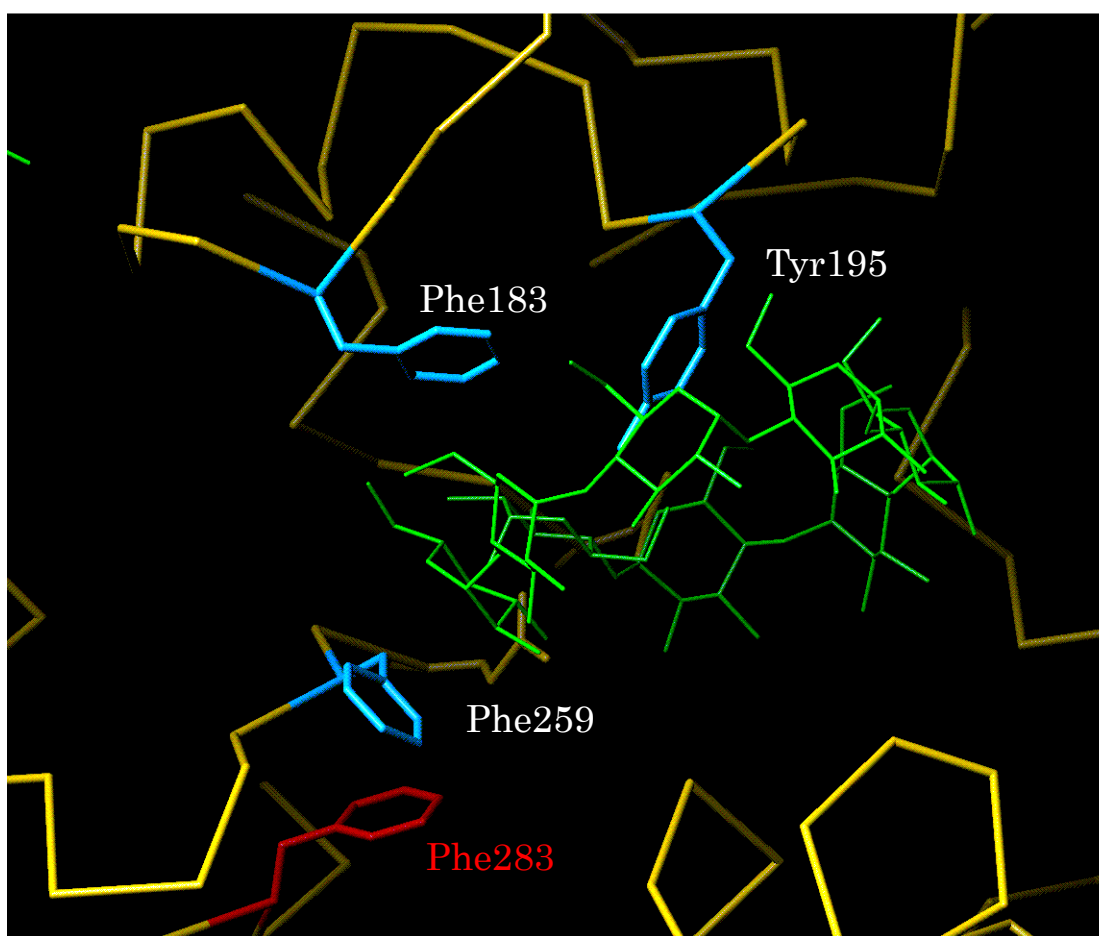
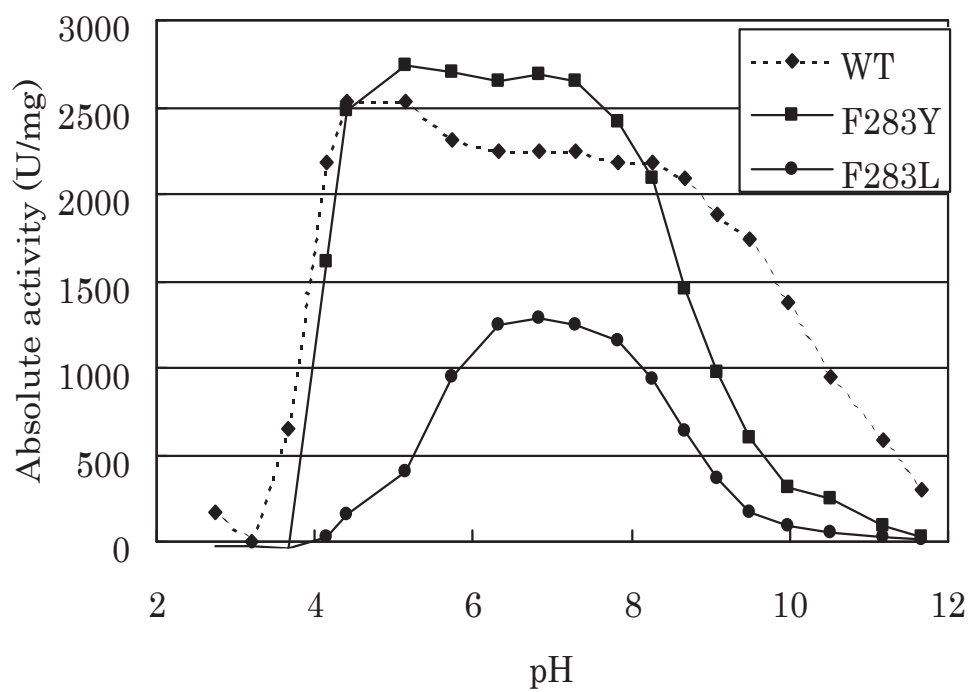


**Figure 11. Absolute (A) and relative (B) starch degrading activities. pH Profiles for F283L (●) (A. Nakamura *et al.* 1994), F283Y mutant (■), and wild type CGTase (◆).**

(A)



(B)

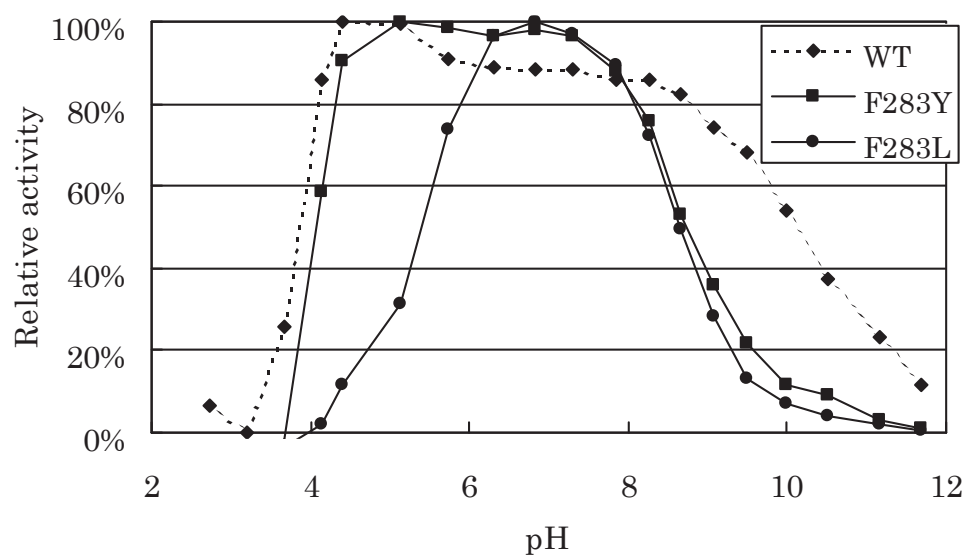
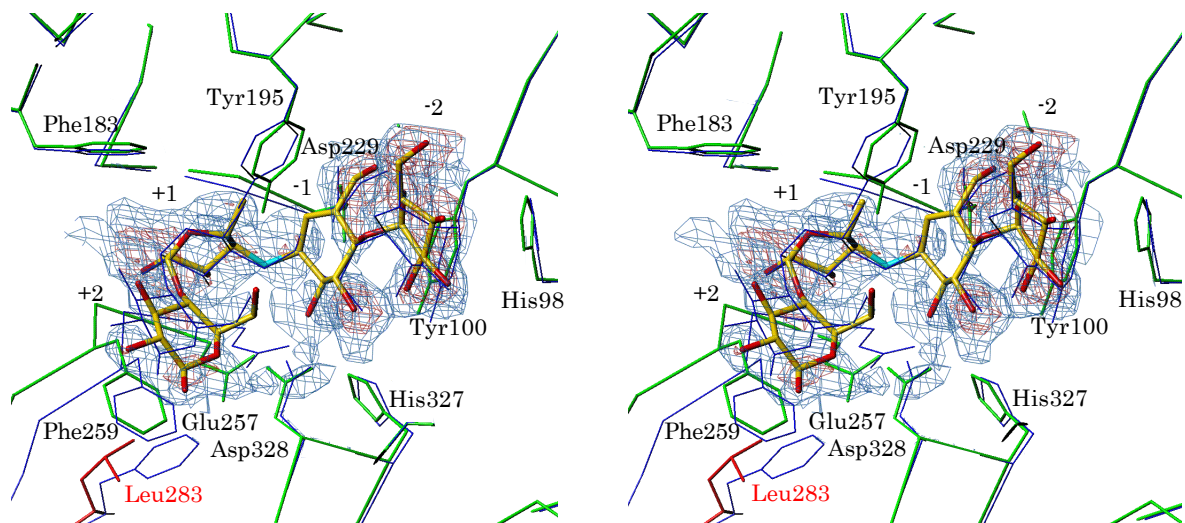


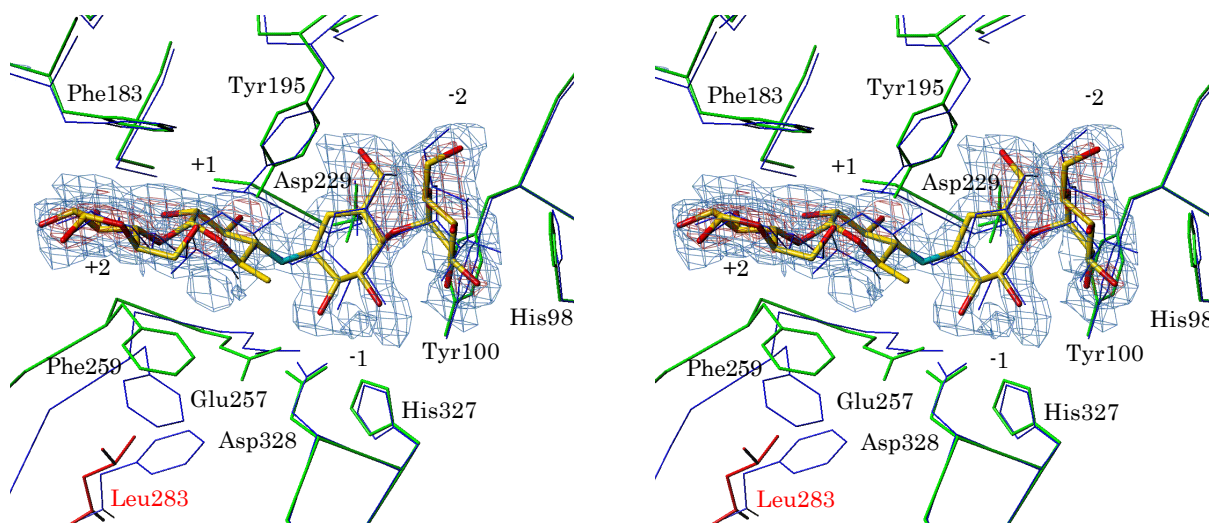
**Figure 12. Stereo views of the structures of pseudo-maltotetraose and catalytic active site of F283L\_ACA and wild type CGTase complexed with acarbose (A:MOL1, B:MOL2). Thick green lines and thin blue lines indicate F283L and wild type CGTases, respectively. Red lines denote the replaced residue Leu283. Omit  $|F_o - F_c|$  electron density of pseudo-maltotetraose in F283L\_ACA is drawn at 1.5  $\sigma$  (blue) and 3.0  $\sigma$  level (red).**

(A)



MOL1

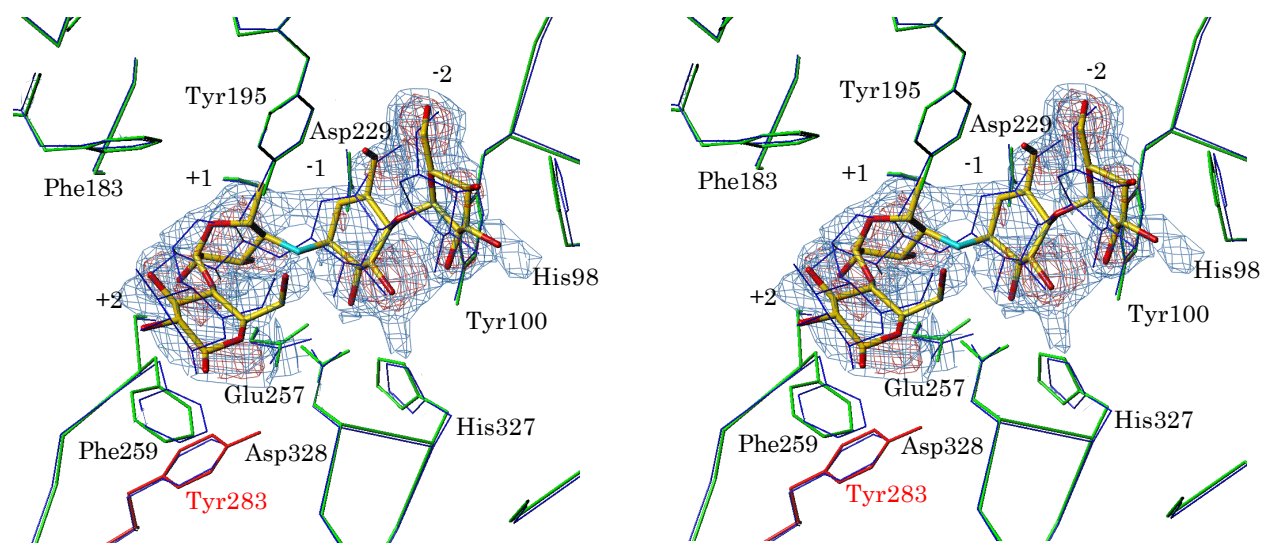
(B)



MOL2

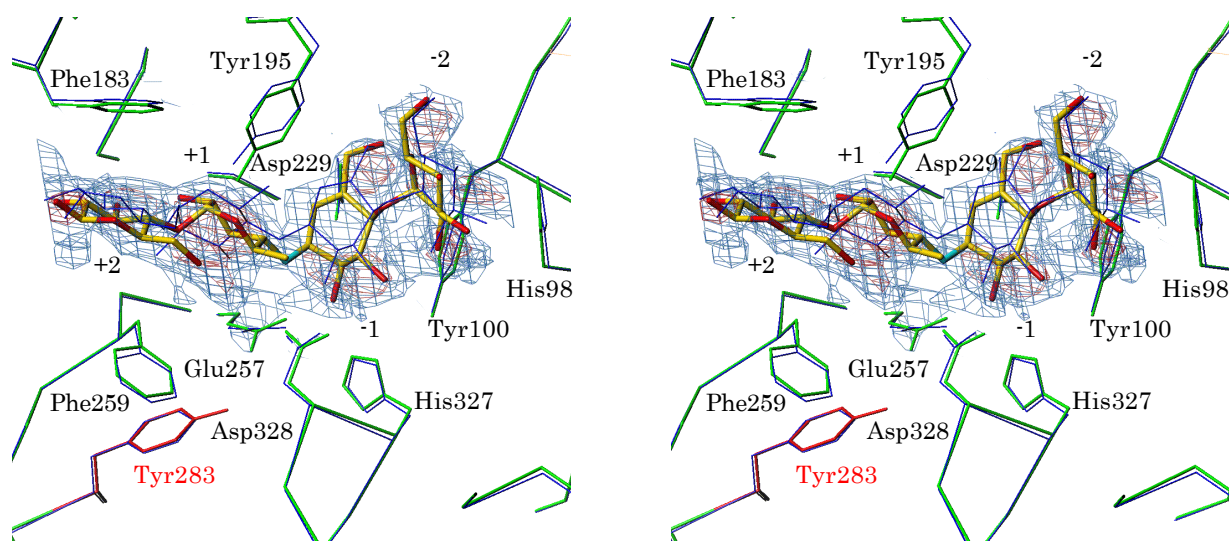
**Figure 13. Stereo views of the structures of pseudo-tetraose and catalytic active site of the acarbose complexes of F283Y and wild type CGTases(A:MOL1, B:MOL2).** Thick green lines and thin blue lines indicate F283Y and wild type CGTases, respectively. Red lines show the replaced residue Tyr283. Omit  $|F_o - F_c|$  electron density of pseudo-tetraose in F283L\_ACA is drawn at 1.5  $\sigma$  (blue) and 3.0  $\sigma$  level (red).

(A)



MOL1

(B)



MOL2

**Figure 14. Comparison of structures and temperature factors.** (A) Difference of isotropic temperature factors for equivalent C $\alpha$  atoms between F283L and wild type CGTase. (B) Difference of isotropic temperature factors for equivalent C $\alpha$  atoms between F283L\_ACA and F283L. (C) Positional difference for equivalent C $\alpha$  atoms in domain A (res. 1 - 138 and 204 - 406) between F283L\_ACA and F283L.



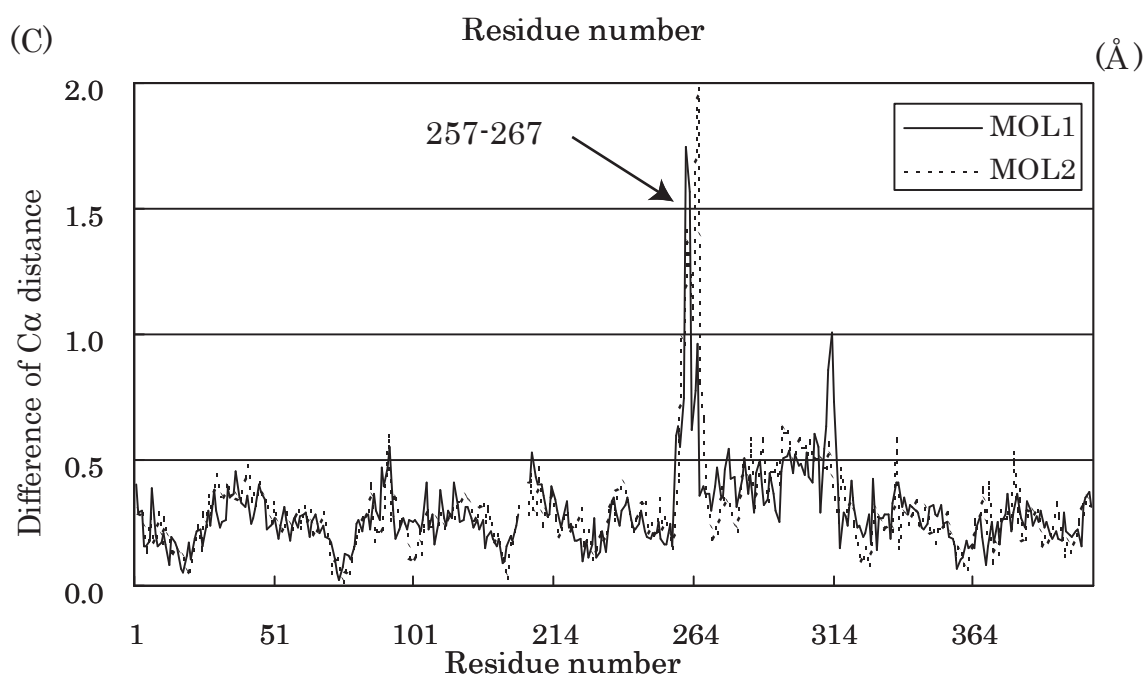
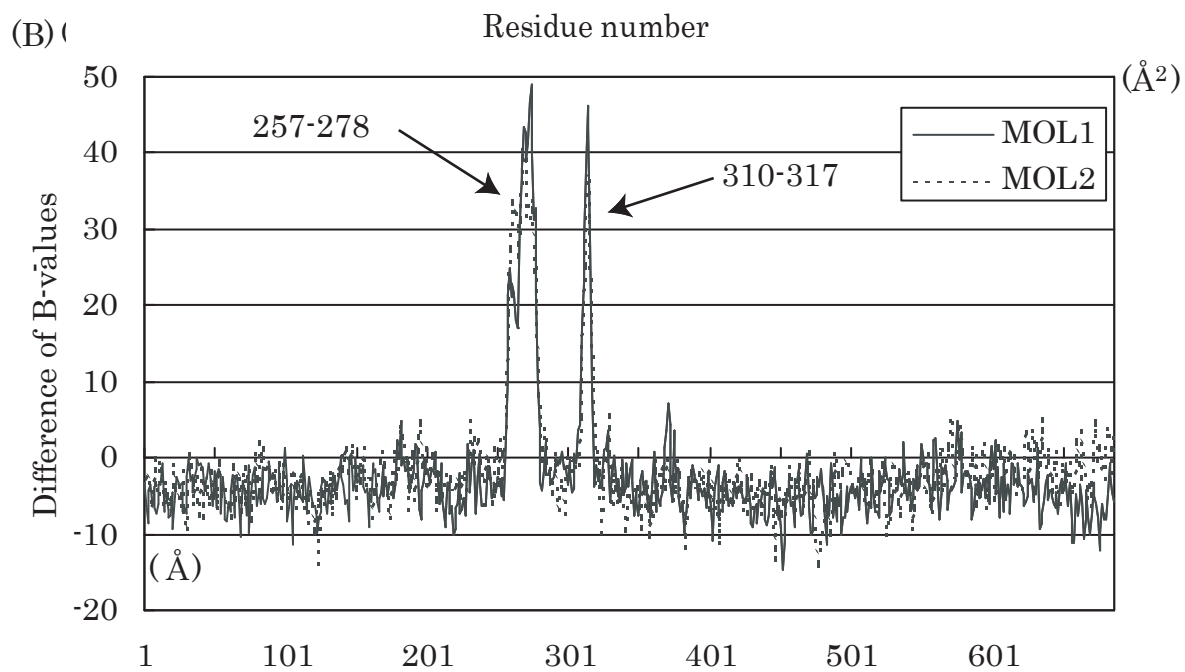
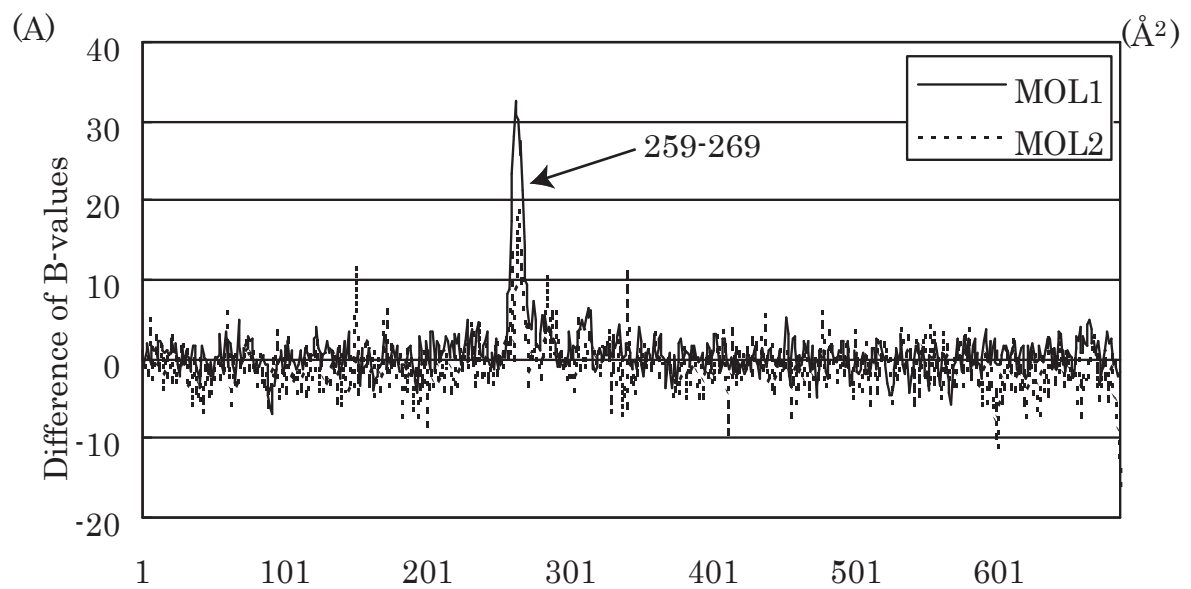
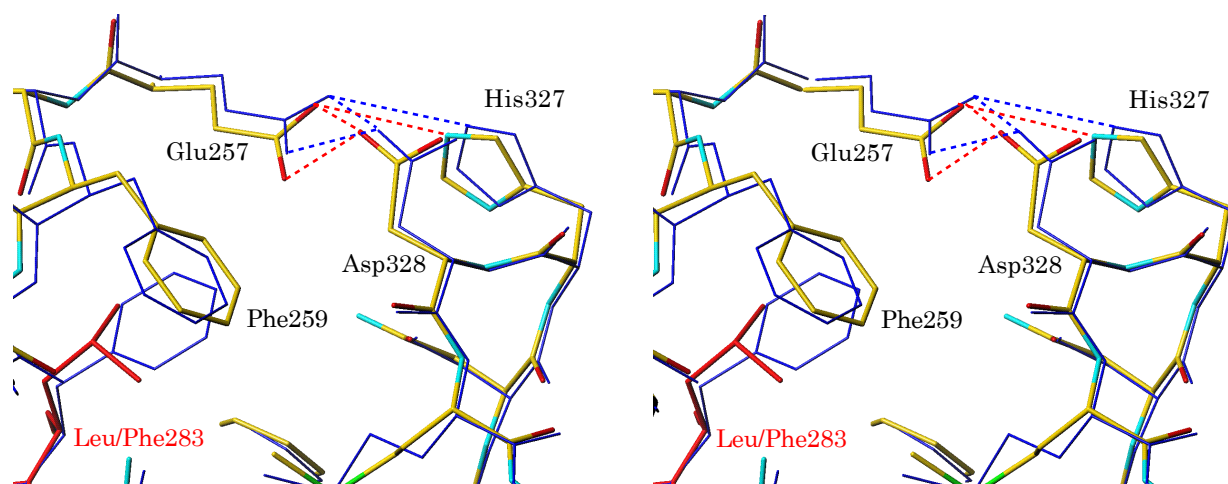
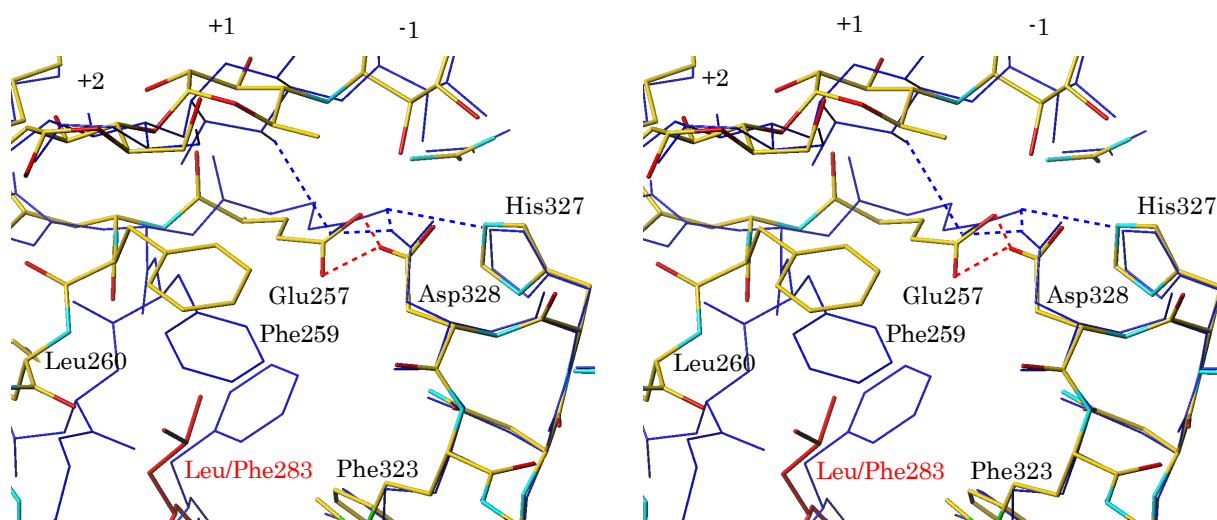


**Figure 15. Comparison of the catalytic active site.** Broken lines denote hydrogen bonds ( $\leq 3.3$  Å). The replaced residue 283 is shown by red lines. (A) MOL1 of F283L (thick lines) and wild type (thin blue lines). (B) MOL2 of F283L\_ACA (thick lines) and wild type complex (thin blue lines). (C) MOL2 of F283Y (thick lines) and wild type (thin blue lines).

(A) F283L



(B) F283L\_ACA



(C) F283Y

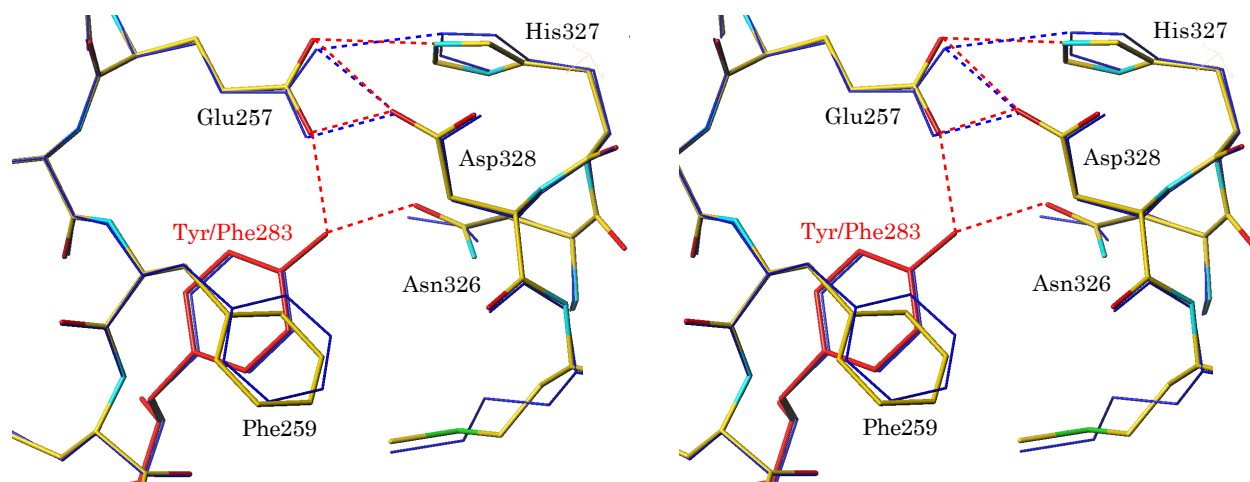
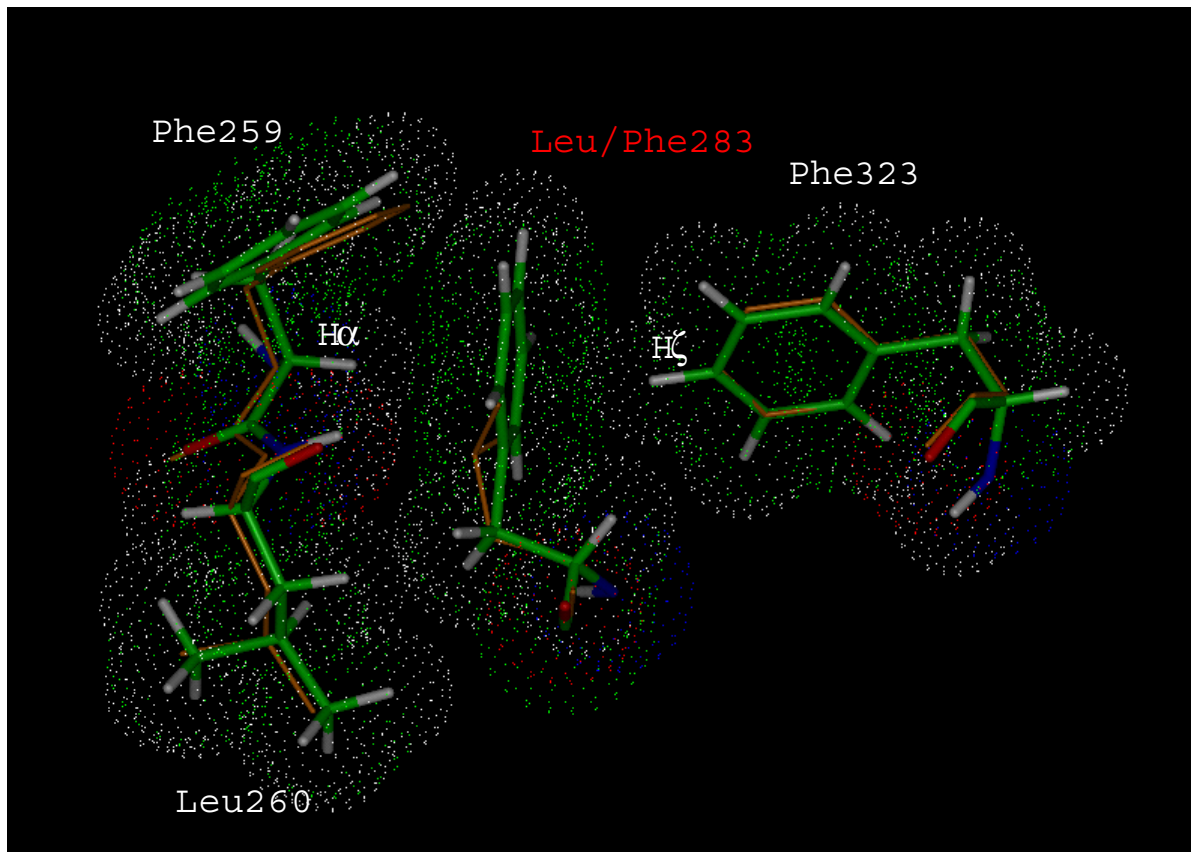
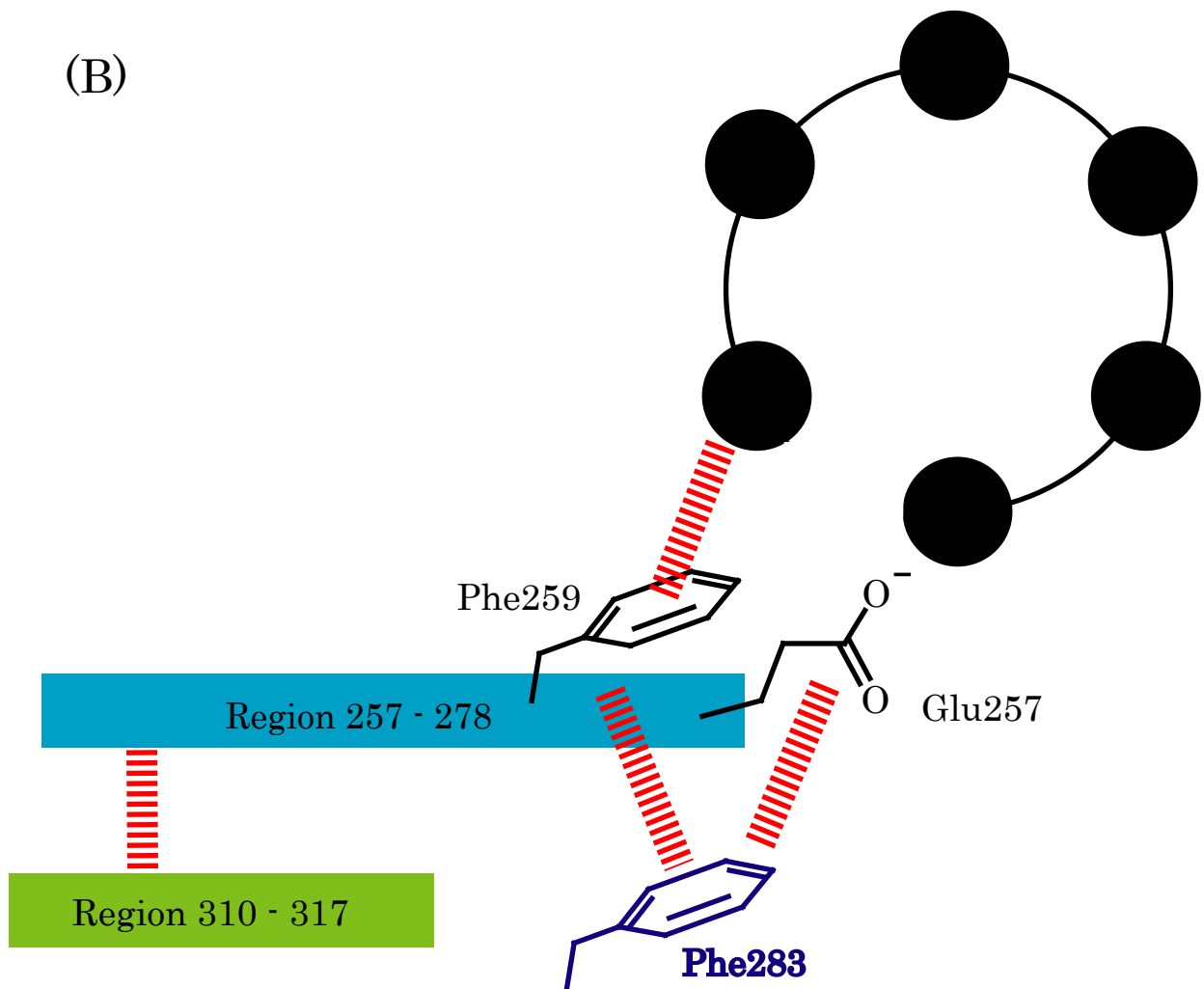


**Figure 16. Structural role of Phe283.** (A) Hydrophobic interaction of Phe283 with Phe259 and Phe323. Wild and F283L enzymes are represented by thick and thin lines, respectively. Dots at 1.0 Å radius represent atomic surface of wild type CGTase. (B) Diagram of interaction of Phe283. Phe283 regulates the structures of the region 257 – 278 containing Glu257 and Phe259, and the region 310 – 317, directly or indirectly.

(A)



(B)



## **Chapter II**

**The Reaction Mechanism of Malto-hexaose Forming Amylase on the Basis of X-ray  
Crystallographic Analysis: Crystal Structures of the Native and  
Pseudo-maltononaose-Complexed Forms.**

## Abstract

Maltohexaose forming amylase (G6-amylase) (E.C.3.2.1.98) from alkalophilic *Bacillus* sp.707 predominantly produces maltohexaose (G6) from starch and related  $\alpha$ -1, 4-glucan. To elucidate its reaction mechanism, the enzymatic activities were assayed and crystal structures of the G6-amylase and its complex with pseudo-maltononaose as pseudo-substrate-enzyme (ES) complex were determined at 2.1 and 1.9 Å resolutions, respectively. The optimal condition for starch degrading reaction activity was found at 45 °C and pH 8.8 and the enzyme produced G6 from amylose (DP=17) more than 30% of total sugar. Sequential and structural similarities of the active site to that of *B. licheniformis* (BLA) indicated that Asp236 is a nucleophilic catalyst and Glu266 is a proton donor/acceptor. The complex formation reduces the  $pK_a$  value of Glu266 as a proton donor/acceptor since the conformational change of Asp333 makes hydrogen bonds with the glycosyl residue at subsite –1. Moreover, the local structure of the region 338 – 340 neighboring to the active cleft is altered to avoid unfavorably close contact with substrate. Subsite –6, which is not identified in the structures of saccharifying  $\alpha$ -amylases, is composed of Lys72, Ala111 and Trp140. Especially, the indole moiety of Trp140 has close contacts within 4 Å to the two glycosyl residues at subsites –6 and –5, respectively. Since Tyr104 in barley  $\alpha$ -amylase, which temporarily produces maltohexaose predominantly, is located at the position equivalent to Trp140 in the G6-amylase, the stack interaction of an aromatic residue with a glucosyl residue at subsite –6 would be important for the maltohexaose production.

## Introduction

Bacterial  $\alpha$ -amylases called maltotetraose (G4), maltopentaose (G5), or maltohexaose (G6)-forming amylases (referred as Gn-amylases), dominantly produce G4, G5 or G6 from starch and related  $\alpha$ -1,4-glucans, while most  $\alpha$ -amylases convert them finally to glucose and/or maltose. Since malto-oligosaccharides (G4 - 6) are useful for their low sweetness, low viscosity, high moisturizing effect, and high efficiency for digestion and absorption, Gn-amylases are important enzymes in food and pharmaceutical industries.

Reaction mechanisms of the Gn-amylases are distinct from that of  $\alpha$ -amylase. Some of  $\alpha$ -amylases also produces G4, G5 or G6 from  $\alpha$ -1,4-glucan temporarily. Especially, many plant  $\alpha$ -amylases are known to temporarily produce G6 mainly in an early stage of starch degrading process (I. Maeda *et al.* 1978). Therefore, an important property of Gn-amylases is presumed to have four, five, or six subsites at the active center at least to produce their particular oligosaccharides by preventing the degradation of them.

G4-amylase (maltotetraose-forming exo-amylase) from *Pseudomonas stutzeri* has been reported to convert short chain amylose (DP=23) to G4 in about 75% of total sugar and to cleavage oligosaccharides (G5-9) to G4 and G1-3 according to the analysis of action pattern (T. Nakakuki *et al.* 1984). Crystal structure of mutant G4-amylase complexed with maltotetraose showed that G4-amylase has four subsites at the non-reducing side and many hydrogen bonds are formed with the glucosyl residue located at subsite -1 (Y. Yoshioka *et al.* 1997). Furthermore, in subsite -4, the side chain of Asp160 and a nitrogen atom in main chain form hydrogen bonds to the O2H and O6H hydroxyl groups of the glucosyl residue, whereas there are a few contacts between the glucosyl residues and subsites -3 and -2 (Y. Yoshioka *et al.* 1997). These previous studies brought us a suggestion that a dominant production of a particular oligosaccharide requires strict and strong interaction between glucosyl residue and subsite corresponding to the non-reducing end of the produced oligosaccharide.

G6-amylase (glucan 1,4- $\alpha$ -maltohexaosidase, E.C. 3.2.1.98) from alkalophilic *Bacillus* sp.707 has been cloned and its DNA sequence has been determined at 1988 (A. Tsukamoto *et al.*). Its



amino acid sequence has 65.5%, 65.9%, and 66.3% identities to those of *Bacillus amyloliquefaciens*, *B. licheniformis*, and *B. stearothermophilus* liquefying  $\alpha$ -amylases, respectively, but is little homologous to bacterial saccharifying  $\alpha$ -amylases and the G4-amylase (A. Tsukamoto *et al.* 1988). Therefore, the G6-amylase is presumed to have the structural property different from the G4-amylase.

In this chapter, I discuss the reaction mechanism of G6-amylase from alkalophilic *Bacillus* sp.707 based on its biochemical analysis and the crystal structures of the native G6-amylase and its complex with pseudo-maltononaose (Figure 17) as an enzyme-substrate (ES) complex.

## Materials and methods

### *Chemicals*

Kanamycin was purchased from Wako Pure Chemical Industry Ltd. Soluble starch was from E. Merck. Short chain amylose EX-I (DP=17) was purchased from Hayashibara Biochemical Laboratories, Inc. Oligosaccharides (G1 – 7) were purchased from Seikagaku Co. Acarbose was a gift from Drs. A. Mullen and K. Hornberg (Bayer AG). All other chemicals were of reagent grade.

### *Bacterial strains and plasmids*

G6-amylase was produced in *B. subtilis* 207-25[m<sub>168</sub> *hsrM recE4 amyE07 aroI906 leuA8 lys-21*] (K. Kimura *et al.* 1988). Plasmid pTUB812 encodes the G6-amylase gene region of an alkalophilic *Bacillus* sp.707 and has resistance genes to kanamycin (K. Kimura *et al.* 1988).

### *Expression and purification of G6-amylase*

G6-amylase from alkalophilic *Bacillus* sp.707 was expressed in *B. subtilis* 207-25 containing the plasmid pTUB812 as described previously (K. Kimura *et al.* 1988). The cells were incubated in Luria-Bertani medium containing kanamycin (10 µg/ml) and 0.2% (w/v) glucose for 3 days at 37 °C. After 28% saturated ammonium sulfate precipitation of the incubation medium, the supernatant was loaded onto TOYOPEARL HW55-F (Tosoh) equilibrated with 28% saturated ammonium sulfate-10 mM sodium phosphate buffer (pH 6.0). The resin was washed and then the target proteins were eluted with gradient of ammonium sulfate from 28% to 0%. After 75% saturated ammonium sulfate precipitation, the protein was desalted by a Bio-Gel P6-DG column (BioRad) equilibrated with Milli-Q water and concentrated to 7.0 mg/ml by using an Amicon concentration kit for crystal preparation. In addition, for the use in biochemical experiments, the protein was loaded onto DEAE sepharose (Pharmacia) equilibrated with 10 mM Tris-HCl (pH 7.5) and eluted by linear gradient of sodium chloride from 0 to 500 mM. The protein was desalted by a HiTrap Desalting column (Pharmacia) equilibrated with Milli-Q water and concentrated to 0.48 mg/ml. The purity was over 99% according to SDS-PAGE. The protein concentration was

determined by using the BCA protein assay reagent (Pierce) with bovine serum albumin as standard.

### *Enzyme assays*

Starch degrading activities were routinely measured at 37 °C in the analysis of pH optima, stability and thermostability by the blue value method with slight modification (A. Nakamura *et al.* 1994) using a 0.9 ml reaction mixture that contained 0.6 ml of a 0.5%(w/v) soluble starch solution and 0.3 ml of an enzyme solution containing 10 µg/ml bovine serum albumin. After the pre-incubation of 5 minutes and the incubation of 5, 10, and 15 minutes, the reaction was halted and starch was colored by adding a stop solution (0.17 mM I<sub>2</sub>, 1.7 mM KI and 1.7 mM HCl). One unit of starch degrading activity was defined as the amount that generated a 1% decrease in absorbance at 660 nm per minute. In the assay of pH optima, each enzyme solution was diluted suitably by Britton-Robinson pH buffer that contains 50 mM phosphoric, acetic and boric acids and adjusted to various pH values by NaOH. In the assay of pH stability, each enzyme solution was kept at various pH values for 30 minutes at 37 °C and then adjusted to pH 8.8 with a 12.5 mM sodium chloride and 50 mM sodium borate buffer. In the assay of thermostability, an enzyme solution suitably diluted by the sodium borate buffer (pH 8.8) was left for 30 minutes at various temperatures and pre-incubated at 37 °C after cooling on ice water for 5 minutes. In the assay of optimal temperature, the each enzyme solution diluted by the sodium borate buffer (pH 8.8) was pre-incubated at various temperatures and the activity at various temperatures was measured as same manner described above.

### *Analysis of reaction products*

Reactions was performed at 40 °C in a 1.2-ml reaction mixture that contained 0.8 ml of 1.0% (w/v) amylose EX-I (DP=17) solution and 0.4 ml of an enzyme solution (final 1 or 40 U/mg amylose) diluted by the sodium borate buffer (pH 8.8). After sampling of a 0.1 ml reaction mixture, the enzyme reaction in various reaction times was stopped by boiling for 10 minutes.

Quantitative analysis of the products was carried out by using HPLC. After desalting the samples and filtration with 0.22  $\mu\text{m}$ -pore size, the reaction products detected by RI detector RI-71 (Shodex) were eluted from LiChrosorb  $\text{NH}_2$  column (Cica-Merck) equilibrated with 68% (v/v) acetonitril at a flow rate of 0.8 ml/min. The products (G1 to G7) were quantified by each liner calibration curve of standard G1 to G7.

#### *Reaction pattern using G5, G6, and G7*

All reactions were performed at 40 °C in reaction mixtures of 60  $\mu\text{l}$  of 20 mM G5, G6, or G7 and 240  $\mu\text{l}$  of the enzyme (final 8 U/ $\mu\text{mol}$  substrate) in the sodium borate buffer (pH 8.8). After the incubation of 10, 20, and 30 minutes, the enzymatic reactions were stopped by boiling for 10 minutes. The reaction products were analyzed by using TLC. The TLC plates (Silica gel 60 F<sub>254</sub>, 5 x 7.5 cm (Merck)) loaded samples were developed in a solution of 2-propanol / ethyl acetate / water (3 : 1 : 1, v/v/v) for 1 hour and dried. After the three times repeat of this manipulation, all carbohydrates were visualized by spraying an ethanol solution of 20% (v/v) sulfuric acid and baking at 120 °C.

#### *Crystallization of native G6-amylase and complex with pseudo-maltononaose*

G6-amylase was crystallized by the hanging drop vapor diffusion method using the reservoir solution containing 50% (v/v) 2-methylpentane-2, 4-diol, 100 mM Tris-HCl (pH 8.5) and 200 mM ammonium phosphate. The drop solution contained equi-volume of sample and reservoir solutions and calcium chloride and sodium chloride were added to final 1 mM. Rod-like crystals of  $0.3 \times 0.1 \times 0.05 \text{ mm}^3$  were grown in 4 days at room temperature. A crystal of the complex with pseudo-maltononaose was obtained by soaking in the same crystallization solution but containing 10 mM acarbose (Figure 17) and 10 mM maltotriose for 3 days.

#### *Measurement of diffraction data*

The X-ray diffraction data of the crystals of native enzyme and its complex were collected to

1.94 Å resolution at 100 K at the BL-6A and AR-NW12 station of the Photon Factory and processed with the program HKL2000 (Z. Otwinowski *et al.* 1997). The acarbose and maltotriose-soaked crystal was isomorphous with the native crystal. Statistics of the data collection were summarized in Table 4.

#### *Structure determination and refinement.*

All the calculations were performed by the program CNS (A.T. Brünger *et al.* 1998). The crystal structure of the native G6-amyase at 2.1 Å resolution was determined by molecular replacement using a set of coordinates of a mutant  $\alpha$ -amylase from *B. licheniformis* (PDB code, 1OB0) (M. Machius *et al.* 2003) as the starting model. The crystal structure was corrected manually using the program TURBO-FRODO for  $|3F_o - 2F_c|$  and  $|F_o - F_c|$  electron density maps and three calcium, one sodium, phosphate and Tris ions were located. Water molecules were picked during the refinement cycle but were omitted in the case of the B-factor larger than 60 Å<sup>2</sup>.

The crystal structure of the G6-amyase complex at 1.9 Å resolution was determined by molecular replacement using the native structure. The  $|3F_o - 2F_c|$  and  $|F_o - F_c|$  electron density maps indicated the presence of pseudo-maltononaose at the subsites -6 to +3. At first, the sugar molecule was built as an  $\alpha$ -1, 4-linked chain of nine 6-deoxy-D-glucoses, and then corrected to an Acv-Glc-Glc-Glc- Acv-Glc-Glc (Acv; acarviosine, Glc; glucose) pseudo-maltononaose (Figure 17) on the electron density maps after some refinement cycles. The stereochemical qualities of the structures were checked by the program PROCHECK (A.R. Laskowski *et al.* 1993). Statistics of the structure determination are summarized in Table 4.

#### *Theoretical calculation of $\Delta pK_a$ s*

The calculation of  $\Delta pK_a$  was performed by using the program DELPHI (M.K. Gilson *et al.* 1987) for a finite difference solution to the nonlinear Poisson-Boltzmann equation. Electrostatic potential were calculated with formal charges, a grid size of 0.3 x 0.3 x 0.3 Å<sup>3</sup>, ionic strength of 0.145 M, interior and external dielectric constants of 2.0 and 80.0, respectively.  $\Delta pK_a$  of the target

residue was calculated by the equation:

$$\Delta pK_a = \frac{\sum \phi_n \times q_n}{2.303}$$

where  $\phi_n$  is the electrostatic potential of atom n induced by the charge of the target residue and  $q_n$  is the formal charge of atom n (B. Honig *et al.* 1993).

## Results

### *Enzyme assays*

The analysis of pH optima for the starch degrading activity showed that G6-amylase has a maximal activity (18800 U/mg) at pH 8.8 and keeps the relative activity higher than 50% between pH 6.5 and 10.0 (Figure 18A). The pH stability analysis showed that the enzyme is stable more than 50% in the pH range from 4.7 to 10.8 (Figure 18B). The optimal temperature of the G6-amylase was 45 °C at pH 8.8 and the enzymatic activity decreased lower than 20% in over 60 °C (Figure 2C). The thermostability analysis showed that the enzyme retains the activity more than 90% at 45 °C but the activity lowered less than 20% at over 55 °C (Figure 18D). The amino acid sequence of the G6-amylase was ca. 65% identical to those of BLA and BSTA (A. Tsukamoto *et al.* 1988), but its optimal temperature was lower than those of BLA and BSTA by about 40 and 20 °C, respectively (S. Narimasa 1973; S.L. Pfuehler *et al.* 1969).

### *Product ratios of the G6-amylase for short amylose*

In a low concentration (1U enzyme/mg amylose) of the G6-amylase (Figure 19A), the production rates (% of total sugar/min) of G3, G6 and G7 were 0.49 (50.2 µM/min), 0.35 (18.1 µM/min), and 0.37 (16.5 µM/min), respectively, in 40 minutes incubation. The amount of G3 after 90 minutes was 24 – 28% (2.5 – 2.9 mM) constantly. The production of G6 slowly increased to 31.4% (1.6 mM) in 40 minutes and had no large change in 24 hours. The highest product ratio of G7 was 18.4% after 60 minutes and decreased to 0% after 24 hours. In the high concentration (40U enzyme/mg amylose) of G6-amylase (Figure 19A), the production of G3 at each reaction time was about 25% (2.2 mM). The G6 production increased to 32.0% (1.4 mM) at 20 minutes but decreased to 0% after 24 hours. In contrast, the production of G1, G2 and G5 reached to 13.0% (3.3 mM), 25.0% (3.3 mM) and 35.4% (1.9 mM) after 24 hours. These degradation patterns were similar to that for 1% starch used as a substrate (data not shown).

### *Reaction pattern of G5, G6, and G7*

The TLC analysis of the products of the G6-amylase (8 U enzyme/ $\mu$ mol substrate) for 4 mM G5 and G6 as substrates after 30 minutes incubation showed that the G6-amylase is inactive for G5 and slightly converted G6 to G5 (Figure 19B). In contrast, the enzyme produced G1 – G6 from G7 (Figure 19C). Since the spots of G5 and G6 were relatively dense, G7 was mostly cleaved to G5 and G2 or G6 and G1.

#### *Crystal structure of native G6-amylase at 2.1 Å resolution*

The protein structure consists of three domains A, B and C (Figure 20A). The domain A (5 – 105, 208 – 396) forms a  $(\beta/\alpha)_8$  barrel like the other enzymes of  $\alpha$ -amylase family. The domain B (106 – 207) is composed of six  $\beta$ -strands and some loops and the two  $\beta$ -strands form a long  $\beta$ -sheet fold. The *cis* peptide bond is observed between Trp189 and Glu190. The domain C (397 – 485) consists of eight  $\beta$ -strands and some loops.

The backbone structure of G6-amylase is similar to liquefying  $\alpha$ -amylases, BLA (M. Machius *et al.* 1998) and BSTA (D. Suvd *et al.* 2001) with the average difference of their equivalent Ca position less than 1.0 Å (Figure 20B). The relatively large difference was observed in the regions 172 – 177, 181 – 185, 311 – 316 and 373 – 380. These regions except for the region 311 – 316 involve the deletion or insertion of some amino acid residues. G6-amylase contains Ca-Na-Ca metal triad at the interface between domain A and domain B as found in BLA (M. Machius *et al.* 1998) and BSTA (D. Suvd *et al.* 2001). The side chains of six aspartic acids (Asp163, Asp188, Asp199, Asp205, Asp207 and Asp209), one asparagine (Asn106), three carbonyl groups of the backbone and two water molecules are coordinated to the three metal ions. Comparing with the other enzymes of the  $\alpha$ -amylase family, saccharifying  $\alpha$ -amylase (Z. Fujimoto *et al.* 1998), barley  $\alpha$ -amylase (A. Kadziola *et al.* 1994), CGTase (C.L. Lawson *et al.* 1994), G4-amylase (Y. Yoshioka *et al.* 1997), and maltogenic amylase (Z. Dauter *et al.* 1999), the structure of domain A and C of G6-amylase is similar to their corresponding domains but there is a large structural difference in domain B.

The sequential and structural similarities to the other enzymes of the  $\alpha$ -amylase family indicate



that Asp236 in G6-amylase is a nucleophilic catalyst and the Glu266 is a proton donor/acceptor catalyst. The amino acid residues (Tyr58, Asp102, Lys239, His240, His332 and Asp333) conserved around the catalytic residues in many  $\alpha$ -amylases have similar conformations observed in those  $\alpha$ -amylases (Y. Yoshioka *et al.* 1997; M. Machius *et al.* 1998; Z. Fujimoto *et al.* 1998).

#### *Crystal structure of the G6-amylase complexed with pseudo-maltononaose*

A pseudo-maltononaose molecule is located at the subsites  $-6$  to  $+3$  of G6-amylase like an enzyme-substrate ES complex (Figure 21A). The structure of the pseudo-maltononaose, Acv-Glc-Glc-Glc-Acv- Glc-Glc (Figure 21B), suggests that this oligosaccharide is derived from some acarbose and maltotrioses by transglycosylation and hydrolysis. In the many crystals of  $\alpha$ -amylase complex with ligand as reported previously, acarbose is converted to an oligosaccharide that inhibits more effectively (R. Mosi *et al.* 1988; M. Qian *et al.* 1994; A.M. Brzozowski *et al.* 2000; K. Haga *et al.* 2004).

#### *Conformation of the pseudo-maltononaose*

Intramolecular hydrogen bonds linking  $O2H_n$  and  $O3H_{n+1}$  hydroxyl groups are observed between the glycosyl residues at subsites  $-6/-5$ ,  $-4/-3$ ,  $+1/+2$ , and  $+2/+3$  (Figure 21B). Torsion angles ( $\phi$ :  $O5(C7)_n - C1_n - O4(N4)_{n+1} - C4_{n+1}$ ,  $\psi$ :  $C1_n - O4(N4)_{n+1} - C4_{n+1} - C5_{n+1}$ ) of all glycosidic linkages are energetically permissible for  $\phi$  angles of  $75.4^\circ$  to  $125.0^\circ$  and  $\psi$  angles of  $-160.7^\circ$  to  $-118.9^\circ$ , except for the  $\phi$  angle at subsite  $-1/+1$  of  $20.5^\circ$  (Figure 21B). Half chair forms are observed in two glycosyl residues at subsites  $-6$  and  $-1$  (Figure 21B).

#### *Contacts of the pseudo-maltononaose with the G6-amylase*

Many hydrogen bonds are observed between the glycosyl residues and amino acids (Tyr198, Glu194, Arg234, Asp236, Lys239, His240, Glu266, His332 and Asp333) located at the subsites  $-1$  to  $+2$  (Table 5 and Figure 22A). The carboxyl group of Asp236, a nucleophile, is close to C1 atom of the glycosyl residue at the subsite  $-1$  in  $3.1 \text{ \AA}$  distance and the side chain of Glu266, a proton

donor/acceptor catalyst, has close contact in 2.8 Å distance to N4 atom of the pseudo-glycosidic bond between subsites –1 and +1 (Table 5 and Figure 22B). Such close contacts of catalytic residues have been found in many acarbose- $\alpha$ -amylase complexes reported previously (R. Mosi *et al.* 1998; Z. Dauter *et al.* 1999; A.M. Brzozowski *et al.* 2000). Moreover, aromatic ring of Tyr58 is parallel to the pyranose ring of the cyclitol residue at the subsite –1 within 4Å distance (Figure 22A) indicating the hydrophobic stack as observed in the other  $\alpha$ -amylase-carbohydrate complexes (Y. Yoshioka *et al.* 1997; Z. Dauter *et al.* 1999; J.C.M. Uitdehaag *et al.* 1999b; A.M. Brzozowski *et al.* 2000).

The glucosyl residues at the subsites –3 and –2 forms hydrogen bonds with water molecules and have few contacts with the enzyme (Table 5). The carboxyl group of Asp166 forms strong hydrogen bonds until O2H and O3H hydroxyl groups of the glucosyl residue at subsite –4 with 2.5 and 2.6 Å distances, respectively, and the aromatic ring of Tyr203 is parallel to the pyranose ring indicating the hydrophobic stack in about 4 Å distance. The hydrogen bonding contacts between the glycosyl residues and the subsites –6 and –5 are fewer than those at subsites –1 to +2, but the aromatic ring of Trp140 closely contacts within 4Å distance to the C4 atom of the glycosyl residue at subsite –5 and the C1 atom in the residue at the subsite –6 (Figure 23), indicating the strong hydrophobic interaction.

#### *Structural comparison of native G6-amylase with its complex.*

There are some structural changes at catalytic active site. In the complexed form, the carboxyl group of Glu266 no more forms such hydrogen bonds with the side chains of Asp333 and Arg234 within 3.2 Å as observed in the native structure (Figure 22B). The carboxyl group of Glu266 moves to the sugar ligand with the change of its  $\chi_2$  angle from 172.15° to –126.65° and forms hydrogen bonds with backbone peptide and O3H hydroxyl group, and a salt bridge with the N4 amino group of the sugar residue at subsite +1 (Figure 22B). Furthermore, C $\alpha$  atoms of Asp333 and His332, which form hydrogen bonds to the ligand, shift by 1.1 and 0.6 Å in comparison with its native structure (Figure 22A). The calculated  $\Delta pK_a$  values of the carboxyl group of Glu266

referred as a proton donor/acceptor catalyst are +17.6 and +4.4 for the native and complex structures, respectively. The effect of Asp333 on the  $\Delta pK_a$  of Glu266 is decreased by  $-10.9$  in the complexed form. This indicates that the structural change of Glu266 and Asp333 affects on their electrostatic environment and protonation/deprotonation (Figure 22B).

The C $\alpha$  atoms of Glu338, Ala339 and Leu340 are moved toward His332 and Asp333 by 1.0, 1.7 and 0.9 Å, respectively (Figure 22A). In the complex structure, the carbonyl oxygen atom in the backbone of Asp333 forms a hydrogen bond with the backbone peptide of Leu340 and the C $\delta$ 1 atom of Leu340 is close to the aromatic ring of Trp268 within 4Å distance (Figure 22A).

## Discussion

### *Crystal structure of G6-amylase*

The backbone structure of G6-amylase resembles to the structure of BLA (M. Machius *et al.* 1998) and BSTA (D. Suvd *et al.* 2001) that are liquefying  $\alpha$ -amylases (Figure 20B). Their structure of domain B is most different from other  $\alpha$ -amylases because the amino acid sequence of domain B is longer by 20 to 40 a. a. than those of the other  $\alpha$ -amylases. BLA produces G5 from starch and related  $\alpha$ -1, 4-glucans. Therefore, the structure of domain B of these enzymes should be specific for G5 or G6 production. In fact, Lys72, Trp140, Asp166 and Tyr203 in domain B, which are conserved in BLA (M. Machius *et al.* 1998), participate to construct the subsite structure as described above (Table 5 and Figure 23).

### *Structural changes of the G6-amylase gone with ES complex formation*

The movement of Asp333 in the complex with pseudo-maltononaose (Figure 22) should be induced by the substrate binding to optimize the interaction between protein and substrate. Furthermore, since the carboxyl group of Asp333 causes the decrease of the  $pK_a$  value of Glu266 in the ES complex, the structural changes of Glu266 and Asp333 would be important for efficient catalytic activity. The carboxyl group of Glu266 in the native form may not be ionized even if in high pH environment, but in the ES complex, would more easily release the proton to donate it to the glycosidic oxygen atom at the cleavage site (Figure 22B).

The movement of the region 338 – 340 to the region 332 – 333 may be caused to release the steric hindrance of the side chain of Leu340 to the ligand and impose restriction on the flexibility of ligand conformation. If the structural change does not occur, the side chain of Leu340 would be too close within 3.5 Å to the glycosyl residues at subsites +1 and +2 and the side chain of Ala339 is far from the glycosyl residues at subsites –2 and –1 (Figure 22A). Trp268 may contribute to the movement of the region 338 – 340 by the hydrophobic interaction with Leu340 (Figure 22A). The regions 332 – 333 and 338 – 340 would interact with each other and include the structural change to accommodate the substrate in the active cleft in the process of ES complex formation.

As a result, the enzyme-substrate interaction would be optimized by such structural changes as described in terms of the induced-fitting.

#### *Binding of subsites to glucosyl residues*

The structure of the enzyme-inhibitor complex indicates three and six subsites at reducing and non-reducing-end sides, respectively (Figure 24A). Many hydrogen bonds at subsites  $-1$  and  $+1$  and the stack interaction of Tyr58 with the glycosyl residues (Table 5 and Figure 22A) indicate that subsites  $-1$  and  $+1$  binds the glucosyl residues strongly enough to distort and cleave the glycosidic bond between the glucosyl residues at subsites  $-1$  and  $+1$ .

Since the aromatic ring of Trp140 is stacked on the cyclitol and deoxyglucose residues at subsites  $-6$  and  $-5$  by the hydrophobic interaction and these subsites have also hydrogen bonding contacts with the sugar (Table 5 and Figure 23), the glucosyl residues should be strongly bound to the subsites  $-6$  and  $-5$ . Moreover, the hydrogen bonds of Asp166 and the stacking of the aromatic ring of Tyr203 to the glucosyl residue (Table 5) suggest the strong interaction between the glucosyl residue and subsite  $-4$ . We tried to determine crystal structures of the enzyme complexed with various maltodextrins and the electron density of glucosyl residues located at subsites  $-6$  to  $-4$  was more visible than those at the other subsites (data not shown). Despite of the break of the intra-molecular hydrogen bond between secondary hydroxyl groups of the deoxyglucose and glucose residues at subsites  $-5$  and  $-4$ , respectively (Figure 21B), their structural flexibility is strictly limited by interactions with the subsites. In contrast, few contacts of subsites  $-3$  and  $-2$  to glucosyl residues (Table 5) indicates the weak binding of these residues to the subsites. However, these glucosyl residues at subsites  $-3$  and  $-2$  caused the structural change of the region 338 – 340 (Figure 22A).

#### *Amylose degradation and maltohexaose production of the G6-amylase.*

Since the product ratio analysis of short chain amylose (Figure 19A) showed the high production (about 25% total sugar) of G3 in the early stage, a substrate, Gn ( $n \geq 9$ ), may occupy

subsites from +3 toward the subsite at non-reducing end side and be hydrolyzed to G3 and Gn-3 (Figure 24B). This is also supported by the fact that BLA produces G3 from reducing end side of G8, G9 or G10 (L. Kandra *et al.* 2002). However, if such a binding of substrate were dominated much, the enzyme would produce G3 mostly. In the fact, there is no structural “barrier” preventing substrate from approach toward far reducing-end side. Therefore, the hydrolysis to G3 and Gn-3 would be followed by the random cleavage of long chain substrate and, when amylose is shorten to G7, G8 or G9, these substrates may be incorporated to occupy six subsites of non-reducing-end side and be hydrolyzed to G6 and G1, G2 or G3 (Figure 24B) because of the strong binding to subsites –6 and –5. Therefore, the interaction of subsites –6 and –5, especially, Trp140 to cyclitol residues play an important role for the G6 production. The strong interaction of subsite –6 with the glucosyl residue indicates a possibility to form non-productive binding (enzyme-product (EP) complex) of G6 that occupies from subsites –6 to –1.

#### *Importance of an aromatic residue at subsite –6 on maltohexaose production*

Barley  $\alpha$ -amylase temporarily produces maltohexaose from starch and finally produces glucose and/or maltose (I. Maeda *et al.* 1978). The structure of barley  $\alpha$ -amylase complex with pseudo-maltononaose, which is generated by docking simulation using its native structure (A. Kadziola *et al.* 1994), showed that the location of Tyr104 is equivalent to that of Trp140 at subsite –6 of G6-amylase (Figure 25A). Despite of low sequence similarity (Figure 25B) and the large difference of the backbone structures of domains B in them (Figure 25A), the structural similarity of subsite –6 indicates the importance of the interaction of an aromatic residue at subsite –6 with a glucosyl residue on maltohexaose production. Recently, the biochemical analysis of an aromatic residue (Tyr105) at subsite –6 of barley  $\alpha$ -amylase showed that the replacement of Tyr105 with alanine induces low degrading activity and change of the cleavage pattern of PNP-G<sub>7</sub> (K.S. Bak-Jensen *et al.* 2003). We are examining the importance of Trp140 on maltohexaose production using mutagenesis and biochemical techniques.

**Table 4. Statistics of diffraction data and structure determination.**

Diffraction data	(Native)	(Complex)
Space group	Orthorhombic $P2_12_12_1$	Orthorhombic $P2_12_12_1$
Unit cell param.(a, b, c (Å))	47.62 82.80 127.18	47.41 82.49 126.88
Mosaicity	0.664	0.315
Resolution range (last shell) (Å)	50.0 - 2.04 (2.11 - 2.04)	50.0 - 1.94 (2.01-1.94)
Num. of total reflections	123734	271436
Num. of unique reflections	32772	39906
Completeness (last shell)	99.6% (97.8%)	98.8% (98.8%)
$R_{\text{merge}}$ (last shell)	9.1% (24.8%)	5.1% (10.6%)
Redundancy	2.60	3.40
Structure determination		
Resolution range (last shell) (Å)	6.0 - 2.1 (2.17 – 2.10)	6.0 - 1.9 (1.98 – 1.94)
Num. Of Reflections used ( $> 2\sigma$ )	26098	38141
Completeness (last shell)	90.8% (79.5%)	95.4% (83.3%)
Protein	5-485 (1-4 disordered)	5-485 (1-4 disordered)
Num. of water molecules	282	324
Final $R$ value (last shell)	16.6% (17.7%)	16.9% (18.4%)
Final $R_{\text{free}}$ value (last shell)	21.0% (23.2%)	20.5% (24.5%)
RMSD		
Bond length	0.005 Å	0.005 Å
Bond angle	1.28°	1.24°
Dihedral	23.48°	23.56°
Improper	0.688°	0.732°

Table 5. List of short contacts ( $\leq 3.3$  Å distance) of pseudo-maltononaose to G6-amylase.

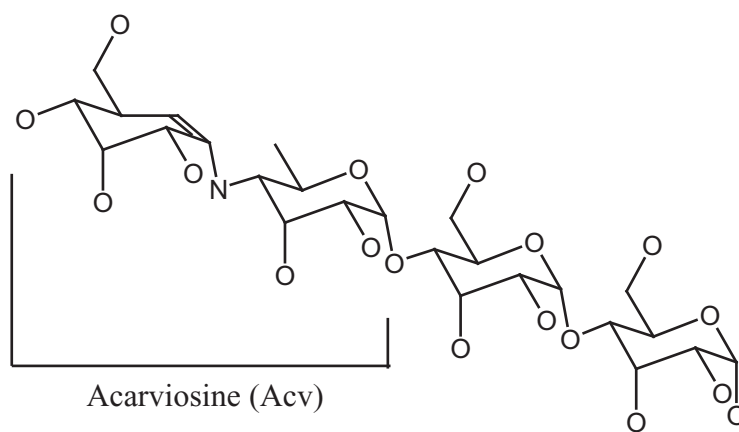
Sugar	Protein	Distance	Sugar	Protein	Distance		
-6 O2	Ala111N	3.3	-1 C1	Asp236Oδ1	3.1		
	Ala111O	2.8		O2	Arg234NH2	3.0	
	O3	Lys72Nζ		2.9		His332Nε2	2.8
-5 O2	Wat734	2.9			Asp333Oδ2	2.3	
	Wat735	2.6			Wat708	3.3	
	O3	Gly110N	3.2	O3	His332Nε2	3.1	
		Ala111N	3.1		Asp333Oδ1	2.7	
	N4	Wat733	3.1		Asp333Oδ2	3.3	
-4 O2	Asp166Oδ2	2.5	O6	Asp236Oδ2	2.7		
	Tyr203N	3.1		C7	Asp236Oδ1	3.1	
	O3	Asp166Oδ1	2.6	+1 O2	His240Nε2	2.6	
		Tyr203N	3.3		O3	Glu266Oε1	3.1
		Wat734	2.9			Glu266Oε2	2.7
-3 O2	Wat858	3.1	N4	Glu266Oε1	2.8		
	Wat862	2.7			Asp333Oδ2	3.1	
	O3	Wat858	3.1	O5	Wat906	2.7	
-2 O2	Asp333Oδ1	3.2	+2 O2	Glu194Oε2	2.6		
	Wat707	2.6			Lys239Nζ	2.9	
	O3	Wat862		2.6	O3	Tyr198OH	3.2
	O6	Wat704		2.6		Lys239Nζ	2.6
		Wat705		2.9	O6	Wat906	3.0
				Wat986	2.7		
			+3 O1	Wat966	3.2		
					Wat979	2.5	
				O2	Asn270N	2.8	

(Å)



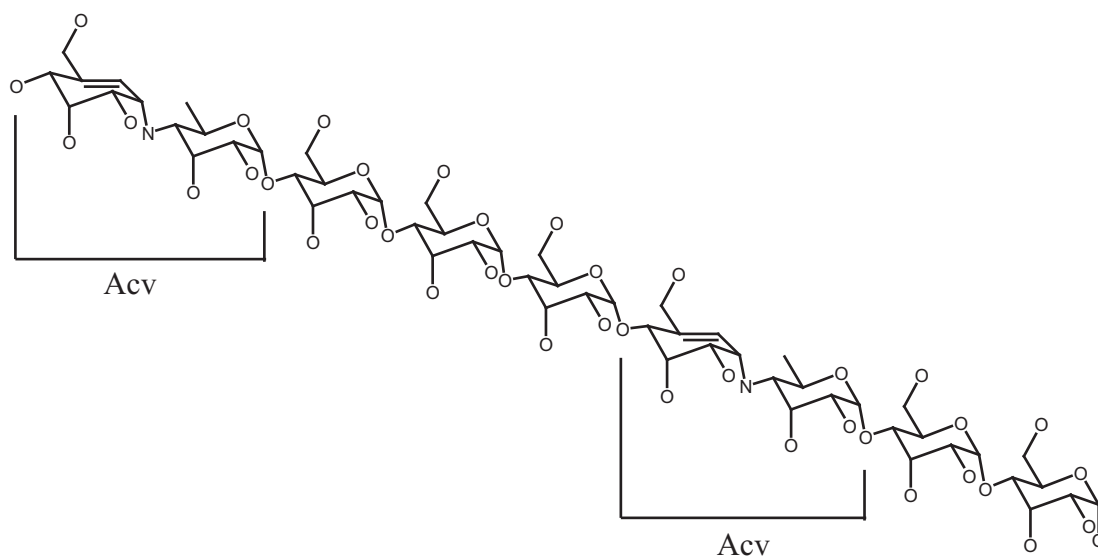
Figure 17. Structure of acarbose (A) and pseudo-maltononaose (B) observed in the crystal structure of the G6-amylase complex.

(A)



Acarbose

(B)



Pseudo-maltononaose

**Figure 18. Characterization of G6-amylase using starch degrading activity.** Effects of pH and temperature on its activity profile (A, C) and stability (B, D). Assays of pH (A and B) were performed at 37 °C and temperature assays (C and D) were performed in 50 mM sodium borate – 12.5 mM sodium chloride buffer (pH 8.8).

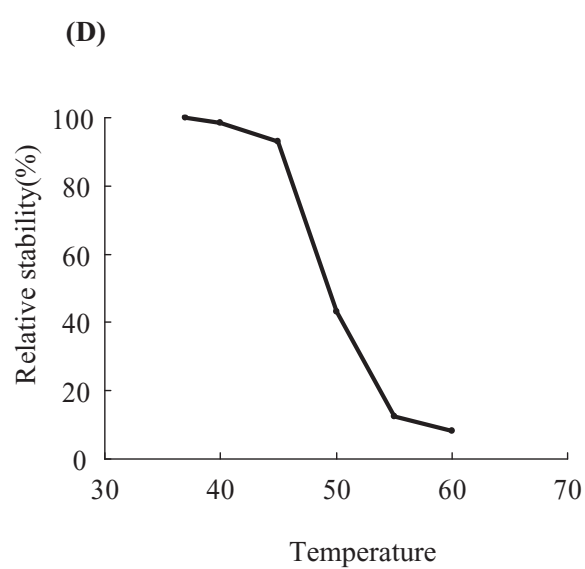
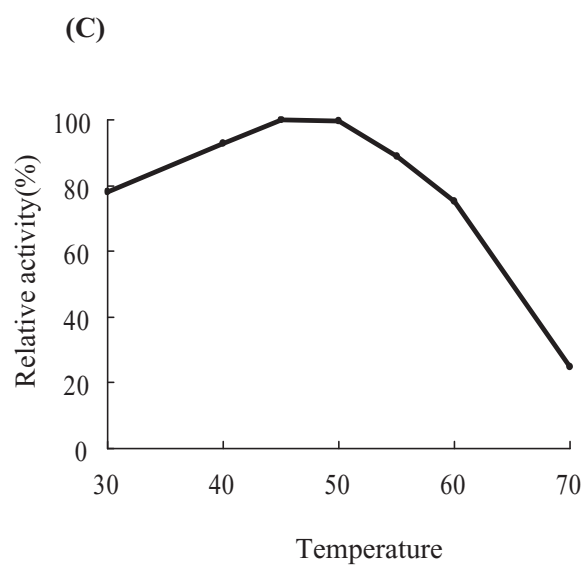
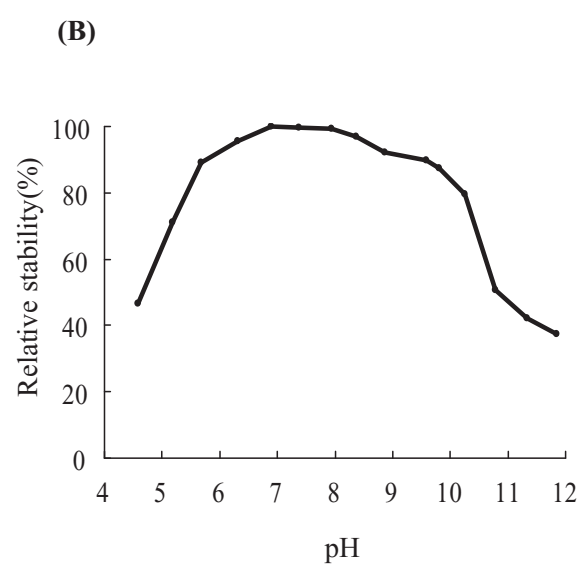
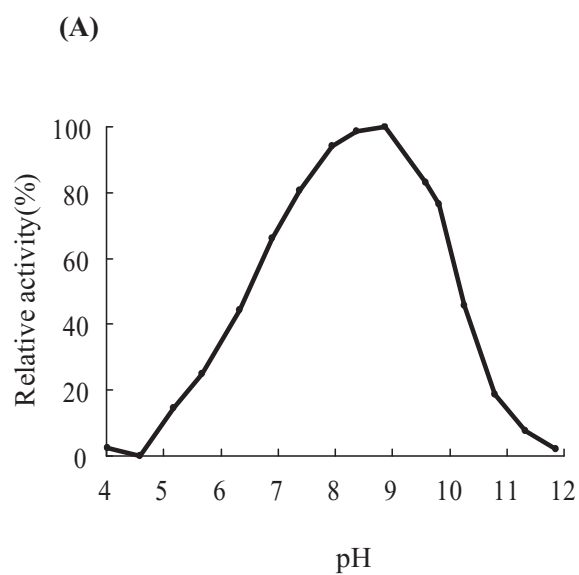
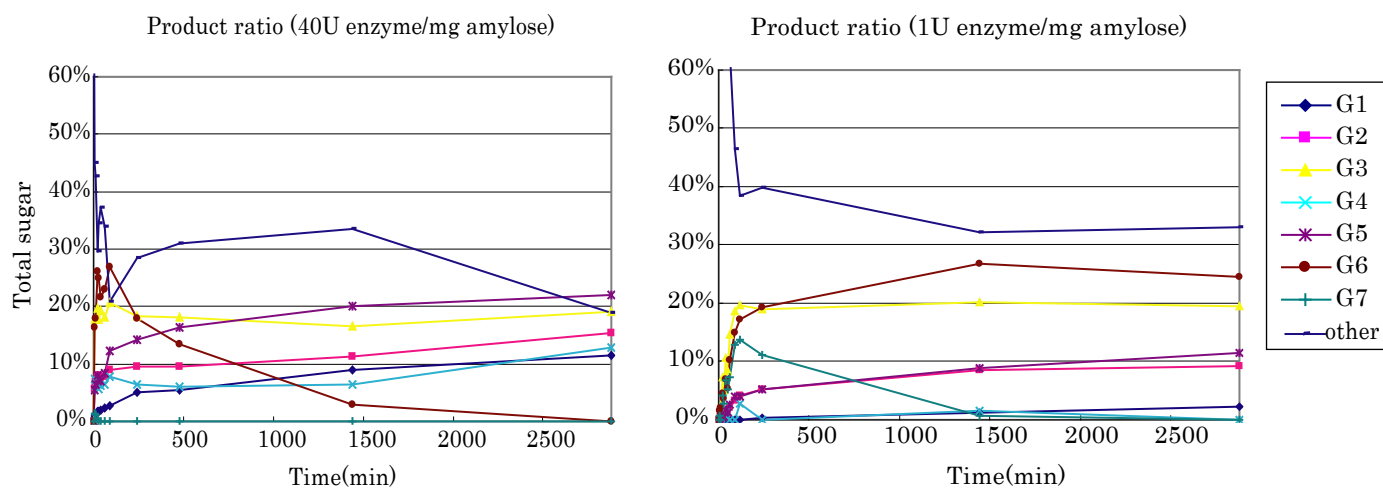
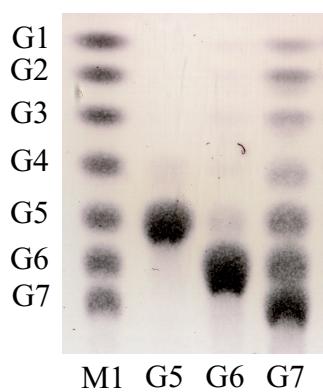


**Figure 19. Products ratio from short amylose (DP=17) and cleavage pattern of G5, G6 and G7 by G6-amylase.** (A) The products ratio of G6-amylase from short amylose (DP=17). The amount of the enzyme is 1 U enzyme/mg (right) or 40 U enzyme/ mg (left) amylose. (B) TLC analysis of the degradation pattern of G5, G6 or G7 after 30 minutes incubation. (C) TLC analysis of degradation pattern of G7 after 10, 20 and 30 minutes incubation. M1 and M2 are markers of G1 – G7 and G7, respectively.

(A)



(B)



(C)

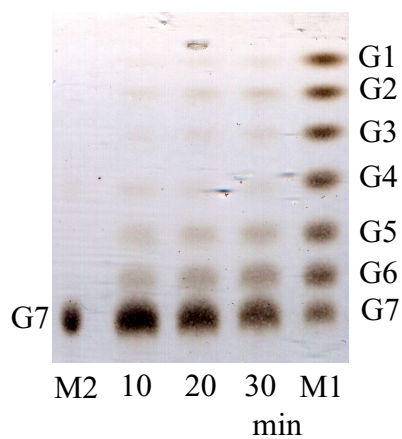


**Figure 20. Overall structure of the native G6-amylase from alkalophilic *Bacillus* sp.707.** (A) G6-amylase is composed of three domains A (blue), B (yellow) and C (green). Asp236 as a nucleophilic catalyst, and Glu266 as a proton donor / acceptor are represented by ball and sticks. Three calcium and one sodium ions are shown by cyan and purple spheres, respectively. (B) Comparison of the backbone structures of G6-amylase (thick yellow line) with BLA (thin blue line) (M. Machius *et al.* 1998) and BSTA (thin green line) (D. Suvd *et al.* 2001).

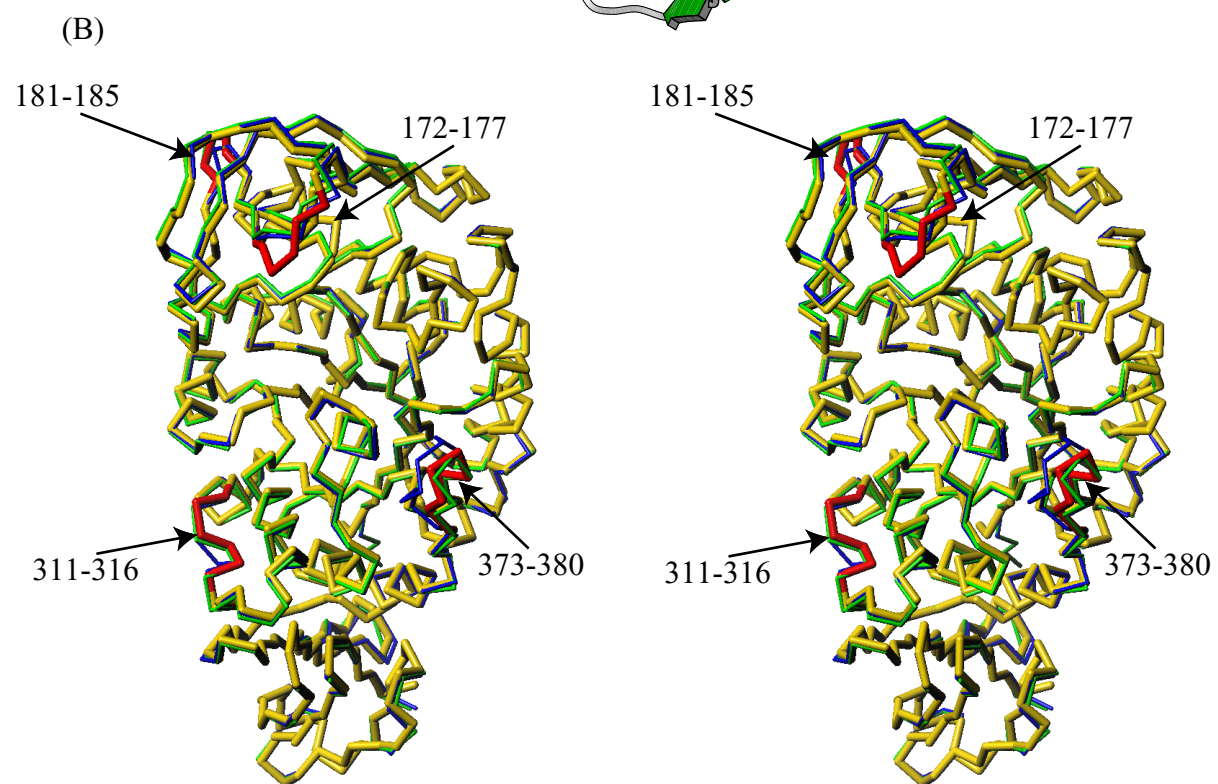
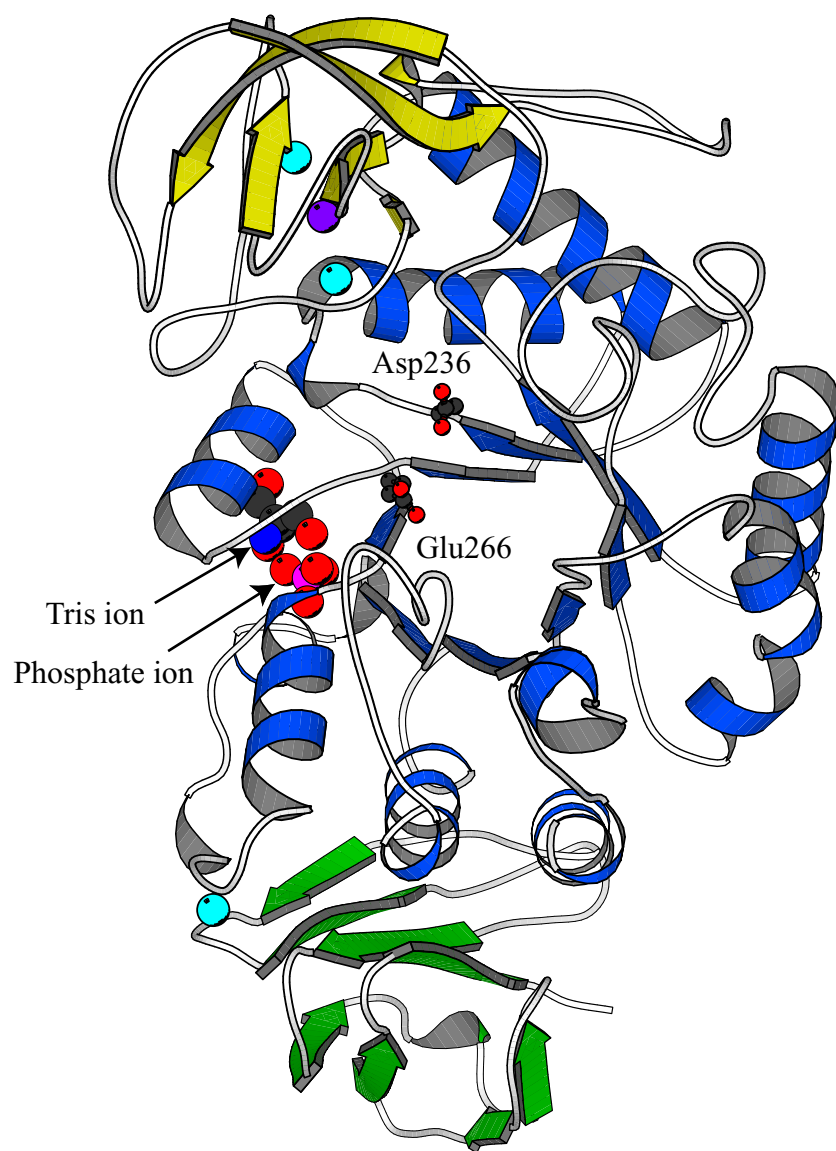
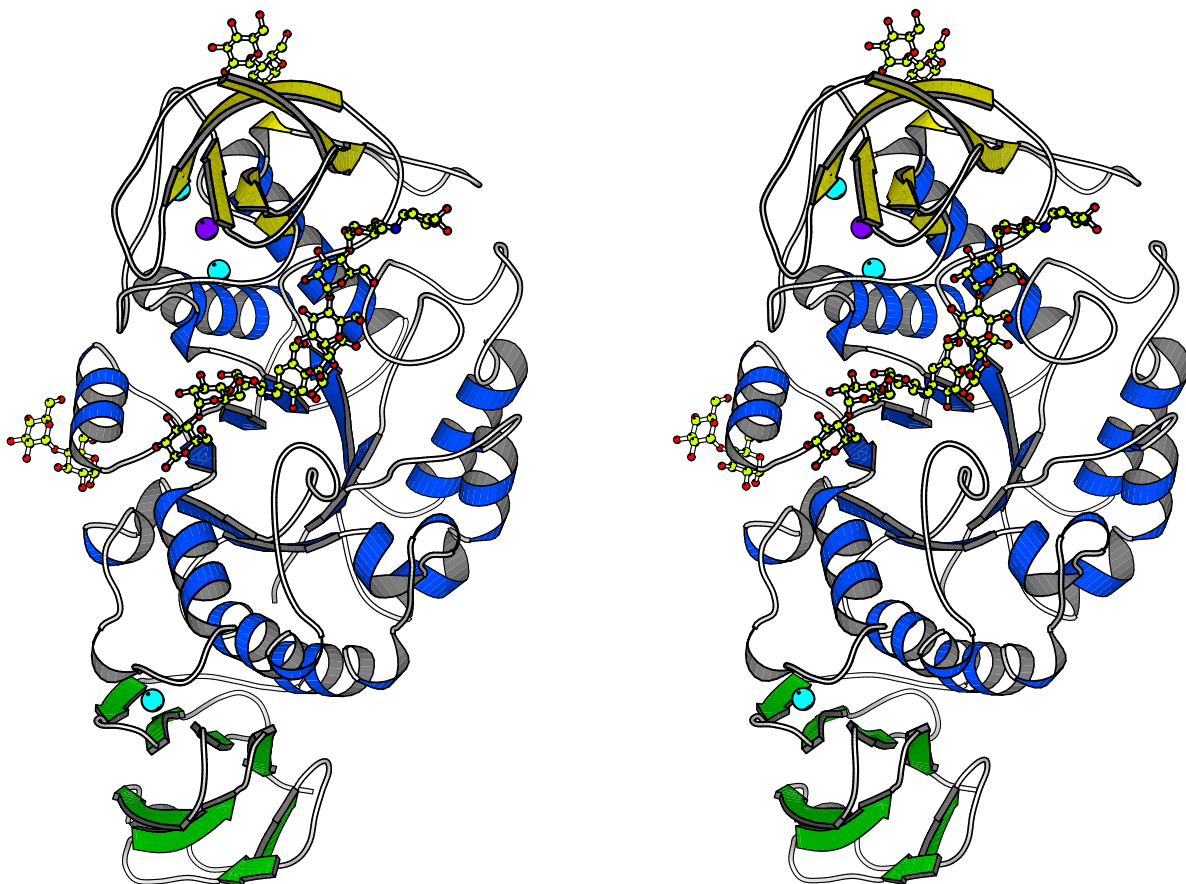


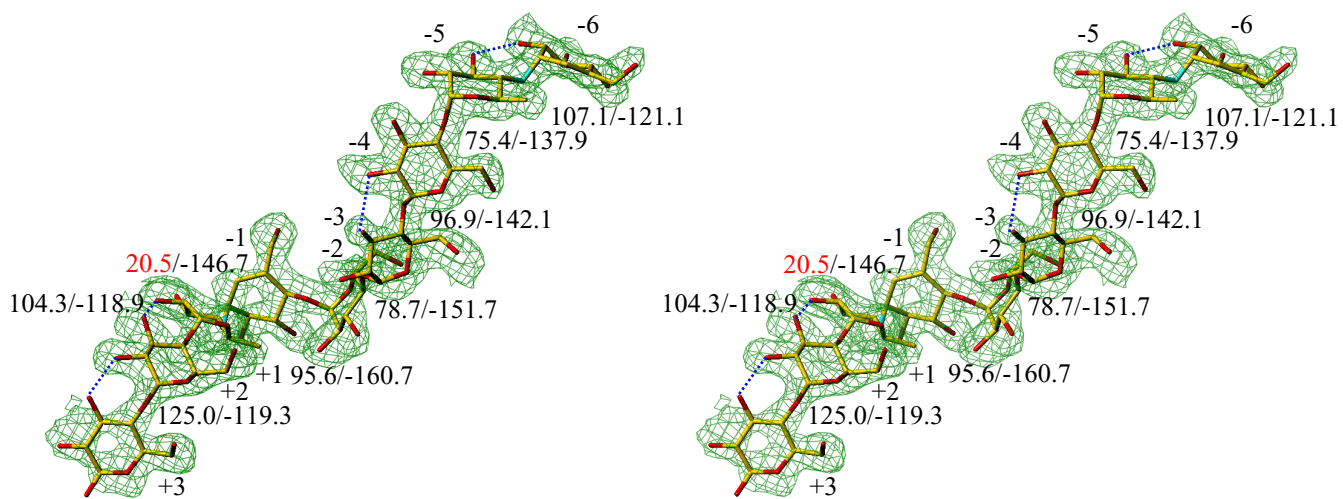


**Figure 21. Crystal structure of G6-amylase complex with pseudo-maltononaose.** (A) Overall structure of the ES complex. Sugar molecules, calcium and sodium ions are represented by ball and sticks, cyan and purple spheres, respectively. (B) Structure of the pseudo-maltononaose with omit  $|F_o - F_c|$  electron density map ( $> 1.5\sigma$ ). Figures are torsion ( $\phi, \psi$ ) angles of glycosidic bonds and are described in and intra-molecular hydrogen bonds are represented by broken lines.

(A)



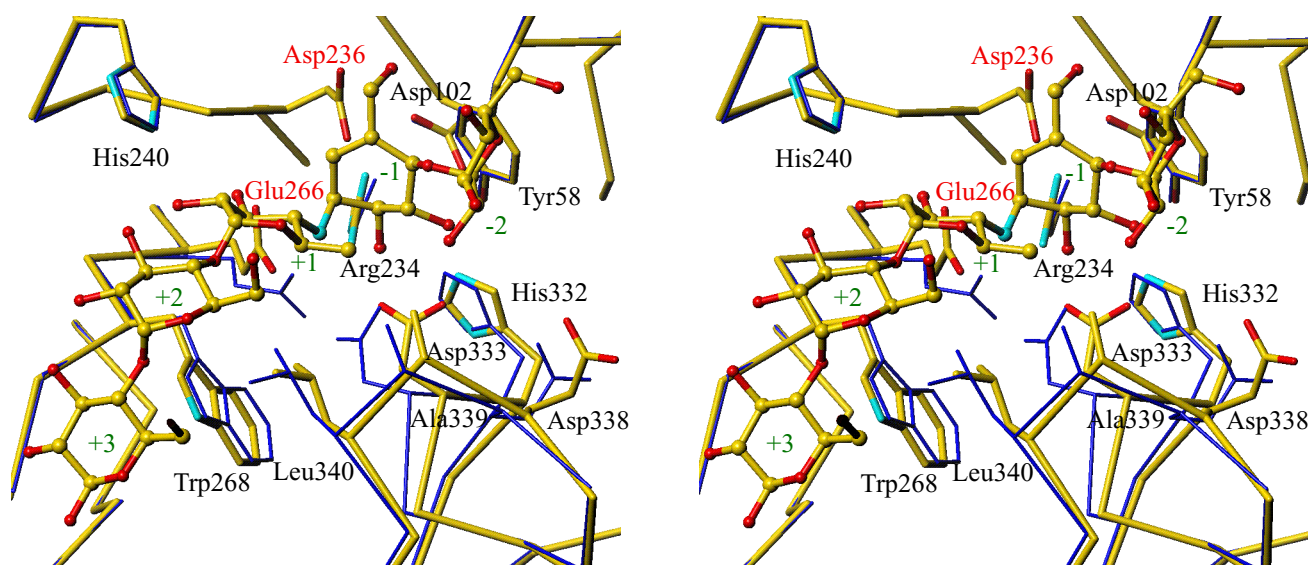
(B)



$\phi/\psi$   $\phi: O5(C7)_n-C1_n-O4(N4)_{n+1}-C4_{n+1}$   $\psi: C1_n-O4(N4)_{n+1}-C4_{n+1}-C5_{n+1}$

**Figure 22. Structural change of the catalytic active site between the native enzyme (thin line) and its complex with pseudo-maltononaose (thick line).** (A) Structural change of the subsites –2 to +3. (B) Structural changes of the catalytic residues (Asp236 and Glu266) and Asp333. Hydrogen bonds and short contacts ( $\leq 3.3$  Å) are shown by broken lines.

(A)



(B)

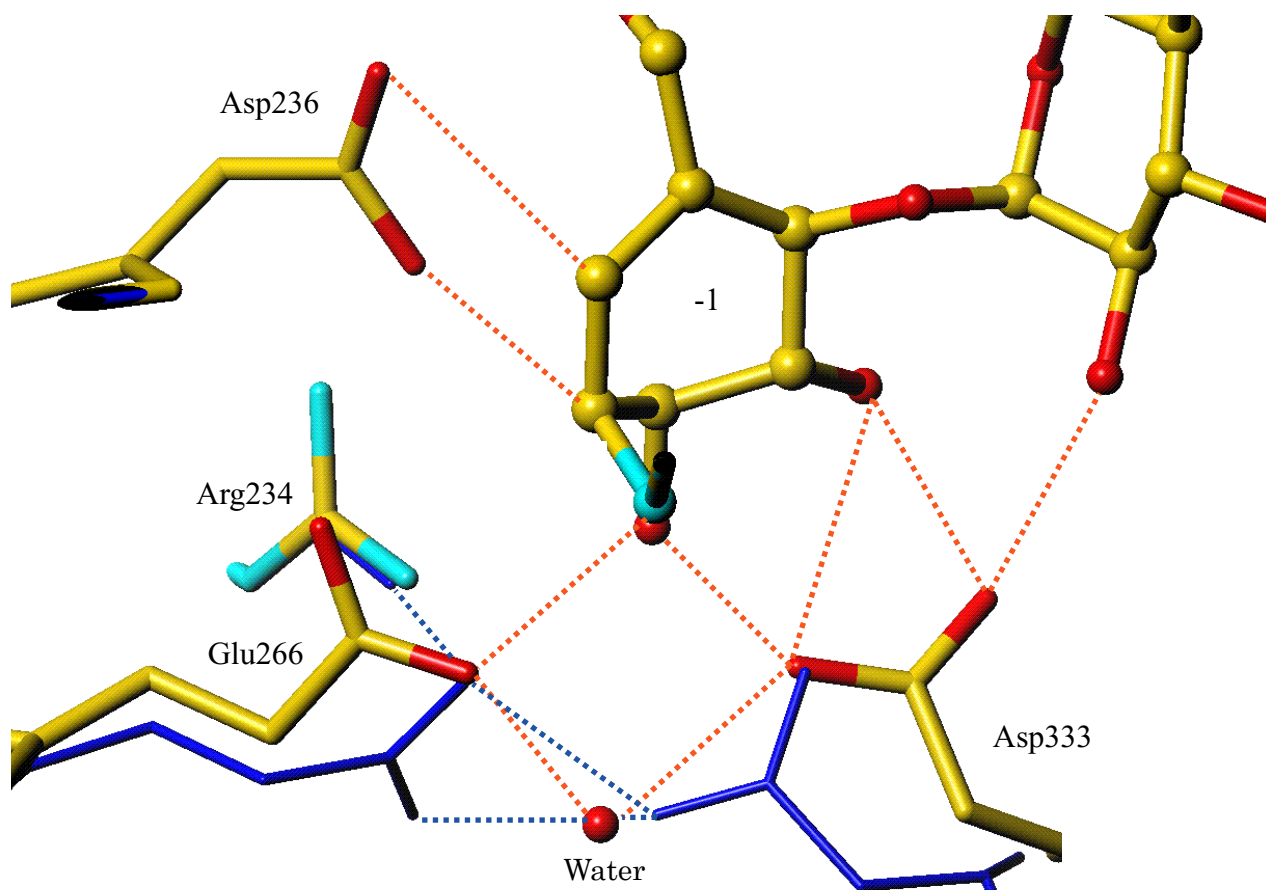
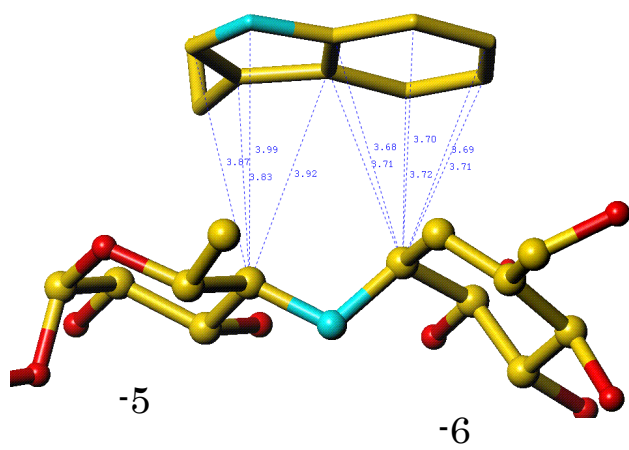
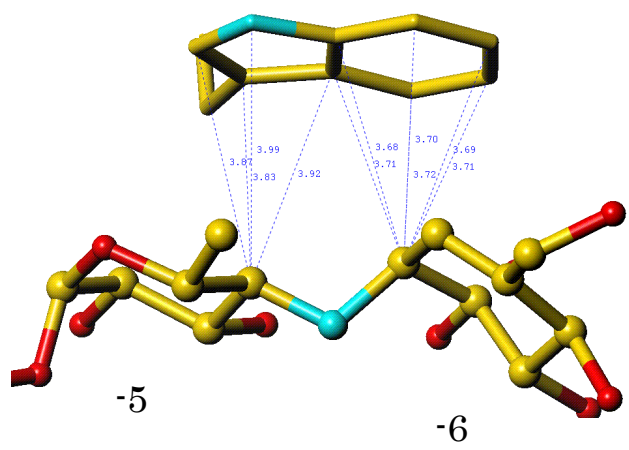


Figure 23. Hydrophobic stack interaction of the aromatic ring of Trp140 with the 4-amino-4, 6-deoxyglucose and cyclitol residues at subsites –5 and –6, respectively.

Trp140

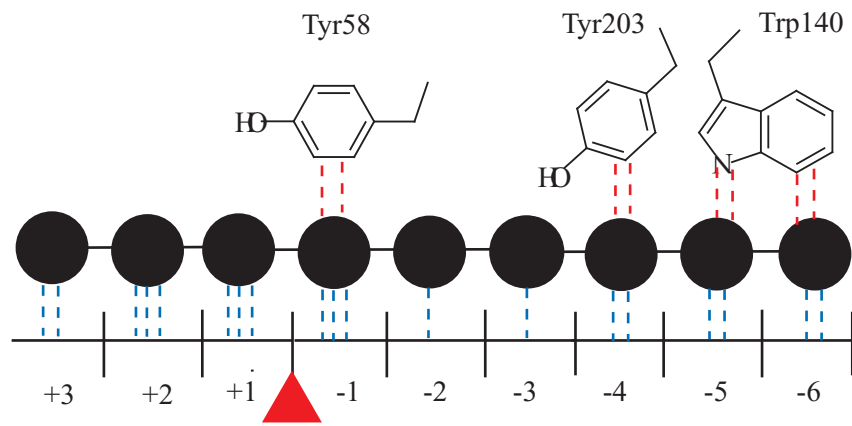


Trp140



**Figure 24. Schematic representation of the reaction mechanism of G6-amylase.** (A) Characteristic drawing of the interactions of the subsites with a substrate. Hydrophobic stacking and hydrogen bonds are shown by red and blue broken lines, respectively. (B) Proposed reaction process for amylose degradation and G6 production by the G6-amylase.

(A)



(B)

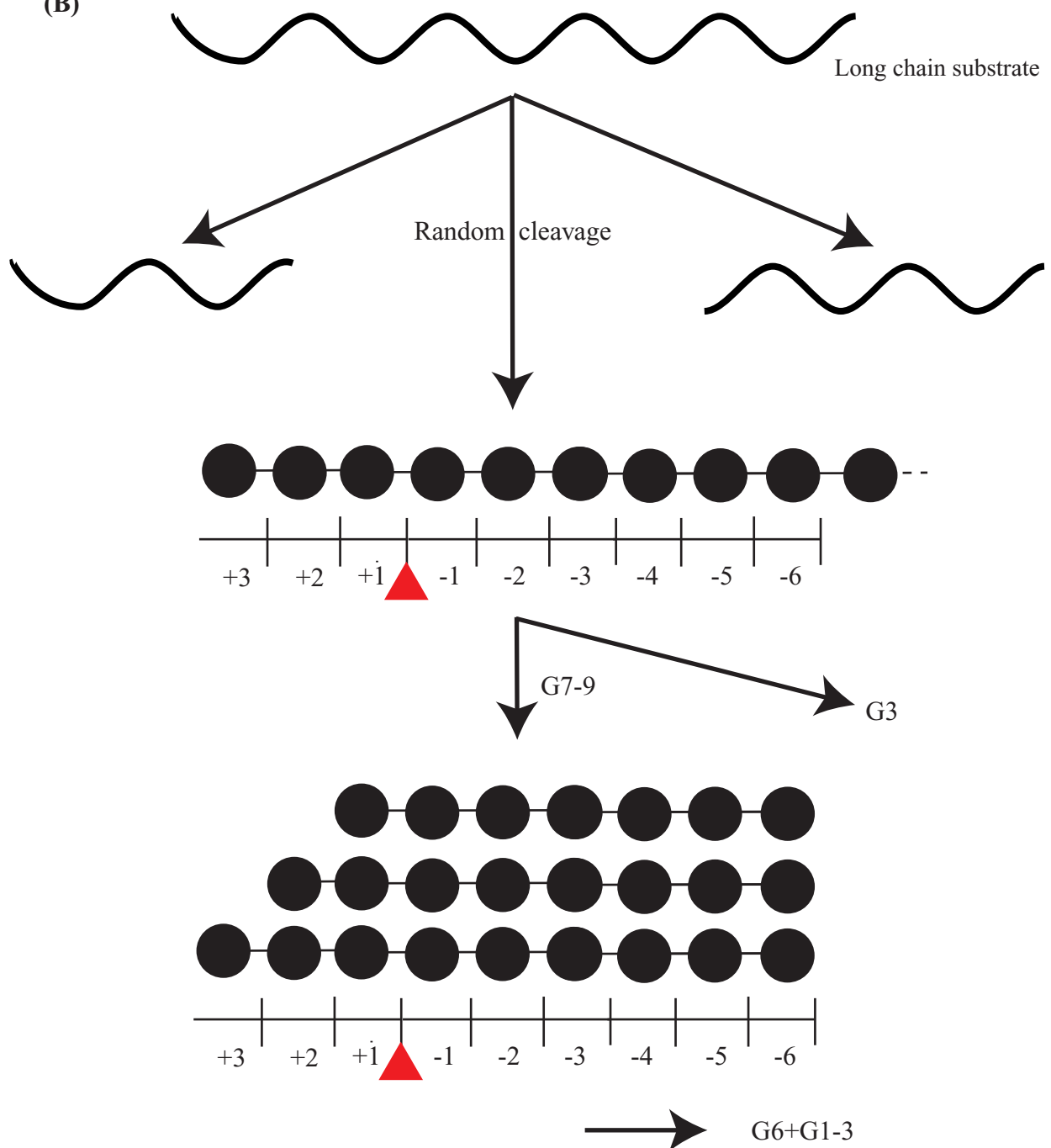
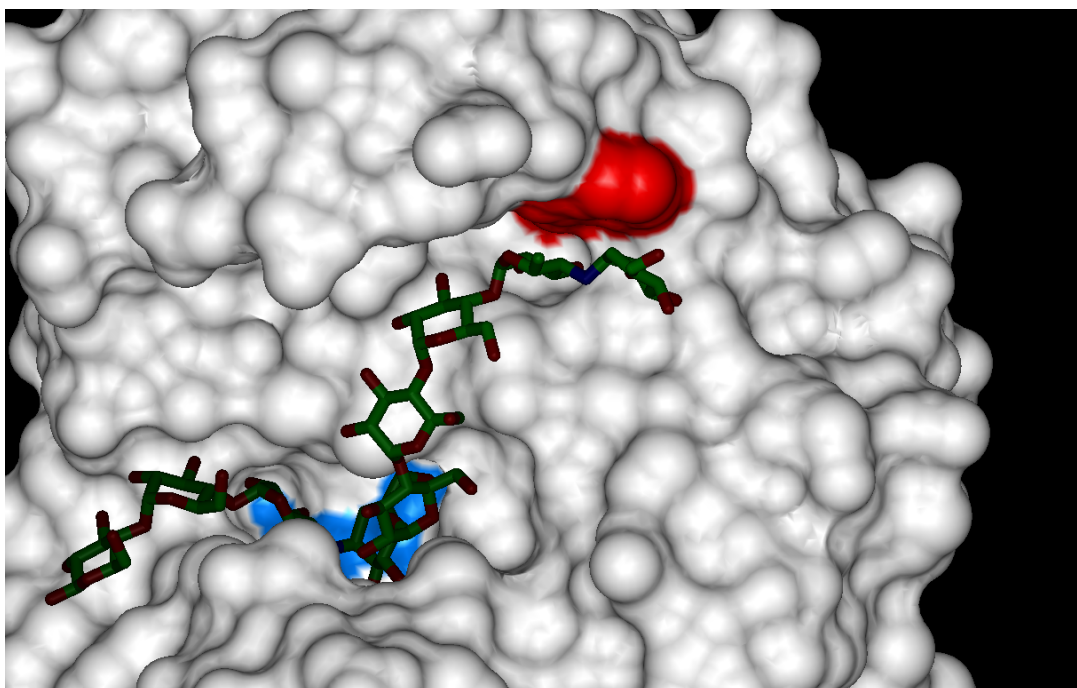


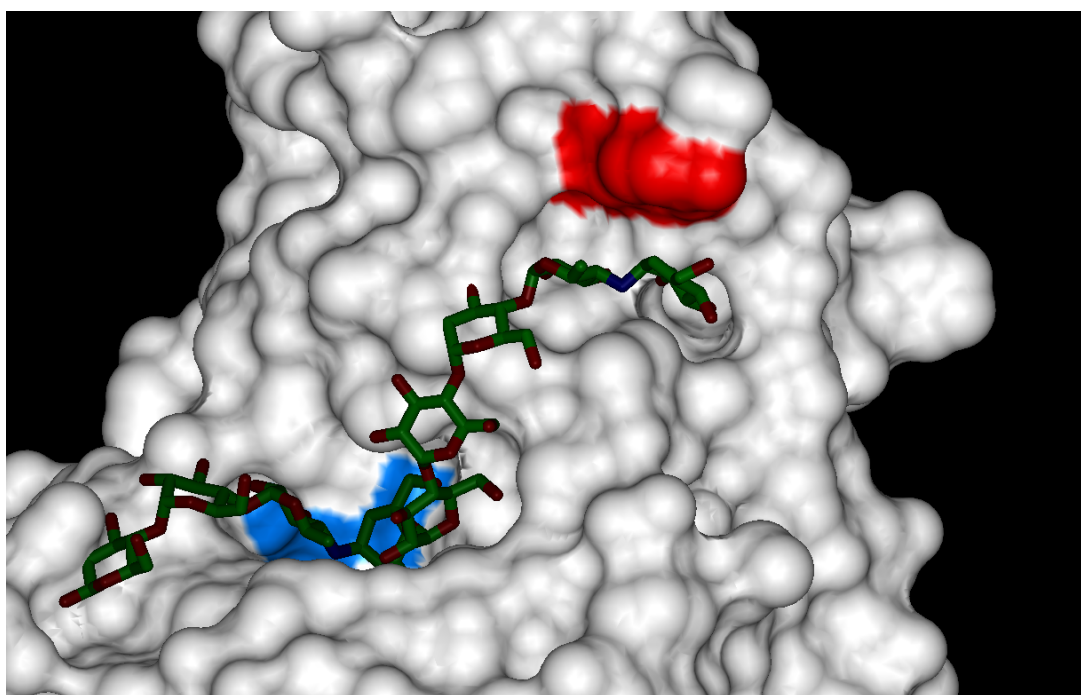


**Figure 25. Structural similarity of subsite –6 between G6-amylase from *Bacillus* sp.707 and barley  $\alpha$ -amylase.** (A) Binding of pseudo-maltononaose with G6-amylase (upper) and barley  $\alpha$ -amylase (lower). The complex structure of barley  $\alpha$ -amylase with pseudo-maltononaose was modeled by docking simulation on the basis of its native structure (A. Kadziola *et al.* 1994). The catalytic residues and the aromatic residue at subsite –6 are colored by cyan and red, respectively. (B) Sequence alignment of the domains B in G6-amylase from *Bacillus* sp.707 (G6AMY) and barley  $\alpha$ -amylase (BAA) according to their structural similarity.

(A)



*Bacillus* sp.707 G6-amylase



Barley  $\alpha$ -amylase

(B)

BAA	NHRT-AEHKD GR-----	-----	104 --GIYCIFEG	-GTPD---AR LDWGPHMICR
G6AMY	NHKGGA DATE	MVRAVEVNPN NRNQEVTGEY	TIEAWTRFDF	PGRGNTHSS- FKWRWYHFD-
			140	
BAA	DD-----	-----RPYA DGTGNPDT--	G-----AD FGAAPDID	
G6AMY	-GVDWDQSRR	LNNRIYK--F RGHGKAWDWE	VDTENGNYDY	L-MYADID

## General Discussion

Many crystal structures of various sugar- $\alpha$ -amylase complexes have been reported. The catalytic mechanism is fundamentally identical in the enzymes of  $\alpha$ -amylase family and the crystallographic studies have shown that the structure of subsites -1 and +1 are similar in  $\alpha$ -amylase family but the structural properties of the other subsites are very different among them.

In this study, the crystal structure of the acarbose-complexed CGTase revealed the four subsites (-2 to +2) and the specific stack interaction of Phe183/259 at subsite +2, which are not observed in  $\alpha$ -amylases. This indicates that Phe183/259 are involving in guiding the glucosyl residue at non-reducing terminal to acceptor-binding site (subsites +1 and +2). This reaction mechanism is currently supported by many biochemical and crystallographic analyses (A. Nakamura *et al.* 1994; J.C.M. Uitdehaag *et al.* 2001; K. Haga *et al.* 2004). Nakamura *et al.* (1994) have reported the biochemical analysis of the four mutant CGTases in which each of specifically conserved aromatic amino acid residues (Phe183, Tyr195, Phe259, and Phe283) of the catalytic active site is replaced with leucine. Stochastic reaction path calculations of the process to form  $\gamma$ -CD from malto-octaose showed that Phe183 transports the non-reducing end of a donor molecule to subsite +1 at the acceptor binding site through the stacking interaction between the aromatic ring of phenylalanine and the pyranose ring of the sugar molecule and Tyr195 cooperatively acts with Phe183 as a hydrophobic center to guide linear substrates to the acceptor-binding site where they are cyclized compactly (J.C.M. Uitdehaag *et al.* 2001). Phe259 plays an important role in binding the substrate, especially as an acceptor residue, to cooperatively cyclize the linear substrate on Phe183 (A. Nakamura *et al.* 1994; J.C.M. Uitdehaag *et al.* 2001; K. Haga *et al.* 2004).

Moreover, Nakamura *et al.* (1994) have reported the biochemical property of the mutant CGTase in which Phe283 is replaced with leucine, but the role of Phe283 in the enzymatic reaction has been unclear. In this study, I have found that Phe283 fixes the motion of the side chain of Phe259 and the interaction of these residues makes the region 257 – 278 and 310 – 317

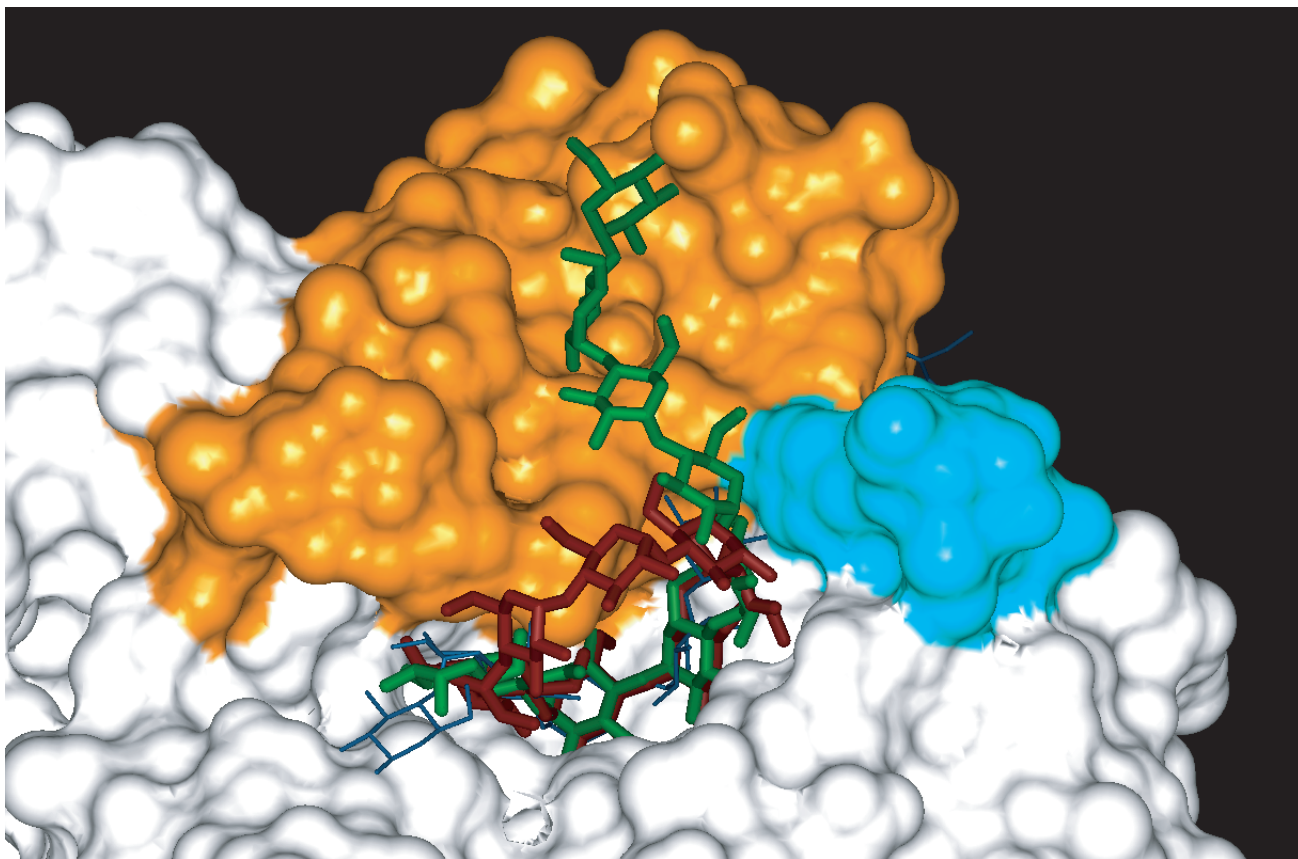
less flexible. Such fixation of the side chain of Phe259 is essential in the cyclization process for regulating the conformation of the glucosyl residue at the non-reducing terminal.

In contrast, structural and biochemical analyses of G6-amylase have been reported little. The crystal structure of G4-amylase in oligo-saccharide forming amylase has been determined (Y. Yoshioka *et al.* 1997). In this study, I have first determined the crystal structure of G6-amylase. The structure of its pseudo-maltonaose complex showed that there are six subsites at the non-reducing-end side and the indole ring of Trp140 makes stack interaction with a cyclitol residue at subsite -6. A similar structural property is observed in the structure of barely  $\alpha$ -amylase-pseudo-maltonaose complex generated by docking simulation. Therefore, maltohexaose production requires the six subsites at non-reducing-end side and the interaction of an aromatic amino acid residue with glucosyl residue at the subsite -6.

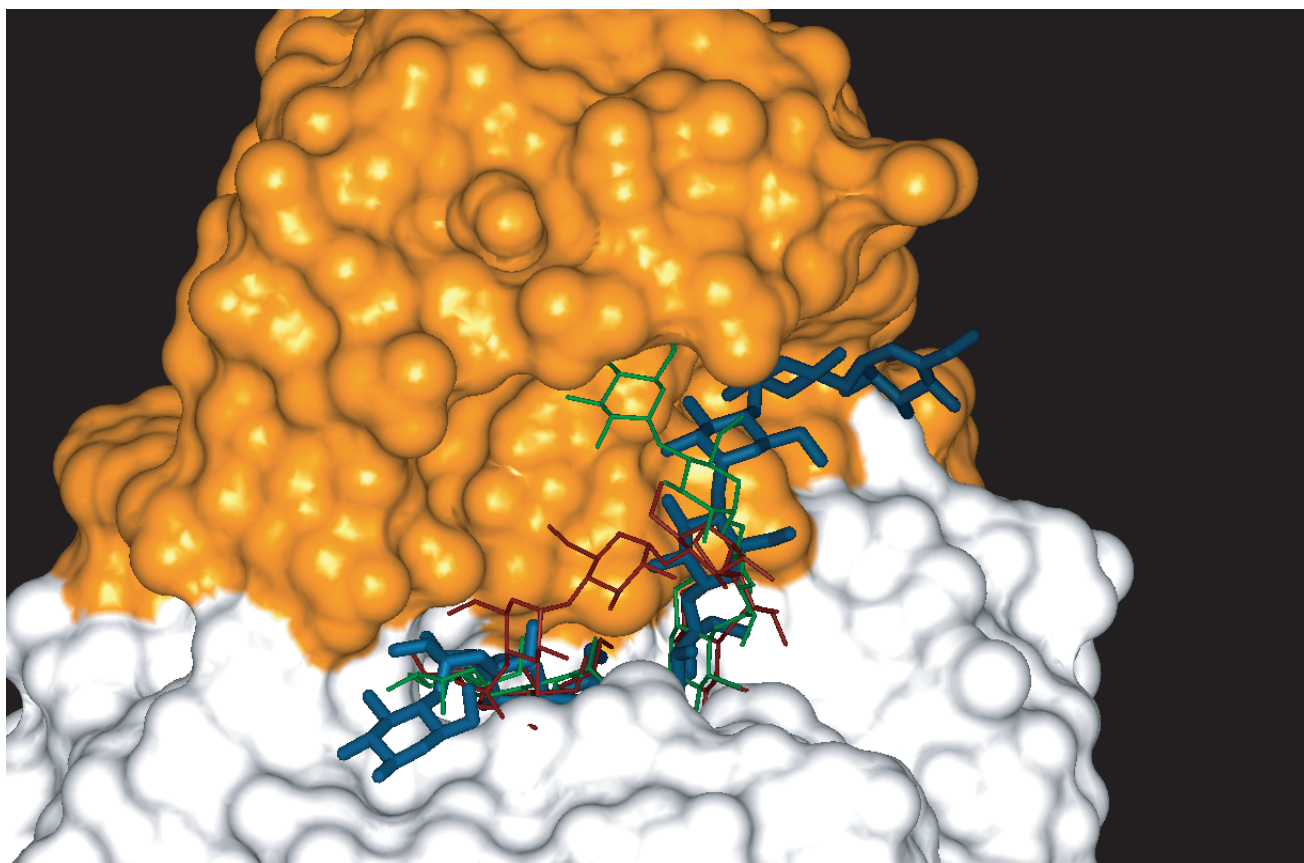
Uidtehaage et al. (1999a and b) reported the crystal structures of inactive double mutant D229N/E257Q CGTase complexed with maltonaose or  $\gamma$ -cyclodextrin. In comparison with the pseudo-maltonaose-G6amylase complex, the additional region 86 – 95 composing of subsites -3 and -4 in CGTase seems to act as a “barrier” to bend sugar chain (Figure 26). As a result, in maltonaose-CGTase complex, the glucosyl residue at the non-reducing end reaches to the top of domain B (Figure 26). This binding manner would be effective for cyclization. In contrast, the structural barrier to bend sugar chain is not observed in G6-amylase and a deep binding cleft is formed between domains A and B. Domain B has a structural barrier not to bend the sugar chain toward the top of the domain B as observed in CGTase (Figure 26). Therefore, if the same substrates are bound to CGTase and G6-amylase, their binding manner is very different because of the difference in the backbone structure of domain B and some loops in domain A. Furthermore, the specific amino acid residues presented in each enzyme may function in their effective and specific production of cyclodextrins or maltohexaose.

**Figure 26. Comparison of the substrate binding mode between CGTase and G6-amylase.** The domain B is shown by orange color. (A) Superposition of maltononaose (green color) and  $\gamma$ -cyclodextrin (red color) in the active site cleft of CGTase (J.C.M. Uitdehaag *et al.* 1999a and b). The region 85 – 95 is rendered by cyan color. Pseudo-maltononaose located at the position equivalent to that in G6-amylase is shown with thin and blue sticks. (B) pseudo-maltononaose (blue color) bound to the active site of G6-amylase. Maltononaose and  $\gamma$ -cyclodextrin shown with thin sticks are located in the same manner as that observed in the CGTase complexes.

(A)



(B)



## References

- Abe, S., Nagamine, Y., Omichi, K., and Ikenaka, T. (1991) Investigation of the active site of *Bacillus macerans* cyclodextrin glucanotransferase by use of modified maltooligosaccharides. *J. Biochem.* **110**, 756 – 761.
- Bak-Jensen, K.S., Andre, G., Gottschalk, T.E., Paes, G., Tran, V., and Svensson, B. (2003) Tyrosine 105 and threonine 212 at outermost substrate binding subsites –6 and +4 control substrate specificity, oligosaccharide cleavage patterns, and multiple binding modes of barley  $\alpha$ -amylase I. *J. Biol. Chem.* In press.
- Brünger, A.T., Adams, P.D., Clore, G.M., DeLano, W.L., Gros P, Grosse-Kunstleve, R.W., Jiang, J.S., Kuszewski, J., Nilges, M., Pannu, N.S., Read, R.J., Rice, L.M., Simonson, T., and Warren, G.L. (1998) Crystallography & NMR system: A new software suite for macromolecular structure determination. *Acta. Cryst.* **D54**, 905-921.
- Brzozowski, A.M., Lawson, D.M., Turkenburg, J.P., Bisgaard-Frantzen, H., Svendsen, A., Borchert, T.V., Dauter, Z., Wilson, K.S., and Davies, G.J. (2000) Structural analysis of a chimeric bacterial  $\alpha$ -amylase. High-resolution analysis of native and ligand complexes. *Biochemistry* **39**, 9099-107.
- Brünger, A. T., Kuriyan, J., and Karplus, M. (1987) Crystallographic *R* factor refinement by molecular dynamics. *Science* **235**, 458 - 460.
- Chan, S. J., Weiss, J., Konrad, M., White, T., Bahl, C., Yu, S. D., Marks, D., and Steiner, D. F. (1981) Biosynthesis and periplasmic segregation of human proinsulin in *Escherichia coli*. *Proc. Natl. Acad. Sci. U. S. A.* **78**, 5401 - 5405.

Dauter, Z., Dauter, M., Brzozowski, A. M., Christensen, S., Borchert, T. V., Beier, L., Wilson, K. S., and Davies, G. J. (1999) X-ray structure of novamyl, the five-domain "maltogenic"  $\alpha$ -amylase from *Bacillus Stearothermophilus*: maltose and acarbose complexes at 1.7Å resolution. *Biochemistry* **38**, 8385 – 92.

Fujimoto, Z., Takase, K., Doui, N., Momma, M., Matsumoto, T., and Mizuno, H. (1998) Crystal structure of a catalytic-site mutant  $\alpha$ -amylase from *Bacillus subtilis* complexed with maltopentaose. *J. Mol. Biol.* **277**, 393 – 407.

Gilson, M.K., Sharp, K.A., and Honig, B.H. (1987) Calculating the electrostatic potential of molecules in solution. *J. Comp. Chem.* **9**, 327 – 35.

Haga, K., Harata, K., Nakamura, A., and Yamane, K. (1994) Crystallization and preliminary X-ray studies of cyclodextrin glucanotransferase from alkalophilic *Bacillus* sp.1011. *J. Mol. Biol.* **237**, 163 - 164.

Haga, K., Kanai, R., Sakamoto, O., Aoyagi, M., Harata, K., and Yamane, K. (2004) Effects of essential carbohydrate/aromatic stacking interaction with Tyr100 and Phe259 on substrate binding of cyclodextrin glycosyltransferase from alkalophilic *Bacillus* sp.1011. *J. Biochem.* In press.

Harata, K., Haga, K., Nakamura, M., Aoyagi, M., and Yamane, K., (1996) X-ray structure of cyclodextrin glucanotransferase from alkalophilic *Bacillus* sp.1011. Comparison of two independent molecules at 1.8 Å resolution. *Acta Cryst.* **D52**, 1136-1145

Harris, E.M.S, Aleshin, A.E., Firsov, L.M., and Honzatko, R.B. (1993) Refined structure for the complex of 1-deoxynojirimycin with glucoamylase from *Aspergillus awamori* var. X100 to 2.4Å



resolution. *Biochemistry* **32**, 1618-1626

Henrissat, B., and Davies, G. (1997) Structural and sequence-based classification of glycoside hydrolases. *Curr. Opin. Struct. Biol.* **7**, 637-644.

Honig, B., and Sharp, K., and Yang, A. (1993) Macroscopic models of aqueous solutions: biological and chemical applications. *J. Phys. Chem.* **97**, 1101-9.

Kandra, L., Gyemant, G., Remenyik, J., Hovanszki, G., and Liptak, A. (2002) Action pattern and subsite mapping of *Bacillus licheniformis*  $\alpha$ -amylase (BLA) with modified maltooligosaccharide substrates. *FEBS Lett.* **518**, 79 – 82.

Kadziola, A., Abe, J., Svensson, B., and R. Haser. (1994) Crystal and molecular structure of barley  $\alpha$ -amylase. *J. Mol. Biol.* **239**, 104 – 121.

Kaneko, T., Kudo, T., and Horikoshi, K. (1990) Comparison of CD composition produced by chimeric CGTases. *Agric. Biol. Chem.* **54**, 197 - 201.

Kimura, K., Kataoka, S., Ishii, Y., Takano, T., and Yamane, K. (1987) Nucleotide sequence of the  $\beta$ -cyclodextrin glucanotransferase gene of alkalophilic *Bacillus* sp. strain 1011 and similarity of its amino acid sequence to those of  $\alpha$ -amylases. *J. Bacteriol.* **169**, 4399 - 4402.

Kimura, K., Tsukamoto, A., Ishii, Y., Takano, T., and Yamane, K. (1988) Cloning of a gene for maltohexaose producing amylase of an alkalophilic *Bacillus* and hyper-production of the enzyme in *Bacillus subtilis*. *Appl. Microbiol. Biotech.* **27**, 372 – 377.

Klein, C., Hollender, J., Bender, H., and Schulz, G.E. (1992) Catalytic center of cyclodextrin

glycosyltransferase derived from X-ray structure analysis combined with the site-directed mutagenesis. *Biochemistry* **31**, 8740 – 8746.

Knegtel, R.M.A., Wind, R.D., Rozeboom, H.J., Kalk, K.H., Buitelaar, R.M., Dijkhuizen, L., and Dijkstra, B.W. (1996) Crystal structure at 2.3 Å resolution and revised nucleotide sequence of the thermostable cyclodextrin glycosyltransferase from *Thermoanaerobacterium thermosulfurigenes* EM1. *J. Mol. Biol.* **256**, 611-622

Kobayashi, S., Kainuma, K., and Suzuki, S. (1978) Purification and some properties of *Bacillus macerans* cycloamylose (cyclodextrin) glucanotransferase. *Carbohydrate Research* **61**, 229 - 238.

Kubota, M., Matsuura, Y., Sakai, S., and Katsube, Y. (1991) Molecular structure of *B. stearothermophilus* cyclodextrin glucanotransferase and analysis of substrate binding site. *Denpun Kagaku* **38**, 141-146 (in Japanese).

Laskowski, A. R., MacArthur, M. W., Moss, D. S., and Thornton, J. M. (1993) PROCHECK: a program to check the stereochemical quality of protein structures. *J. Appl. Cryst.* **26**, 283 - 291.

Lawson, C.L., van Montfort, R., Strokopytov, B., Rozeboom, H.J., Kalk, K.H., de Vries, G.E., Penninga, D., Dijkhuizen, L., and Dijkstra, B.W. (1994) Nucleotide sequence and X-ray structure of cyclodextrin glycosyltransferase from *Bacillus circulans* strain 251 in a maltose-dependent crystal form. *J. Mol. Biol.* **236**, 590-600

Machius, M., Declerck, N., Huber, R., and Wiegand, G. (1998) Activation of *Bacillus licheniformis*  $\alpha$ -amylase through disorder→order transition of the substrate-binding site mediated by a calcium-sodium-calcium metal triad. *Structure* **6**, 281 – 92.

Machius, M., Declerck, N., Huber, R., and Wiegand, G. (2003) Kinetic stabilization of *Bacillus licheniformis*  $\alpha$ -amylase through introduction of hydrophobic residues at the surface. *J. Biol. Chem.* **278**, 11546-53.

Maeda, I., Kiribuchi, S., and Nakamura, M. (1978) Digestion of barley starch granules by the combined action of  $\alpha$ - and  $\beta$ -amylases purified from barley and barley malt. *Agric. Biol. Chem.* **42**, 259 – 67.

Matsuura, Y., Kusunoki, M., Harada, W., and Kakudo, M. (1984) Structure and possible catalytic residues of Taka-amylase A. *J. Biochem.* **95**, 697 – 702.

Mosi, R., Sham, H., Uitdehaag, J. C. M., Ruiterkamp, R., Dijkstra, B. W., and Withers, S. G. (1998) Reassessment of acarbose as a transition state analogue inhibitor of cyclodextrin glycosyltransferase. *Biochemistry* **37**, 17192 - 17198.

Nakakuki, T., Azuma, K., and Kainuma, K. (1984) Action patterns of various exo-amylases and the anomeric configurations of their products. *Carbohydr. Res.* **128**, 297-310.

Nakamura, A., Haga, K., Ogawa, S., Kuwano, K., Kimura, K., and Yamane, K. (1992) Functional relationships between cyclodextrin glucanotransferase from an alkalophilic *Bacillus* and  $\alpha$ -amylases. *FEBS Lett.* **296**, 37-40

Nakamura, A., Haga, K., and Yamane, K. (1993) Three histidine residues in the active center of cyclodextrin glucanotransferase from alkalophilic *Bacillus* sp. 1011: effects of the replacement on pH dependence and transition-state stabilization. *Biochemistry* **32**, 6624 - 6631.

Nakamura, A., Haga, K., and Yamane, K. (1994) Four aromatic residues in the active center of

cyclodextrin glucanotransferase from alkalophilic *Bacillus* sp. 1011: effects of replacements on substrate binding and cyclization characteristics. *Biochemistry* **33**, 9929 - 9936.

Narimasa, S. (1973) A thermophilic extracellular  $\alpha$ -amylase from *Bacillus licheniformis*. *Arc. Biochem. Biophys.* **155**, 290-298.

Nitschke, L., Heeger, K., Bender, H., and Schulz, G. E. (1990) Molecular cloning, nucleotide sequence and expression in *Escherichia coli* of the  $\beta$ -cyclodextrin glycosyltransferase gene from *Bacillus circulans* strain no.8. *Appl. Microbiol. Biotechnol.* **33**, 542 - 546.

Otwinowski, Z. and Minor, W. (1997) Processing of X-ray Diffraction Data Collected in Oscillation Mode, in *Methods in Enzymology*, **276**, Macromolecular Crystallography, part A (Carter, Jr., C.W., and Sweet, R. M. Eds.) pp. 307-327, Academic Press (New York).

Pfueller, S.L., and Elliott, W.H. (1969) The extracellular  $\alpha$ -amylase of *Bacillus stearothermophilus*. *J. Biol. Chem.* **244**, 48-54.

Przylas, I., Terada, Y., Fujii, K., Takaha, T., Saenger, W., and Sträter, N. (2000) X-ray structure of acarbose bound to amylomaltase from *Thermus aquaticus*. Implications for the synthesis of large cyclic glucans. *Eur. J. Biochem.* **267**, 6903 – 6913.

Qian, M., Haser, R., Buisson, G., Duee, E., and Payan, F. (1994) The active center of a mammalian  $\alpha$ -amylase. Structure of the complex of a pancreatic  $\alpha$ -amylase with a carbohydrate inhibitor refined to 2.2-Å resolution. *Biochemistry* **33**, 6284-6294.

Sakoda, M., and Hiromi, K. (1976) Determination of the best-fit values of kinetic parameters of the Michaelis-Menten equation by the method of least squares with the Taylor expansion. *J.*

*Biochem.* **80**, 547-555.

Schmidt, A. K., Cottaz, S., Driguez, H., and Schulz, G. E. (1998) Structure of cyclodextrin glycosyltransferase complexed with a derivative of its main product  $\beta$ -cyclodextrin. *Biochemistry* **37**, 5909 - 5915.

Sin, K. A., Nakamura, A., Kobayashi, K., Masaki, H., and Uozumi, T. (1991) Cloning and sequencing of a cyclodextrin glucanotransferase gene from *Bacillus ohbensis* and its expression in *Escherichia coli*. *Appl. Microbiol. Biotechnol.* **35**, 600 - 605.

Suvd, D., Fujimoto, Z., Takase, K., Matsumura, M., and Mizuno, H. (2001) Crystal structure of *Bacillus stearothermophilus*  $\alpha$ -amylase: possible factors determining the thermostability. *J. Biochem.* **129**, 461-468.

Tanaka, M., Muto, N., and Yamamoto, I. (1991) Characterization of *Bacillus stearothermophilus* cyclodextrin glucanotransferase in ascorbic acid 2-O- $\alpha$ -glucoside formation. *Biochim. Biophys. Acta.* **1078**, 127 - 132.

Truscheit, E., Frommer, W., Junge, B., Müller, L., Schmidt, D.D., and Wingender, W. (1981) Chemistry and biochemistry of microbial  $\alpha$ -glucosidase inhibitors. *Angew. Chem., Int. Ed. Engl.* **20**, 744-761

Tsukamoto, A., Kimura, K., Ishii, Y., Takano, T., and Yamane, K. (1988) Nucleotide sequence of the maltohexaose-producing amylase gene from an alkalophilic *Bacillus* sp.#707 and structural similarity to liquefying type  $\alpha$ -amylases. *Biochem. Biophys. Res. Commun.* **151**, 25-31.

Uitdehaag, J.C., Kalk, K.H., van Der Veen, B.A., Dijkhuizen, L., and Dijkstra, B.W. (1999a) The

cyclization mechanism of cyclodextrin glycosyltransferase (CGTase) as revealed by a  $\gamma$ -cyclodextrin-CGTase complex at 1.8-Å resolution. *J. Biol. Chem.* **274**, 34868-34876

Uitdehaag, J.C.M., Mosi, R., Kalk, K.H., van Der Veen, B.A., Dijkhuizen, L., Withers, S.G., and Dijkstra, B.W. (1999b) X-ray structures along the reaction pathway of cyclodextrin glycosyltransferase elucidate catalysis in the alpha-amylase family. *Nat. Struct. Biol.* **6**, 432-436

Uitdehaag, J. C. M., van der Veen, B. A., Dijkhuizen, L., Elber, R., and Dijkstra, B. W. (2001) Enzymatic circularization of a malto-octaose linear chain studied by stochastic reaction path calculations on cyclodextrin glycosyltransferase. *Proteins* **43**, 327 - 335.

van der Veen, B. A., Leemhuis, H., Kralj, S., Uitdehaag, J. C. M., Dijkstra, B. W., and Dijkhuizen, L. (2001) Hydrophobic amino acid residues in the acceptor binding site are main determinants for reaction mechanism and specificity of cyclodextrin-glycosyltransferase. *J. Biol. Chem.* **276**, 44557 - 44562.

Yoshioka, Y., Hasegawa, K., Matsuura, Y., Katsube, Y., and Kubota, M. (1997) Crystal structures of a mutant maltotetraose-forming exo-amylase cocrystallized with maltopentaose. *J. Mol. Biol.* **271**, 619-628.

## Acknowledgements

This work was performed as a collaborative research under the directions of Professor Kunio Yamane (Institute of Biological Sciences, University of Tsukuba) and Deputy Director Kazuaki Harata (Biological Information Research Center, National Institute of Advanced Industrial Science and Technology). I wish to express my appreciations to Professor K. Yamane and Deputy Director K. Harata for great supports, invaluable suggestions and every encouragement during this work.

I sincerely thanks to Research fellow Keiko Haga and Associate Professor Kouji Nakamura (Institute of Biological Sciences, University of Tsukuba) for great supports, valuable discussions and suggestions, Drs. Hiroshi Kakeshita, Keigo Bunai, Miyuki Kumano, Toshihiko Akiba, Mr. Satoshi Suzuma and all members of the Yamane's laboratory and structural analysis team for helpful discussion and support.

I would like to express my gratitude to Professor Haruo Seto (University of Tokyo) for a gift of 1-deoxynojirimycin, Photon Factory staff for technical support on diffraction measurement.

Finally, I would like to thank my family and friends for their encouragement and great support for my research.

February 2004

Ryuta Kanai